DEPARTMENT OF THE NAVY

DAVID TAYLOR MODEL BASIN
WASHINGTON, D.C.

HYDROMECHANICS

o

AERODYNAMICS

o

STRUCTURAL MECHANICS

o

APPLIED MATHEMATICS

o

ACOUSTICS AND VIBRATION

A METHOD FOR PREDICTING THE STATIC AERODYNAMIC CHARACTERISTICS OF LOW-ASPECT-RATIO CONFIGURATIONS

by

Peter T. Eaton

Distribution of this document is unlimited.

AERODYNAMICS LABORATORY
RESEARCH AND DEVELOPMENT REPORT

June 1966 Report 2216

PRNC-TMB-648 (Rev 1-64)

ERRATA

David Taylor Model Basin Report 2216, Aero Report 1112

A METHOD FOR PREDICTING THE STATIC AERODYNAMIC CHARACTERISTICS OF LOW-ASPECT-RATIO CONFIGURATIONS

By Peter T. Eaton

Date of report - June 1966

Typographical errors

Page ii — $d_o - d_{X_o}$ instead of $d_o - d_{25}$

Page 9 — 11th line Figure 3 instead of Figure 1

Page 18 — Equation [B-4] $\sum (S_2 - S_1)\,(X)\,\frac{1}{S_o}$

Small x instead of Cap X

Page 23 — Equation [B-21] Close paren.; $(\ell_B - \ell_T) \geq 2r_T\beta$

Page 36 — Reference 13 Cylinder instead of Dylinder

Page 37 — Reference 21 Donovan instead of Donovon

Page 43 — Dimension ℓ_{N_M} is not shown

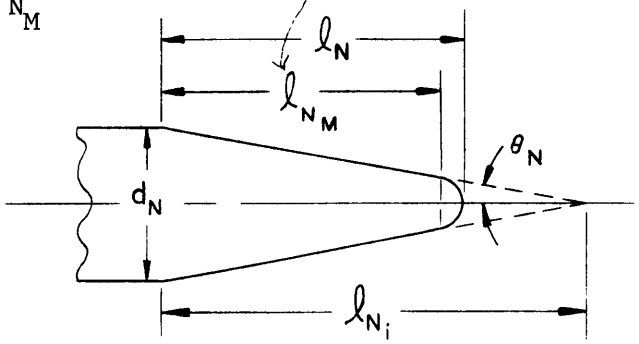

A METHOD FOR PREDICTING THE STATIC AERODYNAMIC CHARACTERISTICS OF LOW-ASPECT-RATIO CONFIGURATIONS

by

Peter T. Eaton

This work was performed under the Foundational Research Program.

June 1966

Report 2216
Aero Report 1112

SYMBOLS

AR_{T_e}	Tails-exposed aspect ratio, $\frac{(b_T)^2}{S_T}$
AR_{W_e}	Wings-exposed aspect ratio, $\frac{(b_W)^2}{S_W}$
b_T	Tail exposed span; i.e., tail span minus body diameter (See Figure 1)
b_W	Wing exposed span; i.e., wing span minus body diameter (See Figure 1)
$\left(c_{d_w}\right)_N$	Forebody (nose) wave-drag coefficient referred to cross-sectional area at nose body juncture
$\left(c_{d_w}\right)_a$	Afterbody (boattail) wave-drag coefficient referred to cross-sectional area at boattail body juncture
$C_{D_{w/W}}$	Wing wave-drag parameter
$\left(c_{d_w}\right)_T$	Tail wave-drag parameter
$\bar{c}_T$	Tail mean geometric chord $\left(\frac{c_{r_T}}{2}\right)(1 + \lambda_T)$
c_{t_T}	Tail tip chord (See Figure 1)
c_{r_T}	Tail exposed root chord at tail-body juncture (See Figure 1)
C_{p_B}	Base pressure coefficient
$\bar{c}_W$	Wing mean geometric chord, $\left(\frac{c_{r_W}}{2}\right)(1 + \lambda_W)$
c_{t_W}	Wing tip chord (See Figure 1)
c_{r_W}	Wing exposed root chord at wing-body juncture (See Figure 1)
$d_o - d_{25}$	Body diameters at aft end of each of 20 equally spaced segments of parabolic body from station 0 to X_o

$d_1 - d_5$	Body diameters at the aft end of each of five equally spaced segments of the nose
d_a	Body diameter at the body-boattail juncture (See Figure 1)
d_b	Diameter of the body at the base (See Figure 1)
d_H	Diameter of hemisphere of a hemispherically modified nose (See Figure 1)
d_N	Body diameter at nose-body juncture (See Figure 1)
d	Body maximum diameter
d_{X_o}	Diameter of parabolic body at station (X_o)
e	Lifting surface efficiency (Oswald) factor
d_{av}	Average body diameter
f_a	Boattail fineness ratio, $\frac{\ell_a}{d_a}$
f_N	Nose fineness ratio, $\frac{\ell_N}{d_N}$
f_W	Spanwise location of wing vortex (See Figure 1)
h_T	Height of wing vortex above body center line at the tail center-of-pressure location
i	Wing-tail downwash interference constant
K_{T_B}	Linear tail lift constant due to angle of attack, accounting for presence of the body
K_{B_T}	Linear body lift constant due to angle of attack, accounting for presence of tails
K'_{T_B}	Linear tail lift constant due to tail deflection angle, accounting for presence of the body
K'_{B_T}	Linear body lift constant due to tail deflection angle, accounting for presence of tails

K_{W_B}	Linear wing lift constant due to angle of attack, accounting for presence of the body
K_{B_W}	Linear body lift constant due to angle of attack, accounting for presence of wings
$(K_2 - K_1)$	Apparent mass factor
K_{w_W}	Wing wave-drag constant
K_{w_T}	Tail wave-drag constant
ℓ_{N_M}	Length of hemispherically modified nose, excluding the hemisphere (See Figure 1)
ℓ_a	Boattail length (See Figure 1)
ℓ_B	Total body length (including nose and boattail) (See Figure 1)
ℓ_R	Arbitrary reference length (usually body maximum diameter)
ℓ_A	Body length excluding nose ($\ell_B - \ell_N$)
ℓ_N	Nose length (See Figure 1)
ℓ_{N_i}	Nose length - blunted nose fictiously extended to point (See Figure 1)
ℓ_W	Distance from foremost point on the body to the wing-leading-edge - body juncture (See Figure 1)
ℓ_T	Distance from foremost point on the body to the tail-leading-edge - body juncture (See Figure 1)
M	Free-stream Mach number
η	Cross-flow drag proportionality factor for nose-body of finite length
N_T	Number of pairs of tail panels
N_W	Number of pairs of wing panels

q	Dynamic pressure, psi or psf (See Figure 27)
$(Re)_B$	Body Reynolds number, $\frac{Re}{\ell} \cdot \ell_B$
$(Re)_W$	Wing Reynolds number, $\frac{Re}{\ell} \cdot \ell_W$
$(Re)_T$	Tail Reynolds number, $\frac{Re}{\ell} \cdot \ell_T$
$\frac{Re}{\ell}$	Reynolds number per unit length
r_T	Body radius at the tails (See Figure 1)
r_W	Body radius at the wings (See Figure 1)
s	Semi-span including body radius ($b/2 + r$)
S_b	Body cross-sectional area at the base
S_{B_V}	Planform area of the cylindrical portion of the body, $(d_{av})(\ell_B - \ell_N)$
$S_{B_{wet}}$	Body wetted area, $(\pi\, d_{av}\, \ell_B)$
$S_{W_{wet}}$	Wing wetted area, $(2S_W N_W)$
$S_{T_{wet}}$	Tail wetted area, $(2S_T N_T)$
S_W	Exposed wing area (one pair of panels)
S_T	Exposed tail area (one pair of panels)
S_N	Body cross-sectional area at nose-body juncture
S_R	Arbitrary reference area (usually body cross-sectional area)
$(t/c)_W$	Wing thickness-to-chord ratio
$(t/c)_T$	Tail thickness-to-chord ratio
V_B	Body volume

	X_{cg}	Distance from foremost point on the body to the chosen center of gravity (See Figure 1)
*	(X_{cp})	Distance from foremost point on the body to the center of pressure
*	$\left(\frac{x}{c}\right)$	Center-of-pressure location as a fraction of exposed root chord
	$\left(\frac{x}{c}\right)_{ref}$	Center-of-pressure travel parameter
	$\Delta\left(\frac{x}{c}\right)$	Center-of-pressure travel parameter
	X_1	Distance from nose or forward-most station of maximum negative change in body cross-sectional area for parabolic body of revolution
	X_o	Parabolic body station where flow ceases to be potential
	$X_{W_{TE}}$	Distance from foremost point on the body to the wing trailing edge (See Figure 1)
	θ_N	Conical nose semi-vertex angle (half enclosed angle at the point) (See Figure 1)
	θ_{N_o}	Ogive nose semi-vertex angle (half enclosed angle of tangent)
	θ_a	Semi-vertex angle of conical boattail (See Figure 1)
	β	Compressibility factor, $\sqrt{M^2-1}$
	α	Angle of attack, in degrees - angle between the body longitudinal axis and the relative-wind vector (nose up is positive) (See sketch)
	δ_T	Tail deflection angle, in degrees - angle between the tail plane of symmetry and the body longitudinal axis (trailing edge down is positive). Both horizontal-tail panels are assumed deflected together for lift and pitching moment and both vertical-tail panels undeflected. (See sketch)
	α_{max}	Angle of attack at maximum lift
	*	See list of subscripts used with this symbol

λ_W	Wing taper ratio, $(c_t/c_r)_W$
λ_T	Tail taper ratio, $(c_t/c_r)_T$
$\Lambda_{W_{LE}}$	Wing leading-edge sweep angle, degrees (See Figure 1)
$\Lambda_{W_{c/2}}$	Wing mid-chord sweep angle, degrees
$\Lambda_{W_{TE}}$	Wing trailing edge sweep angle, degrees
$\Lambda_{T_{LE}}$	Tail leading edge sweep angle, degrees (See Figure 1)
$\Lambda_{T_{c/2}}$	Tail mid-chord sweep angle, degrees
$\Lambda_{T_{TE}}$	Tail trailing edge sweep angle, degrees
$\Lambda_{W_{(t/c)_{max}}}$	Wing maximum thickness sweep angle, degrees
$\Lambda_{T_{(t/c)_{max}}}$	Tail maximum thickness sweep angle, degrees

The coefficients considered here are based on a standard stability axes system with the origin at the vehicle center of gravity and are defined as follows:

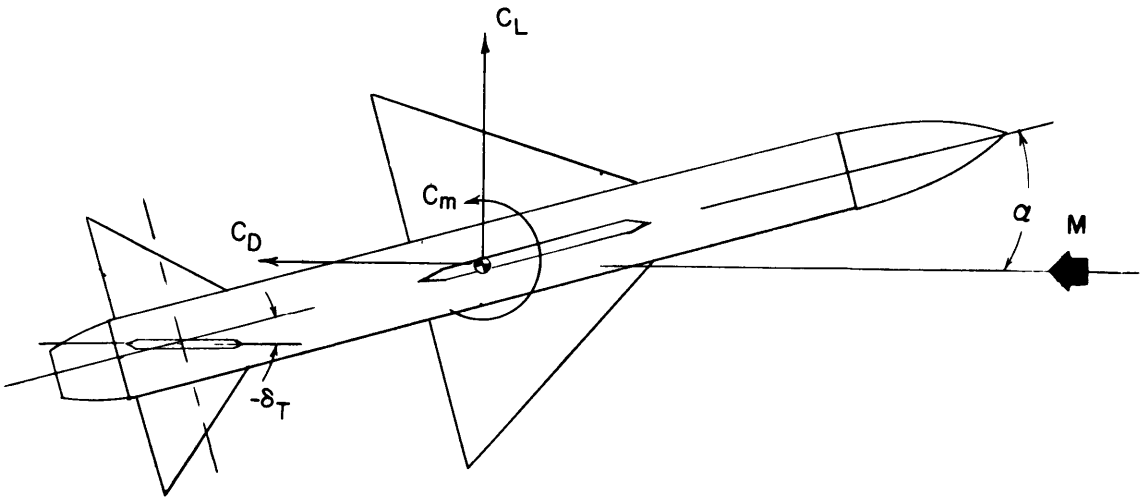

*	C_L	Lift coefficient, $\frac{\text{Lift}}{q\ S_R}$
	C_{L_B}	Total body lift coefficient
	C_{L_W}	Total wing lift coefficient
	C_{L_T}	Coefficient of total tail lift (including downwash lift loss)
	$\left(C_{D_f}\right)_B$	Body friction drag coefficient
	$\left(C_{D_f}\right)_W$	Wing friction drag coefficient
	$\left(C_{D_f}\right)_T$	Tail friction drag coefficient
	C_{D_f}	Total friction drag coefficient
	$\left(C_{D_w}\right)_B$	Body wave-drag coefficient
	$\left(C_{D_w}\right)_W$	Wing wave-drag coefficient
	$\left(C_{D_w}\right)_T$	Tail wave-drag coefficient
	C_{D_o}	Total zero-lift drag (friction drag + wave drag + base drag) coefficient
	C_{D_b}	Base drag coefficient
	C_D	Total drag coefficient, $\frac{\text{Drag}}{q\ S_R}$
	C_{D_i}	Coefficient of induced drag due to lift
*	C_m	Pitching moment coefficient, $\frac{\text{Moment}}{q\ S_R \ell_R}$
	*	See list of subscripts used with this symbol

C_{m_B}	Total pitching moment coefficient due to body lift
C_{m_W}	Total pitching moment coefficient due to wing lift
C_{m_T}	Total pitching moment coefficient due to tail lift
$\left(c_{d_w}\right)_N$	Nose wave-drag coefficient referred to cross-sectional area at nose-body juncture
$\left(c_{d_w}\right)_a$	Boattail wave-drag coefficient referred to cross-sectional area at the body-boattail juncture
$\left(c_{d_N}\right)_1$	Wave-drag coefficient of frustum part of a hemispherically modified nose
$\left(c_{d_N}\right)_2$	Wave drag of the hemispherical part of a hemispherically modified nose
$\left(C_{L_\alpha}\right)_W$	Wing lift-curve slope, per degree
$\left(C_{L_\alpha}\right)_T$	Tail lift-curve slope per degree
$\left(C_{N_\alpha}\right)_B$	Body normal-force curve slope, per radian
C_{f_B}	Body friction coefficient
C_{f_W}	Wing friction coefficient
C_{f_T}	Tail friction coefficient
$\left(c_{d_c}\right)_B$	Body viscous cross-flow constant
$\left(c_{d_c}\right)_W$	Wing viscous cross-flow constant
$\left(c_{d_c}\right)_T$	Tail viscous cross-flow constant

Subscripts

The following subscripts are used with C_L, C_m, X_{cp}, and $\frac{x}{c}$.

B_L	Body, linear
B_V	Body, nonlinear
B_W	Body in presence of wing-linear
W_B	Wing in presence of body-linear
W_V	Wing, nonlinear
B_T	Body in presence of tail-linear
T_B	Tail in presence of body-linear
T_V	Tail, nonlinear
-	Total for the configuration requires no subscript

TABLE OF CONTENTS

TABLE OF CONTENTS

AERODYNAMICS LABORATORY
DAVID TAYLOR MODEL BASIN
WASHINGTON, D. C.

A METHOD FOR PREDICTING THE STATIC AERODYNAMIC CHARACTERISTICS OF LOW-ASPECT-RATIO CONFIGURATIONS

by

Peter T. Eaton

SUMMARY

Equations have been developed which provide the means for rapidly predicting the static aerodynamic characteristics (except rolling moment) of any low-aspect-ratio vehicle at subsonic, transonic, and supersonic speeds for angles of attack and/or tail deflection angles up to stall. These equations are based on existing linear, slender body, and nonlinear cross-flow theories, with some empirical modifications. These equations have been programmed for the IBM 7090 computer in such a manner that the only inputs to the computer program are the specified geometric characteristics of the configuration being studied. Comparisons of theoretical results, obtained using this program, with existing experimental results at Mach numbers between 0.6 and 3.0 at angles of attack up to 20° and tail deflection angles up to 10° indicate acceptable correlation.

INTRODUCTION

The assigned missions of Navy Missiles, and other similar related weapons, are usually such that they require that the vehicle be capable of operating over extremely wide speed and altitude ranges and be capable of performing radical maneuvers. The designs of these vehicles consist of simple bodies of revolution with thin, movable, low-aspect-ratio lifting surfaces.

A study was conducted of the existing theories for the prediction of the static aerodynamic characteristics of low-aspect-ratio configurations and their application to a number of current missile configurations. The study indicated that theories in general tend to be limited in scope, unique in notation, and dependent on extensive, laborious, time-consuming hand calculations. These features, multiplied by the numerous flight conditions that must be considered and the alternate designs that must be investigated if the configuration is to be optimized, make existing procedures highly susceptible to human error, especially if implemented by inexperienced personnel. Similarly, the laborious aspects of these procedures tend to limit the number of conditions studied, and hence unique unfavorable conditions can be overlooked.

Accordingly, an IBM 7090 computer program, whose input consists of only the geometric characteristics of the configuration being considered and whose output consists of the static aerodynamic characteristics (except rolling moment) of the configuration, has been developed to alleviate this situation.

PROCEDURE FOR DETERMINING THEORETICAL CHARACTERISTICS

This theoretical method is applicable to vehicles which consist of: (a) a simple body of revolution which is either parabolic or an ogive or conical nose-cylinder, with or without boattail, and has no significant protuberances, such as inlets, canopies, etc. and (b) wings and tails which are in-line, have exposed aspect ratios of three or less and have thin, simple, symmetrical airfoil sections whose thickness-to-chord ratio is 0.04 or less (see Figure 1).

The linear lift of each component (body, wings, tails), including the lift due to body-lifting surface interaction (carry-over) and the lift loss due to wing-tail interference (downwash) are determined separately by the method shown in Appendix A. Low-aspect-ratio configurations exhibit pronounced nonlinear lift characteristics which are also determined separately. These characteristics are due to strong viscous cross-flow which causes flow separation and free vortices on the upper surfaces of the vehicle. The lift characteristics of a configuration can be determined by hand calculations using Equations [A-1] through [A-25] in Appendix A in conjunction with Figures 2 through 10. These figures indicate the variation with configuration geometry of the parameters on which these equations depend.

The pitching moment contributions of each of the aforementioned component lifts are determined separately by the method shown in Appendix B. The pitching moment characteristics of a configuration can be determined by hand calculations using equations [B-1] through [B-27] in Appendix B in conjunction with Figures 11 through 17. These figures indicate variation with configuration geometry of the parameters on which these equations depend.

The friction drag of each component (body, wings, tails), the wave (or pressure) drag of each component, the body base drag, and the induced drag due to lift (for the entire configuration) are determined separately in Appendix C. The drag characteristics of a configuration can be determined by hand calculations using Equations [C-1] through [C-22] in Appendix C in conjunction with Figures 18 through 25. These figures indicate the variation with configuration geometry of the parameters which affect the drag characteristics.

Equations for each of the curves shown in Figures 2 through 25 were obtained either from the applicable reference cited in the Appendixes or by the method of least squares. These equations and Equations [A-1] through [C-32] from the Appendixes have been programmed for the IBM 7090 computer.

Actually, two computer programs were developed. The first program is designated program UI-28 and is in BELL SYSTEM FORTRAN II language, which, because of computer capacity limitations, was simplified in

some areas and may suffer marginal accuracy for certain extreme conditions. The second program is designated UI-58 and is identical to the first program except that it is in IBSYS SYSTEM, which provides additional capacity and, hence, maximum accuracy for extreme conditions. One additional difference is the ability of the IBSYS program to handle both parabolic and nose-cylinder bodies, whereas the BELL program can only handle nose-cylinders. A technical note, which describes the computer programming characteristics, card preparation procedures, etc. is available and will be provided upon request.

These computer programs are such that the only inputs required are the geometric characteristics of the configuration shown in Table 1. The output of each program consists of the lift, drag, and pitching-moment characteristics of the configuration in coefficient form for the indicated Mach number, angles of attack, and tail deflection. If the configuration is symmetrical, the lift coefficients can be used as side-force coefficients and the pitching-moment coefficients can be used as yawing-moment coefficients. If the configuration is not symmetrical, its geometry in the side view can be used in the program as a separate independent configuration, and the resulting lift and pitching-moment coefficients can be used as side force and yawing moment coefficients of the vehicle.

SPECIAL CONSIDERATIONS

Personnel utilizing this computer program should make note of the following:

a. Computations should not be attempted at a Mach number of one (M=1.00), since this causes the compressibility factor $\left(\beta = \sqrt{M^2-1}\right)$ to go to zero and all equations containing β in the denominator to go to infinity, which stops the computer.

b. If the program is to be applied to a body-wing or body-tail configuration (rather than a body-wing-tail), a fictitious lifting surface must be created to replace the missing lifting surface. This surface can be assigned small dimensions (root, tip and exposed

semispan of 0.1, for instance), which will allow the computer to function while producing zero results for the missing lifting surface.

c. Choice of scale and altitude are arbitrary, but it should be noted that although lift and moment coefficient are independent of these parameters, drag coefficient is not, because of the dependency of friction drag on Reynolds number.

d. Choice of dimensions is also arbitrary (inches, feet, etc.), but must be consistent throughout the input sheet (including Reynolds number per unit length).

THEORETICAL - EXPERIMENTAL CORRELATION

The variation of theoretical lift, drag, and pitching moment characteristics with angle of attack, tail deflection angle, and Mach number obtained using the computer program noted herein is compared with corresponding existing experimental data for a number of missile-type configurations in Figure 26. A study of these comparisons indicates that, in general, satisfactory correlation between theoretical and experimental results can be attained for the specified ranges of applicability. However, these results indicate that for some configurations at high angles of attack and/or tail deflection, small, acceptable errors in the theoretical lift of the tails causes larger, undesirable errors in theoretical pitching moment. This problem exists despite the fact that the center of pressure of this lift is predicted with acceptable accuracy and apparently is due to the fact that the lift error is multiplied by a large moment arm (of the order of four calibers for most missiles) in obtaining the moment. The theoretical lift, and hence pitching moment, at supersonic speeds and high angles of attack is measurably higher than the corresponding experimental results for some configurations, due to the fact that they appear to exhibit little or no nonlinear lift experimentally. These theoretical results include the assumption that the nonlinear lift characteristics which exist at subsonic speeds also exist at supersonic speeds. References 2, 5, 6, and 10 indicate

that the effect of compressibility (due to increasing Mach number) on nonlinear lift is not known and hence this assumption may be invalid for certain configurations, especially those whose lifting surfaces are not highly swept and hence are not designed for optimum supersonic operation.

CONCLUSIONS

The development of a computer program which will produce the static aerodynamic characteristics of low-aspect-ratio vehicles has led to the following conclusions:

1. Equations can be derived for the theoretical prediction of the lift, drag, and pitching moment characteristics at subsonic, transonic, and supersonic speeds and angles of attack and tail deflection up to stall for vehicles with simple bodies of revolution and lifting surfaces with low-aspect-ratio planforms and thin simple symmetrical airfoil sections.

2. These equations, and equations which express the variation with vehicle geometry of the parameters on which they depend, have been programmed for the IBM 7090 computer so that the geometric characteristics of the vehicle are the only inputs required.

3. Theoretical results obtained using this computer program show satisfactory agreement with existing experimental results for a number of missile-type configurations at Mach numbers up to 3.0, angles of attack up to 20°, and tail deflection angles up to 10°.

4. Accurate theoretical prediction of pitching moment due to tail deflection at high deflection angles for some configurations is difficult, since any small error in the prediction of lift is multiplied by such a large moment arm.

5. Accurate prediction of lift at high angles of attack at supersonic speeds is difficult for some configurations, since the behavior of nonlinear lift due to viscous cross flow is not sufficiently well defined for these conditions.

Aerodynamics Laboratory
David Taylor Model Basin
Washington, D. C.
May 1966

APPENDIX A

EQUATIONS FOR DETERMINING LIFT CHARACTERISTICS

1. LINEAR BODY LIFT

SUBSONIC SPEEDS - The linear lift acting on a relatively simple nose-cylinder type body at subsonic speeds and small angles of attack (assuming incompressible flow) can be predicted by potential theory as shown by Munk and given by the relation

$$C_{L_{B_L}} = 2.0 \ (\sin \alpha) \qquad [A\text{-}1]$$

This expression has been modified by Kelly in Reference 1 and Hopkins in Reference 2, by a so-called apparent mass factor $(K_2 - K_1)$, which is shown in Figure 2 as a function of the body length-to-diameter ratio. The expression for subsonic linear body lift referred to some arbitrary reference area, S_R, becomes

$$C_{L_{B_L}} = 0.0349 \ (K_2 - K_1) \ (\alpha) \left(\frac{S_o}{S_R} \right) \qquad [A\text{-}2]$$

Where S_o is the body cross-sectional area at station X_o, which is the station at which the flow ceases to be potential. Station X_o is determined from the expression

$$X_o = \left[0.378 + 0.527 \left(\frac{X_1}{\ell_B} \right) \right] \ell_B \qquad [A\text{-}3]$$

Where ℓ_B is the body total length and X_1 is the forward-most station of maximum negative change in body cross-sectional area. For a body whose shape is parabolic over its entire length, X_1 is the body base; while for parabolic body modified by a conical boattail, it would be the juncture of the parabolic and conical sections. For a nose-cylinder, X_1 is the nose-cylinder juncture and $S_o = S_N$. Experimental results such as those in Reference 3 indicate that linear body lift is

essentially unaffected by increasing Mach number at transonic as well as subsonic speeds up to a Mach number of approximately 1.4 (i.e., $\beta = 1$).

SUPERSONIC SPEEDS - The linear body lift at supersonic speeds ($M > 1.4$, $\beta > 1$) can be predicted by the second-order shock expansion method of Reference 4. The variation of body linear normal-force slope $\left(C_{N_\alpha}\right)_B$ with Mach number and body fineness ratio obtained in Reference 4 has been converted to a more usable form in Figure 4.2.1.1 - 7 of the stability and control handbook (Reference 5), which is reproduced here in Figure 4. Supersonic linear body lift can then be expressed as

$$C_{L_{B_L}} = \left(C_{N_\alpha}\right)_B (\cos \alpha)\ (\alpha) \left(\frac{S_N}{S_R}\right). \qquad [A\text{-}4]$$

2. NONLINEAR BODY LIFT

Similar methods for predicting the nonlinear body lift due to viscous cross flow have been developed by Kelly in Reference 1, by Hopkins in Reference 2, and Allen and Perkins in Reference 6. These methods are essentially the same except the Allen and Perkins' method and Kelly's method assume that the viscous forces act over the entire body, whereas the Hopkins method assumes that they act only on that portion of the body which is aft of the body station X_o, where the flow over the body ceases to be potential (see Equation [A-3]).

Comparisons of theoretical and experimental results for nose-cylinder configurations indicate that Hopkin's method appears to predict values that are too low and the method of Allen and Perkins appears to give values that are slightly high. A compromise was effected by assuming that the viscous cross-flow acts only on the cylindrical portion of the body (S_{B_V}). Therefore, nonlinear body lift can be obtained from the expression

$$C_{L_{B_V}} = \left(c_{d_c}\right)_B (\eta) (\sin^2 \alpha) \left(\frac{S_{B_V}}{S_R}\right) \qquad [A\text{-}5]$$

where the body viscous cross-flow drag coefficient $\left(c_{d_c}\right)_B$ is obtained from Reference 5, Figure 4.2.1.2 -9, which is reproduced here as Figure 5. The effective body planform area assumed to be affected by viscous cross flow as noted above is assumed to be the cylindrical portion of the body; namely,

$$S_{B_V} = d_N \left(\ell_B - \ell_N\right) \qquad [A-6]$$

The term η is a correction constant derived to account for distortions in the flow around the ends of the body, which is required, since this theory was developed for an infinite cylinder and is being applied to a finite body. This parameter is obtained from Figure 3, Reference 2, and is reproduced herein in Figure 1. The nonlinear body lift for a parabolic body can be obtained using equation [A-5] if the body planform area (S_{B_V}) is obtained from Hopkins' expression in Reference 2; that is,

$$S_{B_V} = \left(\frac{d_{x_o} + d_b}{2}\right)\left(\ell_B - X_o\right) \qquad [A-7]$$

Where d_{x_o} and d_b are the diameter at X_o and the base diameter, respectively, and ℓ_B and X_o are the body length and the station where the flow ceases to be potential, respectively (see equation [A-3]).

3. LINEAR WING LIFT

Low-aspect-ratio vehicles of the type considered herein generally have body diameters which are large relative to the spans of the lifting surfaces and hence the effects of body-wing and body-tail interaction or "carryover" is significant. Similarly, low-aspect-ratio lifting surfaces generally have thin, symmetrical simple airfoil sections and hence their lift characteristics are primarily a function of speed, planform shape, and aspect ratio, rather than airfoil section. Hence the linear lift of a wing in the presence of a body is expressed in Reference 7 as

$$C_{L_{W_L}} = \left(K_{W_B} + K_{B_W}\right)\left(C_{L_\alpha}\right)_W (\alpha)\left(\frac{S_W}{S_R}\right) \qquad [A\text{-}8]$$

where the constants K_{W_B} for lift on the wing in the presence of the body and K_{B_W} for lift on the body in the presence of the wing are obtained from Reference 7, Figures 1 and 4a, which are reproduced here in Figure 6. (It is assumed that there is sufficient afterbody behind the wings.) The lift-curve slope of the isolated wing $\left(C_{L_\alpha}\right)_W$ is obtained from Reference 8, Figures 9 and 10, which are reproduced here in Figure 7, by taking the ordinate of these curves $\frac{C_{L_\alpha}}{AR}$ and converting it to lift-curve slope per degree:

$$\left(C_{L_\alpha}\right)_W = \left(\frac{C_{L_\alpha}}{AR_{W_e}}\right)\left(\frac{AR_{W_e}}{57.3}\right) \qquad [A\text{-}9]$$

4. NONLINEAR WING LIFT

Nonlinear lift peculiar to low-aspect-ratio lifting surfaces is the result of viscous cross flow which causes lateral flow separation and the formation of free vortices on the upper surface. This nonlinear lift increases with increasing angle of attack but its magnitude is dependent on flow separation and hence it is difficult to predict accurately. Analysis of this phenomenon by Flax and Lawrence (Reference 9) and Gersten (Reference 10) has provided the general expression for this lift, referred to exposed wing area

$$C_{L_{W_V}} = \left(c_{d_c}\right)_W (\sin^2 \alpha) \qquad [A\text{-}10]$$

This expression is based on incompressible lifting surface theory which assumes a symmetrical, thin, airfoil section. Since low-aspect-ratio vehicles of the type considered herein usually have wing sections of this type, this restriction should not be too limiting. Linear theory and experimental results indicate that flow around slender wings of this type is not seriously affected by increasing Mach number and

hence it can be assumed that this expression for nonlinear lift is not Mach-number dependent. The most accurate values for $\left(c_{d_c}\right)_W$ appear to be those obtained from Figure 12 of Reference 10. However, a study of the values for C_1 shown in the theoretical curves in Figure 12 of Reference 10 and comparison with values of c_{d_c} (called C_1) computed from the experimental data presented in Figures 13 through 16 of Reference 10 and Figures 5, 8, 11, and 14 of Reference 11 indicate that the theoretical curve for delta wings is too low. Hence, a new curve for wings with unswept trailing edges, for low taper ratios (between 0 and 0.5) has been derived. This curve and Gersten's curves for untapered planforms are presented in Figure 8 as functions of planform shape and exposed aspect ratio. Hence, nonlinear wing lift based on an arbitrary reference area can be expressed as:

$$C_{L_{W_V}} = \left(c_{d_c}\right)_W (\sin^2 \alpha) \left(\frac{S_W}{S_R}\right) \qquad [A\text{-}11]$$

5. LINEAR TAIL LIFT

The linear lift of the tails consists of: (a) lift on the tails in the presence of the body due to angle of attack, (b) lift on the body in the presence of the tails due to angle of attack, (c) lift on the tails in the presence of the body due to tail deflection angle, and (d) lift on the body in the presence of the tails due to tail deflection angle. The entire linear tail lift due to angle of attack and tail deflection angle can be obtained from the method presented in Reference 7, which, when referred to an arbitrary reference area, is expressed as

$$C_{L_{T_L}} = (K_{T_B} + K_{B_T}) \left[\left(C_{L_\alpha}\right)_T (\alpha) \left(\frac{S_T}{S_R}\right)\right] + (K'_{T_B} + K'_{B_T}) \left[\left(C_{L_\alpha}\right)_T (\delta_T) \frac{S_T}{S_R}\right] \qquad [A\text{-}12]$$

The tail lift constants K_{T_B} and K'_{T_B} due to α and δ, respectively, are obtained from Reference 7, Figure 1, which is reproduced here in Figure 6a. Two additional curves are obtained from Reference 7, and

are reproduced in Figure 6, which gives the tail lift carryover and the body constants K_{B_T} and K'_{B_T} for

$$\ell_B \geq (\ell_T + c_{r_T} + 2r_T \beta)$$

and

$$(\beta AR_{T_e})(1 + \lambda_T)\left(\frac{1}{\beta \cot \Lambda} + 1\right) \leq 4.0$$

The lift carryover constant K_{B_T} for the condition

$$(\beta AR_{T_e})(1 + \lambda_T)\left(\frac{1}{\beta \cot \Lambda} + 1\right) > 4.0$$

is obtained from Reference 7, Figure 4, which is reproduced here in Figure 6b for the condition of sufficient afterbody; that is,

$$\ell_B \geq \ell_T + c_{r_T} + 2r_T \beta$$

and for the condition of no afterbody at all:

$$\ell_B \leq \ell_T + c_{r_T}$$

A means for determing this constant for the conditions where there is some afterbody but not enough to support all of the carryover is not available in Reference 7, but a method is available in Figure 1 of Report RS-TR-65-4 of the U.S. Army Missile Command at Redstone Arsenal, Alabama, which is as follows:

(a) Values obtained from Figure 6b for sufficient afterbody are defined as K_1, and values obtained for no afterbody are defined as K_2.

(b) For the condition $(\ell_B - \ell_T) \geq 2r_T \beta$,

$$K_{B_T} \text{ or } K'_{B_T} = K_1 \left[\frac{1.0 - (RI)(2r_T\beta - \ell_B + \ell_T + c_{r_T})}{4.0\, c_{r_T}\, r_T}\right]$$

where

$$RI = \left(2r_T\beta - \ell_B + \ell_T + c_{r_T}\right)\left(\frac{1}{\beta}\right) \qquad [A\text{-}13]$$

(c) For the condition $(\ell_B - \ell_T) < 2r_T\,\beta$,

$$K_{B_T} \text{ or } K'_{B_T} = (K_1 - K_2)\left(\frac{A_1}{A_1+A_2}\right) + K_2 \qquad [A\text{-}14]$$

where

$$\frac{A_1}{A_1+A_2} = \frac{\ell_B - \ell_T - c_{r_T}}{2r_T\,\beta - \frac{c_{r_T}}{2}}$$

The term $\frac{A_1}{A_1+A_2}$ is the ratio of body surface available to support lift on the body in the presence of the tails to the body surface required to support such lift. The lift-curve slope $\left(C_{L_\alpha}\right)_T$ is obtained from Reference 8, Figures 9 and 10, which are reproduced in Figure 7, by taking the ordinate of these curves, $\frac{C_{L_\alpha}}{AR}$ per radian, and converting it to lift-curve slope per degree as follows:

$$\left(C_{L_\alpha}\right)_T = \left(\frac{C_{L_\alpha}}{AR_{T_e}}\right)\left(\frac{AR_{T_e}}{57.3}\right) \qquad [A\text{-}15]$$

This method is similar to the method for predicting linear wing lift detailed in Section A-3, except for taking into account the possibility of insufficient afterbody, which is not necessary for the wings. The lift created by deflecting four "X" oriented tails is assumed to be

$$C_L = 2C_L' \cos 45^\circ \approx 1.4\ C_L' \qquad [A\text{-}16]$$

where C_L' is the lift due to δ for two deflected tails in the horizontal plane as determined in equation [A-12].

6. NONLINEAR TAIL LIFT

The nonlinear tail lift due to viscous cross-flow effects can be obtained by the same method used to obtain nonlinear wing lift in Section 4, with provision made for the effect of tail deflection angle in addition to the effect of angle of attack. Hence, tail nonlinear lift, referred to an arbitrary reference area (S_R) is expressed as:

$$C_{L_{T_V}} = \left(c_{d_c}\right)_T (\sin^2\alpha + \sin^2 \delta_T) \left(\frac{S_T}{S_R}\right) \qquad [A\text{-}17]$$

The cross-flow drag constant $\left(c_{d_c}\right)_T$ can be obtained from Figure 8.

7. LIFT LOSS DUE TO WING-TAIL INTERFERENCE

Loss of lift on the tail due to wing-tail interference, or wing "downwash," is obtained from line-vortex theory by the method presented in Reference 7, which assumes a single fully rolled-up vortex at the mid semispan of each wing panel. The lift loss due to downwash, referred to an arbitrary reference area, can be expressed as:

$$C_{L_i} = \frac{\left(C_{L_\alpha}\right)_W \left(C_{L_\alpha}\right)_T \left(\frac{b_T}{2}\right) (57.3)\ (S_W)\ (i) \left(K_{W_B}\right) (\alpha)}{2\pi\ (AR_{T_e})\ (f_W - r_W)\ (S_R)} \qquad [A\text{-}18]$$

The linear lift-curve slopes $\left(C_{L_\alpha}\right)_W$ and $\left(C_{L_\alpha}\right)_T$ can be obtained from Figure 7 by converting the ordinate $\frac{C_{L_\alpha}}{AR}$ to lift curve slope per degree as noted in equations [A-9] and [A-15], namely:

$$\left(C_{L_\alpha}\right)_W = \left(\frac{C_{L_\alpha}}{AR_{W_e}}\right)\left(\frac{AR_{W_e}}{57.3}\right)\left(\frac{S_W}{S_R}\right) \qquad [A\text{-}19]$$

$$\left(C_{L_\alpha}\right)_T = \left(\frac{C_{L_\alpha}}{AR_{T_e}}\right)\left(\frac{AR_{T_e}}{57.3}\right)\left(\frac{S_T}{S_R}\right) \qquad [A\text{-}20]$$

The linear wing lift constant K_{W_B} can be obtained from Figure 6, The wing vortex spanwise location ($f_W - r_W$) is obtained from Reference 7, Figures 5 and 6, which are reproduced in Figure 9, and the expression

$$f_W - r_W = \left(\frac{f_W - r_W}{\frac{b_W}{2}}\right)\left(\frac{b_W}{2}\right) \qquad [A\text{-}21]$$

The critical term in Equation [A-18] is the wing-tail interference constant (i) which is evaluated by a combination of strip theory and slender body theory. This term is obtained from Reference 7, Figure 7, which is reproduced in Figure 10 or from the equations of Appendix B of Reference 7. The ordinates and abscissas of Figure 10 are obtained from the expressions:

$$\left(\frac{h_T}{r_T + \frac{b_T}{2}}\right) = \frac{\left[\left(X_{cp}\right)_{T_B} - X_{W_{T.E.}}\right](\alpha)}{(57.3)\left(\frac{b_T}{2} + r_T\right)} \qquad [A\text{-}22]$$

$$\frac{f_T}{r_T + \frac{b_T}{2}} = \frac{f_W - r_W + r_T}{\frac{b_T}{2} + r_T} \qquad [A\text{-}23]$$

where the location of the center of pressure of the tail linear lift (in the presence of the body)$\left(X_{cp}\right)_{T_B}$ can be obtained from the expression

$$\left(X_{cp}\right)_{T_B} = \left(\frac{x}{c}\right)_{T_B} c_{r_T} + \ell_T \qquad [A\text{-}24]$$

where$\left(\frac{x}{c}\right)_{T_B}$is obtained from Reference 7, Figures 10 and 11, which are reproduced in Figure 11.

8. TOTAL LIFT

The individual lift contributions detailed in this Appendix are summed to obtain the total lift acting on a low-aspect-ratio vehicle at a given angle of attack and tail deflection angle at zero sideslip as follows:

$$C_L = C_{L_B} + C_{L_{B_V}} + C_{L_{W_L}} + C_{L_{W_V}} + C_{L_{T_L}} + C_{L_{T_V}} + C_{L_i} \quad \text{[A-25]}$$

Equation: $\begin{Bmatrix}\text{[A-2]}\\ \text{[A-4]}\end{Bmatrix}$ [A-5] [A-8] [A-11] [A-12] [A-17] [A-18]

APPENDIX B

EQUATIONS FOR DETERMINING PITCHING MOMENT CHARACTERISTICS

1. PITCHING MOMENT DUE TO LINEAR BODY LIFT

The general expression for pitching moment can be stated as

$$C_m = C_L \left(\frac{X_{cg} - X_{cp}}{\ell_R} \right) \qquad [B\text{-}1]$$

The location of the center of pressure of the linear lift of a simple body $(X_{cp})_{B_L}$ can be determined from the general method of Hopkins shown in Reference 2 as follows:

$$X_{cg} - \left(X_{cp}\right)_{B_L} = \int_0^{\ell_N} \frac{dS}{dx} \, (X_{cg} - x) \, dx \qquad [B\text{-}2]$$

The body lift center of pressure is obtained as follows:

a. If the body nose is blunted, extend the nose to a point, e.g.:

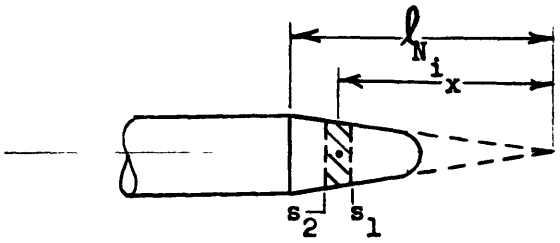

b. Divide the nose into a number of segments of equal length.

c. Compute the difference between the cross-sectional areas at the ends of each segment $(S_2 - S_1)$.

d. Compute the distance from the forward-most point of the extended nose to the midpoint of each segment (x).

e. Multiply (c) by (d) for each segment, sum the results for all segments, and divide by the area at nose-body juncture (S_N).

$$\sum_{o}^{\ell_{N_i}} (S_2 - S_1)\ (x)\ \left(\frac{1}{S_N}\right) = \left(X_{cp}\right)_{B_L} \qquad [B\text{-}3]$$

This equation applies to parabolic bodies of revolution if the summation is made from the nose to station X_o; for example,

$$\left(X_{cp}\right)_{B_L} = \sum_{o}^{X_o} (S_2 - S_1)\ (X)\ \frac{1}{S_o} \qquad [B\text{-}4]$$

The expression for pitching moment due to linear body lift is then

$$C_{m_{B_L}} = C_{L_{B_L}} \left[\frac{X_{cg} - \left(X_{cp}\right)_{B_L}}{\ell_R} \right] \qquad [B\text{-}5]$$

This approach is part of Hopkins' Method of predicting the characteristics of slender bodies detailed in Reference 2 and hence is based on slender body theory, which assumes subsonic incompressible flow. References 2 and 7 indicate that for slender bodies this method will provide accurate results at supersonic speeds. However, a study of experimental data for non-slender bodies made by Douglas using data from Reference 4 resulted in the family of curves presented in Reference 5, Figures 4.2.2.1 to 7, which are reproduced in Figure 12. The data indicate that the Hopkins' Method is not applicable for bodies where $\frac{\ell_B - \ell_N}{\ell_N} < 4$ at supersonic speeds. Hence, for these conditions the linear body lift center of pressure is obtained from

$$\left(X_{cp}\right)_{B_L} = \left(\frac{X_{cp}}{\ell_B} \text{ from Figure 12}\right) \left(\ell_B\right) \qquad [B\text{-}6]$$

and pitching moment due to linear body lift is then obtained from Equation [A-30].

2. PITCHING MOMENT DUE TO NONLINEAR BODY LIFT

The nonlinear body lift for a nose-cylinder was assumed (section A-2) to exist from the nose-body juncture to the aft end of the body.

The center of pressure of this lift is shown in Reference 6 at the body midpoint for a pointed body. Hence, under the assumptions of Section A-2:

$$\left(X_{cp}\right)_{B_V} = \frac{\ell_B - \ell_N + \ell_{N_i}}{2} \qquad [B-7]$$

For a parabolic body of revolution Reference 2 indicates that Equation [25] is applicable if stated as

$$\left(X_{cp}\right)_{B_V} = \frac{X_o + \ell_B}{2} \qquad [B-8]$$

Hence, from the general expression for pitching moment in Equation [B-1] and the expression for nonlinear body lift in Equation [A-5] we obtain the equation for pitching moment due to nonlinear body lift:

$$C_{m_{B_V}} = C_{L_{B_V}} \left[\frac{\left(X_{cg} - X_{cp}\right)_{B_V}}{\ell_R}\right] \qquad [B-9]$$

A study of the information in References 6 and 10 seems to indicate that this center-of-pressure location is not seriously affected by increasing Mach number or angle of attack.

3. PITCHING MOMENT DUE TO LINEAR WING LIFT

Linear wing lift consists of lift on the wing in the presence of the body and lift on the body in the presence of the wing as noted in Section A-3. The center-of-pressure location for each of these two lift contributions is determined separately by the method presented in Reference 7. However, the method of Reference 7 is limited to small angles of attack and does not include the effect of center-of-pressure travel with increasing angle of attack. A method for predicting this center-of-pressure travel with angle of attack for the lift on the wing in the presence of the body is presented in section 4.1.4.3 of Reference 5. Apparently there is no existing method for predicting center-of pressure travel for the lift on the body in the presence of the wing and hence its location is assumed independent of angle of attack.

The distance from the nose of the body to the center of pressure of the lift on the body in the presence of the wing is calculated as follows:

$$\left(X_{cp}\right)_{B_W} = \left(\frac{x}{c}\right)_{B_W} \left(c_r\right)_W + \ell_W \qquad [B\text{-}10]$$

where $\left(\frac{x}{c}\right)_{B_W}$ is obtained from Reference 7, Figures 15 and 16, which are reproduced in Figure 13. The assumption is made that there is sufficient body to support the lift on the body in the presence of the wing at all speeds, as noted in Section A-3, and hence $(X_{cp})_{B_W}$ is not dependent upon body length.

Similarly, the center of pressure of lift on the wing in the presence of the body including the effect of travel with increasing angle of attack is determined by the expression from Reference 5; namely,

$$(X_{cp})_{W_B} = \left[\left(\frac{x}{c}\right)_{W_B} \left(c_{r_W}\right) (\cos \alpha) + \ell_W\right] + \left[\left(\frac{x}{c}\right)_{ref_W} + \Delta\left(\frac{x}{c}\right)_{3_W} + \Delta\left(\frac{x}{c}\right)_{4_W}\right]\left(c_{r_W} \sin \alpha\right) \qquad [B\text{-}11]$$

where $\left(\frac{x}{c}\right)_{W_B}$ is obtained from Reference 7, Figures 10 and 11, which are reproduced in Figure 11. The incremental terms $\Delta\left(\frac{x}{c}\right)_{3_W}$ and $\Delta\left(\frac{x}{c}\right)_{4_W}$ are obtained from Reference 5, Figures 4.1.4.3-12 and 4.1.4.3-13, which are reproduced here in Figures 14 and 15.

The term $\left(\frac{x}{c}\right)_{ref_W}$ is defined in Reference 5 as:

$$\left(\frac{x}{c}\right)_{ref_W} = \left[\frac{0.6 + \Delta\left(\frac{x}{c}\right)_{2_W}}{\sin \alpha_{max}}\right] - \left[\left(\frac{x}{c}\right)_{W_B} \cot \alpha_{max}\right] \qquad [B\text{-}12]$$

where $\Delta\left(\frac{x}{c}\right)_{2_W}$ is obtained from Reference 5, Figure 4.1.4.3-11, which is reproduced in Figure 16 and the angle for maximum lift, α_{max} is obtained from Reference 5, Figure 4.1.3.4-18, which is reproduced in Figure 17.

Hence, the pitching moment due to linear wing lift including terms for the interaction between body and wing and for center of pressure travel with angle of attack is expressed as:

$$C_{m_{W_L}} = \left[K_{W_B}\left(X_{cg} - X_{cp}\right)_{W_B} + K_{B_W}\left(X_{cg} - X_{cp}\right)_{B_W}\right]\left[\left(C_{L_\alpha}\right)_W \left(\frac{\alpha}{\ell_R}\right)\left(\frac{S_W}{S_R}\right)\right] \qquad [B\text{-}13]$$

where K_{W_B}, K_{B_W}, $\left(C_{L_\alpha}\right)_W$ have previously been determined in Equations [A-8] and [A-9].

It is noted in Reference 5 that this method is essentially a subsonic method. However, for thin low-aspect-ratio lifting surfaces, this method probably can be used with fair accuracy at supersonic speeds.

4. PITCHING MOMENT DUE TO NONLINEAR WING LIFT

The center of pressure of the nonlinear wing lift due to viscous cross flow, derived in Section A-4, is assumed to be at the same location as the center of pressure of the linear lift on the wing in the presence of the body determined in Equation [B-11] Section B-3 in accordance with the assumptions in Reference 5, Section 4.1.4.3. A study of Gersten's theoretical data in Reference 10 seems to indicate that this center of pressure should be 10 to 20 percent of the root chord rearward of the linear lift center of pressure, while data in Flax and Lawrence (Reference 9) seem to indicate that this center of pressure is near the wing mid-chord. However, a comparison of theoretical and experimental results for several configurations indicates that the assumption that the centers of pressure of the linear and nonlinear lift are coincident (Reference 5) gives the most accurate results. Hence, the center of pressure of the nonlinear wing lift can be expressed as

$$X_{cp_{W_V}} = \left[\left(\frac{x}{c}\right)_{W_V}\right] c_{r_W} + \ell_W \qquad [B\text{-}14]$$

However,

$$\left(X_{cp}\right)_{W_V} = \left(X_{cp}\right)_{W_B} \qquad [B\text{-}15]$$

where $\left(X_{cp}\right)_{W_B}$ was obtained in Equation [B-11].

Pitching moment due to nonlinear wing lift is then expressed in the form of Equation [B-1] as follows:

$$C_{m_{W_V}} = C_{L_{W_V}} \left[\frac{X_{cg} - \left(X_{cp}\right)_{W_V}}{\ell_R} \right] \qquad [B\text{-}16]$$

where nonlinear wing lift $C_{L_{W_V}}$ is obtained from Section A-4 Equation [A-11].

5. PITCHING MOMENT DUE TO LINEAR TAIL LIFT

Four separate linear tail lift terms were noted in Section A-5; e.g., lift on the tail in the presence of the body and lift on the body in the presence of the tail due to angle of attack and due to tail deflection angle. A pitching moment term is calculated for each lift term making use of the tail lift equation (Equation [A-12]) and the general moment equation (Equation [B-1] as follows:

$$C_{m_{T_L}} = \left\{ K_{T_B} \left[X_{cg} - \left(X_{cp}\right)_{T_B} \right] + K_{B_T} \left[X_{cg} - \left(X_{cp}\right)_{B_T} \right] \right\} \left[\left(C_{L_\alpha}\right)_T (\alpha) \left(\frac{S_T}{S_R}\right) \left(\frac{1}{\ell_R}\right) \right]$$

$$+ \left\{ K'_{T_B} \left[X_{cg} - \left(X_{cp}\right)_{T_B} \right] + K'_{B_T} \left[X_{cg} - \left(X_{cp}\right)_{B_T} \right] \right\} \left[\left(C_{L_\delta}\right)_T \delta_T \left(\frac{S_T}{S_R}\right) \left(\frac{1}{\ell_R}\right) \right] \qquad [B\text{-}17]$$

The terms K_{T_B}, K_{B_T}, K'_{T_B}, K'_{B_T}, $\left(C_{L_\alpha}\right)_T$ and $C_{L_{\delta_T}}$ have already been given in Section A-5. The distance from the body nose to the center of pressure of the lift on the tail in the presence of the body is obtained from an equation similar to Equation [B-11] developed for the wing; e.g.

$$\left(X_{cp}\right)_{T_B} = \left[\left(\frac{x}{c}\right)_T c_{r_T} \cos \alpha + \ell_T \right] + \left[\left(\frac{x}{c}\right)_{ref\ T} + \Delta\left(\frac{x}{c}\right)_{3_T} + \Delta\left(\frac{x}{c}\right)_{4_T} \right] \left(c_{r_T} \sin \alpha \right) \qquad [B\text{-}18]$$

The term $\left(\frac{x}{c}\right)_{T_B}$ is obtained from Figure 11, $\Delta\left(\frac{x}{c}\right)_{3_T}$ and $\Delta\left(\frac{x}{c}\right)_{4_T}$ are obtained from Figures 14 and 15, and the term $\left(\frac{x}{c}\right)_{ref_T}$ is obtained from an equation that corresponds to Equation [B-12] and is expressed as:

$$\left(\frac{x}{c}\right)_{ref_T} = \left[\frac{0.6 + \Delta\left(\frac{x}{c}\right)_{2_T}}{\sin \alpha_{max}}\right] - \left[\left(\frac{x}{c}\right)_{T_B} \cot \alpha_{max}\right] \qquad [B\text{-}19]$$

The term $\Delta\left(\frac{x}{c}\right)_{2_T}$ is obtained from Figure 16 and the term α_{max} is obtained from Figure 17. The distance from the body nose to the center of pressure of the lift on the body in the presence of the tail can be expressed by an equation that corresponds to Equation [B-7] which was developed for the wing in Section A-5; namely,

$$\left(X_{cp}\right)_{B_T} = \left(\frac{x}{c}\right)_{B_T}\left(c_{r_T}\right) + \ell_T \qquad [B\text{-}20]$$

where $\left(\frac{x}{c}\right)_{B_T}$ is obtained from Figure 13.

It would seem that the lack of sufficient afterbody to support the lift on the body in the presence of the tails, due to angle of attack and tail deflection angle, should affect the center of pressure of this lift $\left(X_{cp}\right)_{B_T}$ but this effect is not accounted for in the references noted thus far. This effect is accounted for herein by multiplying the center-of-pressure location $\left(\frac{x}{c}\right)_{B_T}$ by the ratio of available afterbody to required afterbody area, for all supersonic speeds as follows:

(a) For $M > 1.0$; $(\ell_B - \ell_T - c_{r_T}) < (2r_T\beta)$; $(\ell_B - \ell_T \geq 2r_T\beta$ [B-21]

$$\left(X_{cp}\right)_{B_T} = \left(\frac{x}{c}\right)_{B_T}\left(c_{r_T}\right)\left[\frac{(1.0 - (RI)\ (2r_T\beta) - \ell_B + \ell_T + c_{r_T})}{4r_T\ c_{r_T}}\right] + \ell_T$$

(b) For $M > 1.0$; $(\ell_B - \ell_T) < (2r_T\beta)$ [B-22]

$$\left(X_{cp}\right)_{B_T} = \left[\left(\frac{x}{c}\right)_{B_T}\left(c_{r_T}\right)\right]\left[\frac{\left(\ell_B - \ell_T - c_{r_T}\right)c_{r_T}}{c_{r_T}\left(2r_T\beta + c_{r_T}/2 - \ell_B + \ell_T\right)}\right] + \ell_T$$

where the term in the second bracket of each equation is the above-mentioned area ratio, which is defined in Section A-5.

6. PITCHING MOMENT DUE TO NONLINEAR TAIL LIFT

The pitching moment due to nonlinear tail lift can be obtained from an expression of the form of Equations [B-1] and [B-16]; namely,

$$C_{m_{T_V}} = C_{L_{T_V}}\left[\frac{X_{cg} - \left(X_{cp}\right)_{T_V}}{\ell_R}\right] \qquad [B-23]$$

The nonlinear tail lift has already been obtained in Equation [A-17].

The distance from the body nose to the center of pressure of the nonlinear tail lift is obtained by the same method used to obtain the center-of-pressure location for the nonlinear wing lift in Equations [B-14] and [B-15]; for example,

$$\left(X_{cp}\right)_{T_V} = \left(X_{cp}\right)_{T_B} \qquad [B-24]$$

$$= \left(\frac{x}{c}\right)_{T_B}\left(c_{r_T}\right) + \ell_T$$

where $\left(X_{cp}\right)_{T_B}$ was obtained in Equation [B-18].

Calculation of tail hinge moment has not been included in these equations because of the inherent probability of inaccuracy in such calculations. However, if approximate values of tail hinge moment are desired, they can easily be obtained by hand calculations using the expression

$$\text{Hinge-moment} = \left[X_{HL} - \left(\frac{C_{m_T}}{C_{L_T}} \right) \ell_R - X_{cg} \right] \left(C_{L_T} \; q \; S_R \right) \qquad [B\text{-}25]$$

where

X_{HL} distance from nose to hinge line.

X_{cg} distance from nose to center of gravity.

C_{m_T} tail pitching moment coefficient from output, see Equations [B-17], [B-23], [B-26].

C_{L_T} tail lift coefficient from output, see Equations [A-12], [A-17], [A-18].

q free-stream dynamic pressure (see Figure 27) [Note that dimensions must be consistent.]

7. PITCHING MOMENT DUE TO LIFT LOSS OF WING-TAIL INTERFERENCE

Loss of linear tail lift due to wing-tail interference or "downwash" C_{L_i} was obtained in Equation [A-18]. The location of the center of pressure of this linear tail lift loss is assumed to be the same as the location of the linear tail lift in the presence of the body $X_{cp_{T_B}}$, obtained in Equation [B-18]. These terms are applied to the general moment equation (Equation [B-1]) to produce the pitching moment due to downwash lift loss as follows:

$$C_{m_i} = C_{L_i} \left[\frac{X_{cg} - \left(X_{cp} \right)_{T_B}}{\ell_R} \right] \qquad [B\text{-}26]$$

8. TOTAL PITCHING MOMENT

The individual pitching moment contributions discussed in Sections 9 through 15 are summed to provide the total pitching moment coefficient (C_m) of a low-aspect-ratio vehicle at a given angle of attack and tail deflection angle at zero sideslip angle as follows:

$$C_m = C_{m_{B_L}} + C_{m_{B_V}} + C_{m_{W_L}} + C_{m_{W_V}} + C_{m_{T_L}} + C_{m_{T_V}} + C_{m_i} \qquad [B\text{-}27]$$

Equation: [B-5] [B-9] [B-13] [B-16] [B-17] [B-23] [B-26]

APPENDIX C

EQUATIONS FOR DETERMINING DRAG CHARACTERISTICS

1. BODY FRICTION DRAG

The flows around higher-speed, airborne vehicles of the type considered here usually have characteristic turbulent boundary layers; and skin friction coefficients for bodies of revolution $\left(C_{f_B}\right)$ can be obtained from the expression shown by Hoerner in Reference 12, page 2.5:

$$C_{f_B} = \frac{0.044}{[(Re)_B]^{1/6}} \qquad [C\text{-}1]$$

However, this expression appears to be accurate only for subsonic Mach numbers. Body friction coefficient can be obtained more accurately for all Mach numbers up to 2.0 from the curves derived experimentally by Chapman and Kester, which are shown in Figures 15 of Reference 13, and are reproduced in Figure 18. It should be noted that body Reynolds number $(Re)_B$ is equal to body length ℓ_B times Reynolds number per unit length $(Re_{/\ell})$, which, for convenience, is shown in Figure 19 as a function of Mach number and altitude.

Body friction drag coefficient $\left(C_{D_f}\right)_B$ is dependent on Mach number, Reynolds number, body length and body wetted area; and, when referred to some arbitrary reference area S_R, is expressed as:

$$\left(C_{D_f}\right)_B = C_{f_B}\left(\frac{S_{B_{wet}}}{S_R}\right) \qquad [C\text{-}2]$$

2. WING FRICTION DRAG

The flow over a wing surface at the speeds considered here will tend to have a turbulent boundary layer, similar to the flow on the body; but it is more nearly two-dimensional and the local Mach numbers on the surface tend to be lower. Hence the wing friction coefficient tends to be slightly lower than the body friction coefficients for the same free-stream Mach number and Reynolds number. Expressions for wing friction coefficients are presented in Reference 14, page 40, and

Reference 12, page 2.5. Considering these expressions and the effect of Mach number on friction coefficient shown in Figure 18, wing friction coefficient can be expressed:

$$C_{f_W} = \left(\frac{0.455}{\log(Re)_W^{2.58}} \right) - \left(0.0004\ M \right) \qquad [C\text{-}3]$$

Note that wing Reynolds number $(Re)_W$ is equal to Reynolds number per unit length (Re/ℓ) times a representative length; namely, wing mean geometric chord $\bar{c}_W$, which is defined as follows:

$$\bar{c}_W = \left(\frac{c_{r_W}}{2} \right) (1 + \lambda_W) \qquad [C\text{-}4]$$

Wing friction drag coefficient $\left(C_{D_f}\right)_W$ is dependent on Mach number, Reynolds number, wing mean geometric chord, and wing wetted area; and is expressed as:

$$\left(C_{D_f}\right)_W = C_{f_W} \left(\frac{S_{W_{wet}}}{S_R} \right) = C_{f_W} \left(\frac{S_W}{S_R} \right) (2.0)\ (N_W) \qquad [C\text{-}5]$$

3. TAIL FRICTION DRAG

Tail friction drag is obtained by the same method as wing friction drag. Hence tail mean geometric chord is chosen as the representative length and is expressed as

$$\bar{c}_T = \left(\frac{c_{r_T}}{2} \right) (1 + \lambda_T) \qquad [C\text{-}6]$$

Tail Reynolds number is expressed as:

$$(Re)_T = (Re/\ell)\ \bar{c}_T \qquad [C\text{-}7]$$

Tail friction coefficient is obtained from

$$C_{f_T} = \left(\frac{0.455}{\log(Re)_T^{2.58}} \right) - 0.0004\ M \qquad [C\text{-}8]$$

Tail friction drag coefficient, dependent on Mach number, Reynolds number, tail mean geometric chord, and tail wetted area, is expressed as:

$$\left(C_{D_f}\right)_T = C_{f_T}\left(\frac{S_{T_{wet}}}{S_R}\right) = C_{f_T}\left(\frac{S_T}{S_R}\right)(2.0)(N_T) \qquad [C\text{-}9]$$

4. BODY BASE DRAG

Accurate experimental measurement of body base drag has been found to be extremely difficult. Base pressure measured in the wind tunnel is subject to use of fictitious base location, due to sting clearance requirements, and to sting interference. As a result, measured base pressure is usually used only to reference base pressure to free-stream static pressure and correct drag for the suction or thrust created by the model–sting combination. Methods for measuring full-scale in-flight base pressure of low-aspect-ratio vehicles during flame-off are usually unavailable. Base drag of boattail bodies often accounts for no more than approximately 10 to 20 percent of the drag of a body-wing-tail type vehicle, as noted in Reference 5, Section 4.2.3.1. Hence, use of empirical methods to predict base drag may introduce errors which are measurable as a percentage of base drag but they should not be too significant as a percentage of total vehicle drag.

Considering the above, body base drag is obtained by semi-empirical methods noted in Section 4.2.3.1 of Reference 5 and pages 3-19 and 3-20 of Reference 12, which are expressed as follows:

(a) At subsonic speeds ($M < 1$)

$$C_{D_b} = \left[\frac{0.029}{\sqrt{\left(C_{D_f}\right)_B}}\right]\left(\frac{d_b}{d}\right)^3\left(\frac{S_N}{S_R}\right) \qquad [C\text{-}10]$$

where the body friction drag $\left(C_{D_f}\right)_B$ has been obtained in Equation [C-2].

(b) At supersonic speeds ($M > 1$)

$$C_{D_b} = -C_{p_b}\left(\frac{S_b}{S_R}\right) \qquad [C\text{-}11]$$

where base pressure coefficient C_{p_b} is obtained from Reference 5, Figures 4.2.3.1-40 through 4.2.3.1-45, which are reproduced in more usable form for typical boattails and speed ranges considered here ($1 \leq M \leq 3$) in Figure 20.

The effect of tails, when in close proximity to the body base, on base drag can be significant, as noted in Reference 5, Section 4.2.3.1. A method for predicting this effect is proposed in Reference 14, pages 32 through 37, but the method does not appear to have any experimental verification. Considering the lack of a reliable method for predicting tail effect on base drag and the relatively small magnitude of such a drag contribution, no provision is made in these equations for such a term. Comparison of theoretical drag data obtained by this method with experimental wind-tunnel data should account for the fact that such experimental data are often corrected so that base drag is zero to remove sting effects. This correction is made especially when the vehicle is powered and is expected to fly most of its mission under "flame on" conditions, in which there is little or no base drag. Provision for including or not including base drag in the computer computations is available through a control constant in the inputs. It should be noted that base drag should be computed for all vehicles during captive flight.

5. BODY WAVE DRAG

Bodies of revolution moving at speeds near or above a Mach number of one experience a drag force, due to the local disturbance velocities and pressures on the body surface; this is referred to as pressure, or wave drag. This drag consists of a forebody (nose) component and an afterbody (boattail) component (if there is a boattail), both of which are functions of their respective geometries and the free-stream Mach number. The center portion of the body is assumed to be essentially cylindrical and longer than either the nose or boattail and hence there is little or no interference wave drag component. Provision has been made for a parabolic body of revolution (no cylindrical portion), where the wave drag is contained in a single component. These equations provide

the means for predicting the wave drag of pointed or hemispherically blunted, ogive or conical noses and boattails as well as pointed parabolic bodies of revolution. These equations do not apply to very blunt nose and afterbodies; i.e., those whose length-to-diameter ratio is 0.5 or less. This limitation is not considered critical, since practical vehicle designs usually will not have blunt noses of this type because of the disastrous wave drag penalties they impose even at subsonic speeds. These equations also do not provide a detailed method for predicting drag divergence Mach number or wave drag in the transonic "drag rise" region. The assumption is made here that wave drag is small at Mach numbers below 0.95 and increases linearly from zero to its theoretical value at Mach one for Mach numbers between 0.95 and 1.0. This simplification is not considered critical, since a knowledge of the drag in this region is not as critical as a knowledge of the subsonic and supersonic "drag levels." Theoretical prediction of drag in this "drag rise" region is very hazardous and should be determined only by experimental investigation. Hence, body wave drag referred to some arbitrary reference area is theoretically predicted by the expression:

$$\left(C_{D_W}\right)_B = \left[\left(C_{d_W}\right)_N + \left(C_{d_W}\right)_a\right]\left(\frac{S_N}{S_R}\right) \qquad [C\text{-}12]$$

where the wave drag contributions of the forebody $\left(C_{d_W}\right)_N$ and afterbody $\left(C_{d_W}\right)_a$ are obtained as follows:

a.) POINTED CONICAL NOSE

The wave drag of a pointed conical nose $\left(C_{d_W}\right)_N$ is a function of the cone semi-vertex angle (θ_N) (half the included angle) and Mach number, as shown in Figure 3.2 of Reference 14, Figure 4.2.3.1-51 of Reference 5, and on pages 16-18 of Reference 12. The theoretical curves presented in these three references have been correlated, especially at speeds near a Mach number of one and the resulting curves are presented in Figure 21a.

b.) POINTED OGIVE NOSE

The wave drag $\left(C_{d_W}\right)_N$ of a pointed ogive nose is a function of the nose length to diameter ratio $(\ell/d)_N$ and free-stream Mach number, as shown in Figures 16-14 and 16-16 of Reference 12, Figures 11 and 12 of Reference 15, and Figure S.02.03.06 of Reference 16. The theoretical curves presented in these references (primarily Reference 16), have been correlated, especially at speeds near M = 1, and the resulting curves are presented in Figure 21b.

c.) BLUNTED OGIVE AND CONICAL NOSES

A method for determining the wave drag of Blunted Ogive and Conical Noses is presented in Section 4.2.3 of Reference 5. However, comparisons of theoretical and experimental results indicates that this method usually overestimates the wave drag (as also noted in Reference 16, Section S.02.03.01-page 3). Hence, the wave drag for these noses is obtained herein from Figure 21b, which seems to give more accurate results.

d.) PARABOLIC BODIES

The wave drag for a parabolic body is obtained from Figure 4.2.3.1-19 of Reference 5, modified by information in Figures 6 and 7 of Reference 14 and as presented in Figure 22.

e.) AFTERBODIES OR BOATTAILS

The wave drag of a conical or ogive boattail $\left(C_{d_W}\right)_a$ is obtained from Reference 16, Figures S.02.03.04 and S.02.03.05, which are reproduced in Figure 23, using the following expression

$$\left(C_{d_W}\right)_a = \left(C_{d_a}\right)_1 \left(\frac{d_a^2}{4\,\ell_a^2}\right) \qquad [C\text{-}13]$$

Similar curves of the wave drag of boattails is presented in Figures 4.2.3.1-20 and 21 and of Reference 5.

6. WING WAVE DRAG

Wings experience a drag force, at supersonic speeds, which is referred to as wing pressure, or wave drag. This drag force can be

calculated by integration of the theoretical surface pressures by linear theory for thin symmetrical wing sections ($t/c \leq 0.04$) typical of the low-aspect-ratio type wings considered here. Theoretical studies of wing wave drag indicate that it is dependent on free-stream Mach number, and wing aspect ratio, sweep, taper, and maximum thickness-to-chord ratio.

The wing maximum thickness location is assumed to be at the 50 percent chord for wings whose taper ratio is greater than 0.15. Theoretically, there is a small but measurable effect of maximum thickness location on wing wave drag, as noted for taper ratios near zero and one in Reference 19, in Figure 8 of Reference 17, and in Figure 4 of Reference 18; and this effect is accounted for in these equations. However, most low-aspect-ratio lifting surfaces have a constant thickness or almost constant thickness section for most of the chord; and the assumption of maximum thickness at 50 percent of the chord is believed to be acceptable for medium taper ratio wings with this type wing section. Hence the wave drag for thin symmetrical low-aspect-ratio wings according to References 17 through 20 can be expressed as:

$$\left(C_{D_w}\right)_W = K_{w_W} \left(\frac{t}{c}\right)_W^2 \left(\frac{S_W}{S_R}\right) N_W \qquad [C\text{-}14]$$

The wing wave drag parameter (K_{w_W}), for wing taper ratios (λ_W) less than 0.15, is defined as

$$K_{w_W} = \left(C_{d_w}\right)_W \left(\frac{1}{\beta}\right) \qquad [C\text{-}15]$$

Where $\left(C_{d_w}\right)_W$ is the abscissa of Figures 7 and 9 of Reference 19, reproduced here in Figure 24. For wing taper ratios (λ_W) greater than 0.15, this parameter is defined as

$$K_{w_W} = \left(C_{d_w}\right)_W \left(AR_{W_e}\right) \qquad [C\text{-}16]$$

where $\left(C_{d_w}\right)_W$ is the abscissa of Figure 8 of Reference 17, reproduced in a more usable form in Figure 25.

It is assumed that wing wave drag is zero for $M < 0.95$ and that it increases linearly in the range $0.95 \leq M \leq 1$. This assumption is made in order to avoid making a prediction of drag divergence Mach number and wing wave drag in the Transonic "drag rise" region.

7. TAIL WAVE DRAG

The pressure or wave drag experienced by the tails at supersonic speeds is similar to the wing wave drag discussed in the previous Section (6) and can be expressed as:

$$\left(C_{D_w}\right)_T = K_{w_T} \left(\frac{t}{c}\right)_T \left(\frac{S_T}{S_R}\right) N_T \qquad [C\text{-}17]$$

where the tail wave-drag parameter K_{w_T} for tail taper ratios less than 0.15 is defined as

$$K_{w_T} = \left(C_{d_w}\right)_T \left(\frac{1}{\beta}\right) \qquad [C\text{-}18]$$

where $\left(C_{d_w}\right)_T$ is the abscissa of Figure 24. For tail taper ratios greater than 0.15, it is defined as:

$$K_{w_T} = \left(C_{d_w}\right)_T AR_{T_e} \qquad [C\text{-}19]$$

where $\left(C_{d_w}\right)_T$ is the abscissa of Figure 25.

The assumptions discussed in Section C-6 for wing wave drag apply here to tail wave drag; e.g., the tail airfoil is thin ($\frac{t}{c} \leq 0.04$) and symmetrical, the maximum thickness is assumed to be at the 50 percent chord for medium taper ratio tails and tail wave drag is zero for Mach numbers below 0.95 and increases linearly for Mach numbers between 0.95 and 1.0.

8. INDUCED DRAG DUE TO LIFT

The conventional expression for induced drag due to lift (see Reference 11, Chapter 7-1) is:

$$C_{D_i} = \frac{C_L^{\,2}}{(\pi)\ (AR_W)\ \ (e)} \qquad [C\text{-}20]$$

However, this expression was evolved primarily for aircraft which had thick, high-aspect-ratio, cambered wings which provided most of the vehicle's lift. The efficiency factor or Oswald factor (e) for these wings is actually an experimentally determined factor which defines the shape of the drag parabola. For vehicles of the type considered here, the wings do not provide as large a part of the vehicle lift, total aspect ratio of the wings is a relatively meaningless term, and the efficiency factor is not well defined.

The lifting surfaces of this type vehicle generally have little or no leading-edge suction; and flow separation from the body, wing, and tail surfaces is common, especially at moderate to high angle of attack and/or Mach numbers. The induced drag due to lift or due to increasing angle of attack can therefore be more accurately obtained from Equation 8-21 of Reference 21, e.g.,

$$C_{D_i} = C_L \tan \alpha \qquad [C\text{-}21]$$

The induced drag generated by the tails due to tail deflection angle (δ_T) can be expressed by the same equation; and the total induced drag at any combined angle of attack and tail deflection angle can be expressed as

$$C_{D_i} = (C_{L_1} \tan \alpha) + (C_{L_2} \tan \delta_T) \qquad [C\text{-}22]$$

where C_{L_1} is the linear and viscous lift of the body, wing, and tail due to angle of attack (including wing-tail downwash interference lift) and C_{L_2} is the linear and viscous tail lift due to tail deflection angle (see Appendix A).

9. TOTAL DRAG

The individual drag contributions of the body, wings, and tails discussed in Appendix C are summed to provide the total drag coefficient (C_D) of a low-aspect-ratio vehicle as follows: [C-23]

$$C_D = C_{D_{f_B}} + C_{D_{f_w}} + C_{D_{f_T}} + C_{D_b} + C_{D_{w_B}} + C_{D_{w_w}} + C_{D_{w_T}} + C_{D_i}$$

Equation: [C-2] [C-5] [C-9] [C-10] [C-11] [C-12] [C-14] [C-17] [C-22]

REFERENCES

1. Kelly, Howard R. The Estimation of Normal Force and Pitching Moment Coefficients for Blunt-Based Bodies of Revolution at Large Angles of Attack. China Lake, Calif., May 1953. 70 p. incl. illus. (Naval Ordnance Test Station. TM-998)
2. Hopkins, Edward J. A Semiempirical Method for Calculating the Pitching Moment of Bodies of Revolution at Low Mach Numbers. Wash., May 1951. 27 p. incl. illus. (National Advisory Committee for Aeronautics. RM A51C14)
3. McDevitt, John B. and Robert A. Taylor. Force and Pressure Measurements at Transonic Speeds for Several Bodies Having Elliptical Cross Sections. Wash., Sep 1958. 152 p. incl. illus. (National Advisory Committee for Aeronautics. TN 4362)
4. Syvertson, Clarence A. and David H. Dennis. A Second-Order Shock-Expansion Method Applicable to Bodies of Revolution Near Zero Lift. Wash., 1957. 20 p. incl. illus. (National Advisory Committee for Aeronautics. Rpt. 1328. Formerly TN 3527)
5. Douglas Aircraft Co., Inc. USAF Stability and Control DATCOM. Rev. W-P AFB, Jul 1963. 1v. (loose-leaf) (Contract AF33(616)-6460)
6. Allen, Harry Julian and Edward W. Perkins. A Study of Effects of Viscosity on Flow Over Slender Inclined Bodies of Revolution. Wash., 1951. 13 p. incl. illus. (National Advisory Committee for Aeronautics. Rpt. 1048. Formerly TN 2044)
7. Pitts, William C., Jack N. Nielsen and George E. Kaattari. Lift and Center of Pressure of Wing-Body-Tail Combinations at Subsonic, Transonic and Supersonic Speeds. Wash., 1957. 70 p. incl. illus. (National Advisory Committee for Aeronautics. Rpt. 1307)
8. Frantz, Gerald E. Lift Curve Slopes of Low Aspect Ratio Wings at Transonic Speeds. Columbus, Ohio, Jun 1963. 32 l. incl. illus. (North American Aviation, Inc. Applied Mechanics Tech. Note AM-TN-2-63)

9. Flax, A. H. and H. P. Lawrence. The Aerodynamics of Low-Aspect-Ratio Wings and Wing-Body Combinations. Buffalo, Sep 1951. [66] 1. incl. illus. (Cornell Aeronautical Lab., Inc. Rpt. CAL-37) (Also in Proceedings of Third Anglo-American Aeronautical Conference, Brighton, Eng., 4-7 Sep 1951. London, Royal Aeronautical Society, 1952)

10. Gersten, K. Calculation of Non-Linear Aerodynamic Stability Derivatives of Aeroplanes. Paris, 1961 [i.e. 1962] 20 p. incl. illus. (Advisory Group for Aeronautical Research and Development. Rpt. 342) (Deutsche Forschungsanstalt für Luft - und Raumfahrt. Bericht 143)

11. Emerson, Horace F. Wind-Tunnel Investigation of the Effect of Clipping the Tips of Triangular Wings of Different Thickness, Camber and Aspect Ratio; Transonic Bump Method. Wash., Jun 1956. 183 p. incl. illus. (National Advisory Committee for Aeronautics. TN 3671. Formerly RM A53L03)

12. Hoerner, Sighard F. Fluid Dynamic Drag. [2d. ed.] Midland Park, N. J., 1958.

13. Chapman, Dean R. and Robert H. Kester. Turbulent Boundary-Layer and Skin-Friction Measurements in Axial Flow Along Dylinders at Mach Numbers Between 0.5 and 3.6. Wash., Mar 1954. 53 p. incl. illus. (National Advisory Committee for Aeronautics. TN 3097)

14. Luther, Marvin L. and Ralph H. Upson. On the Prediction of the Aerodynamic Drag of Missiles. China Lake, Calif., Nov 1952. 100 p. incl. illus. (Naval Ordnance Test Station. TM-918)

15. Stoney, William E., Jr. Collection of Zero-Lift Drag Data on Bodies of Revolution From Free-Flight Investigations. Wash., 1961. 188 p. incl. illus. (National Aeronautics & Space Administration. Tech. Rpt. R-100. Formerly NACA TN 4201)

16. Royal Aeronautical Society. Data Sheets: Aerodynamics. Vol. 4. London, Dec 1962.

17. Bishop, R. A. and E. G. Cane. Charts of the Theoretical Wave Drag of Wings at Zero Lift. London, H.M.S.O., 1957. 15 p. illus. (Gt. Brit. Aeronautical Research Council. CP313. 18,872) (Gt. Brit. Royal Aircraft Est. TN Aero 2421, Jun 1956)

18. Nielsen, Jack N. Effects of Aspect Ratio and Taper on the Pressure Drag at Supersonic Speeds of Unswept Wings at Zero Lift. Wash., Nov 1947. 22 p. illus. (National Advisory Committee for Aeronautics. TN 1487)

19. Puckett, A. E. and H. J. Stewart. Aerodynamic Performance of Delta Wings at Supersonic Speeds. Journal of Aeronautical Sciences (New York) V. 14, Oct 1947, p. 567-578.

20. Margolis, Kenneth. Effect of Chordwise Location of Maximum Thickness on the Supersonic Wave Drag of Sweptback Wings. Wash., Mar 1948. 30 p. incl. illus. (National Advisory Committee for Aeronautics. TN 1543)

21. Jones, Robert T. and Doris Cohen. High Speed Wing Theory. Princeton, N. J., Princeton Univ. Press, 1960. 243 p. (Princeton Aeronautical Paperback No. 6) (Also in Donovon, Allen F., ed. Aerodynamic Components of Aircraft at High Speeds. Princeton, N. J., Princeton Univ. Press, 1957. p. 3-243)

Table 1
Inputs Required for Low-Aspect-Ratio
Theory Computer Programs
a)Programs UI-28(BELL)and UI-58(IBSYS)

VARIABLE	SYMBOL	PROGRAM NUMBER	INPUT VALUE	REMARKS
Mach No.	M	V-1		Free-Stream
Reynolds No.	Re/ℓ	V-2		per unit length use units chosen
C.G. Location	X_{cg}	V-3		point about which moments taken
Reference Area	S_R	V-4		usually body maximum Cross-sectional Area
Reference Length	ℓ_R	V-5		usually body maximum cross-section diameter
Body Radius at Wings	r_W	V-7		at wing midchord
Wing Semispan	s_W	V-8		including body radius
Wing Tip Chord	c_{t_W}	V-9		
Wing Root Chord	c_{R_W}	V-10		exposed root chord at wing-body junct.
Wing L.E. Sweep Angle	Λ_{le_W}	V-11		in degrees
Wing Midchord Sweep Angle	$\Lambda_{1/2_W}$	V-160		in degrees
Wing T.E. Sweep Angle	Λ_{te_W}	V-162		in degrees
Wing Location	ℓ_W	V-12		location of wing L.E.-body juncture
Body Radius at Tails	r_T	V-23		at tail midchord
Tail Semispan	s_T	V-24		including body radius
Tail Tip Chord	c_{t_T}	V-25		
Tail Root Chord	c_{R_T}	V-26		exposed root chord at tail-body junct.
Tail L.E. Sweep Angle	Λ_{le_T}	V-27		in degrees
Tail Midchord Sweep Angle	$\Lambda_{1/2_T}$	V-228		in degrees
Tail T.E. Sweep Angle	Λ_{te_T}	V-230		in degrees.
Tail Location	ℓ_T	V-28		location of tail L.E.-body juncture

one of these three angles must be set equal to zero

one of these three angles must be set equal to zero

Table 1 (Continued)
a)(Continued)

VARIABLE	SYMBOL	PROGRAM NUMBER	INPUT VALUE	REMARKS
Nose Semi-Vertex Angle	θ_N	V-38		use 90 for ogive Noses
Body Radius at Nose	r_N	V-39		at nose-body juncture
Nose Length	ℓ_N	V-41		
Body Length	ℓ_B	V-42		including nose and boattail
Effective Nose Length	ℓ_{N_i}	V-43		blunt nose extended to a point
Nose Wetted Area Const.	-	V-48		use 2.0 for cone, 2.67 for ogive
Ogive Nose Semivertex	-	V-46		half included angle of tangent to nose
Nose Hemisphere Diam.	d_H	V-87		use zero for pointed noses
Nose Length Less Hemis.	ℓ_{N_M}	V-88		V-41 minus half of V-87
Angles of Attack	α	V-94		in degrees, positive angles only
Angles of Tail Deflection	δ_T	V-96		in degrees, one pair of tails only
Boattail Length	ℓ_a	V-102		conical or ogive
Number of Pairs of Wings	N_W	V-136		monowing=1.0 cruciform=2.0
Number of Pairs of Tails	N_T	V-141		" " "
Base Diameter	d_b	V-147		at aft end of body
Base Drag Control Const.	-	V-149		1.0 if base drag is desired-zero if not
Tail Thickness to Chord Ratio	$(t/c)_T$	V-150		at max. thickness of MGC
Wing Thickness to Chord Ratio	$(t/c)_W$	V-159		" " " "
Boattail Semi vertex Angle	θ_a	V-152		use 90 for ogive; zero if no boattail

Table 1 (Continued)
a) (Concluded)

VARIABLE	SYMBOL	PROGRAM NUMBER	INPUT VALUE	REMARKS
Sweep of Wing Max. Thick.	$\Lambda_{W(t/c)_{max}}$	V-161		
Sweep of Tail Max. Thick	$\Lambda_{T(t/c)_{max}}$	V-229		
Wing Max. Thick.Location	-	V-164		max. thickness location-fraction of MGC-0.5 for flat plates
Tail Maximum Thick.Location	-	V-232		
Nose Section Diameter	d_1	V-305		diameters at the aft end of each of five equal-length segments of the nose-see Appendix (B),page 17
" " "	d_2	V-306		
" " "	d_3	V-307		
" " " "	d_4	V-308		
" " " "	d_5	V-309		
Body Wave Drag Control Const.	-	V-310		use 1.0 if body is parabolic-all other bodies use zero

a) All angles must be in degrees

b) Lengths and areas may be in any dimensions desired but they must be consistent throughout the program

c) Any scale may be chosen but must be consistent throughout the program and the same scale as the vehicle for which correlative experimental data exists

d) Length in Reynolds Number term must be consistent with other length dimensions

Table 1 (Continued)

b) Program UI-58 (IBSYS) only

VARIABLE	SYMBOL	PROGRAM NUMBER	INPUT VALUE	REMARKS
Body Section Diameter	d_1	V-326		body diameters at the aft end of each of 20 equal-length segments of the body between the foremost point on the body and the station where the flow cease to be potential (X_o) where: $X_o = \left[0.378 + (0.527)\frac{V\text{-}346}{V\text{-}42}\right](V\text{-}42)$ These values are required for parabolic bodies of revolution only input values of zero may be used for nose-cylinder type bodies for further details see Appendix (B)
" "	d_2	V-327		
" "	d_3	V-328		
" "	d_4	V-329		
" "	d_5	V-330		
" "	d_6	V-331		
" "	d_7	V-332		
" "	d_8	V-333		
" "	d_9	V-334		
" "	d_{10}	V-335		
" "	d_{11}	V-336		
" "	d_{12}	V-337		
" "	d_{13}	V-338		
" "	d_{14}	V-339		
" "	d_{15}	V-340		
" "	d_{16}	V-341		
" "	d_{17}	V-342		
" "	d_{18}	V-343		
" "	d_{19}	V-344		
" "	d_{20}	V-345		

Table 1 (Concluded)

b)(Concluded)

VARIABLE	SYMBOL	PROGRAM NUMBER	INPUT VALUE	REMARKS
Maximum Slope Body Station	X_1	V-346		body station where negative rate of change of body cross-sectional area is maximum-required for parabolic bodies only-zero for other type bodies
Body Diameter at Station(Xo)	d_{x_o}	V-348		see definition of of Xo above
Tail Roll Orientation Constant	-	V-96a		use 1.0 for (+) oriented tails and 1.4 for (X) oriented tails(cruciform)

a) the BELL program,UI-28,should be used for configurations which have nose-cylinder type bodies at Mach numbers below 2.0. This program requires only the inputs specified in part (a) of this table,pages 38 thru 40.

b) the IBSYS program,UI-58, can be used for all configurations,including those with parabolic bodies of revolution at Mach numbers up to 3.0. This program requires all the inputs specified in this table, pages 38 thru 42,although zero values may be used for inputs V-326 thru V-348 for configurations having nose-cylinder type bodies.

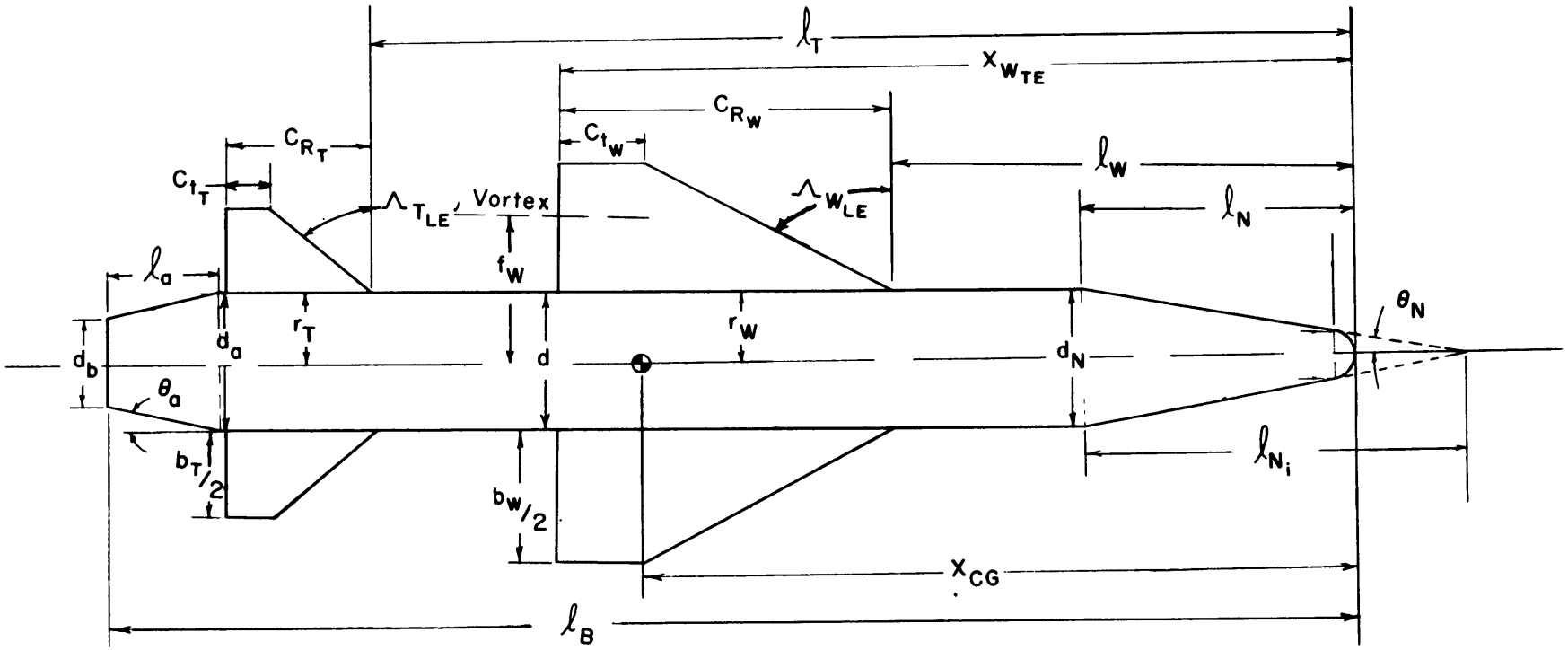

Figure I - Geometric Parameter Identification

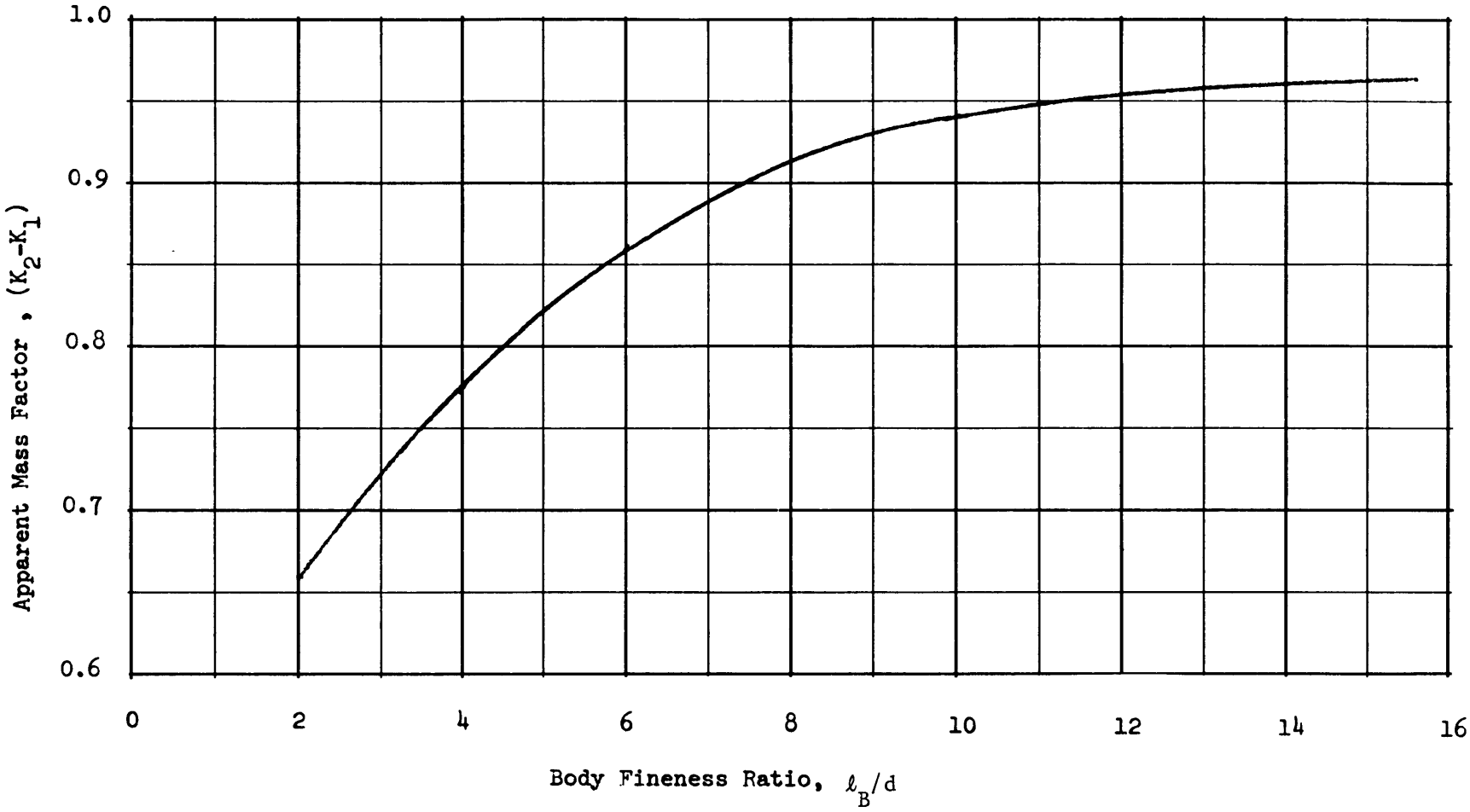

Figure 2 - Variation of Apparent Mass Factor With Body Fineness Ratio

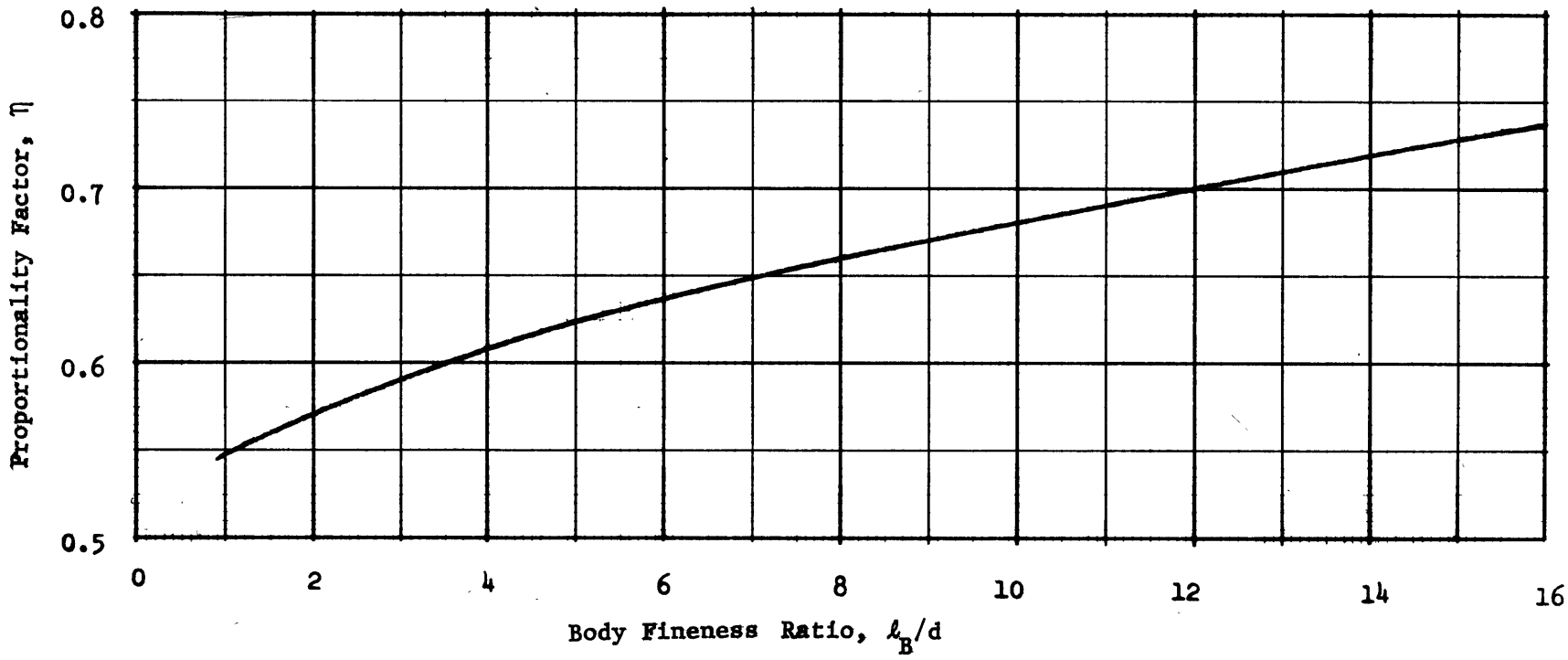

Figure 3 - Proportionality Factor To Account for Body Having a Finite Length

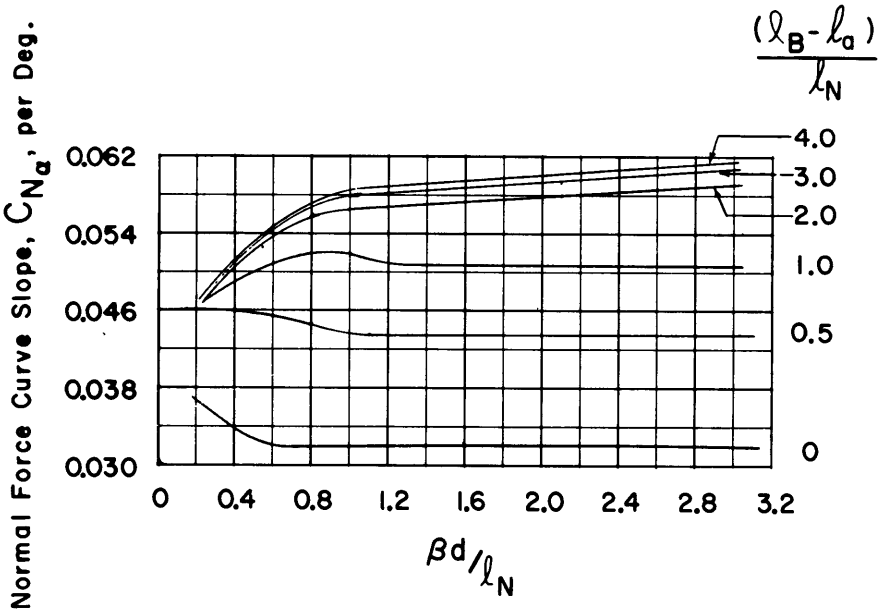

a) Conical Noses

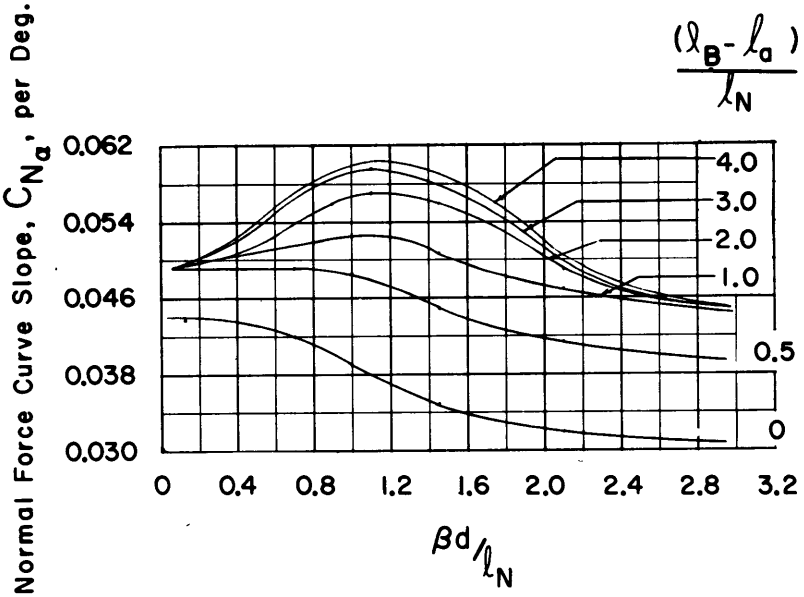

b) Ogive Noses

Figure 4 - Linear Body Normal Force at Supersonic Speeds

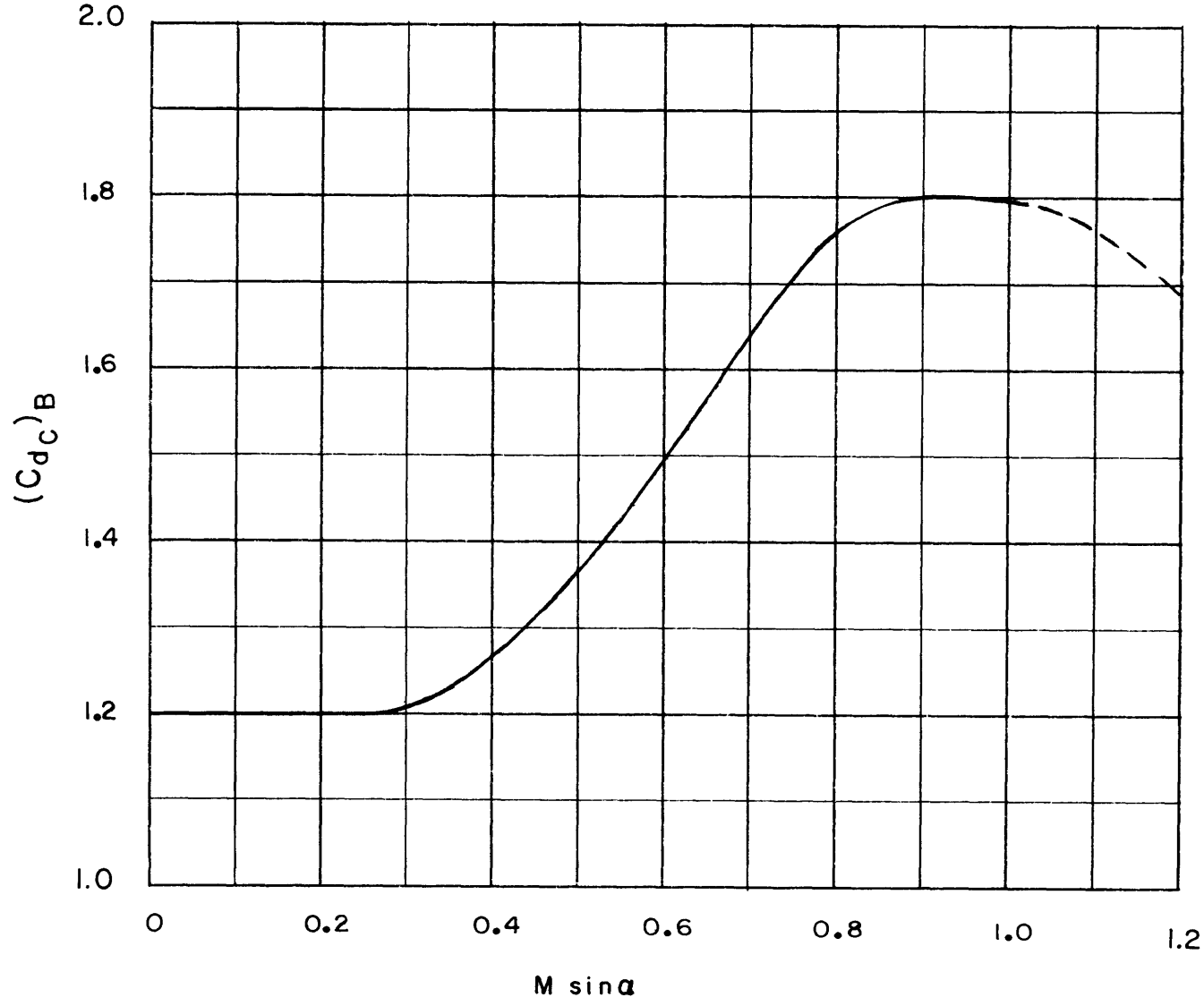

Figure 5 - Variation of Body Non-Linear Lift Constant with Crossflow Mach Number

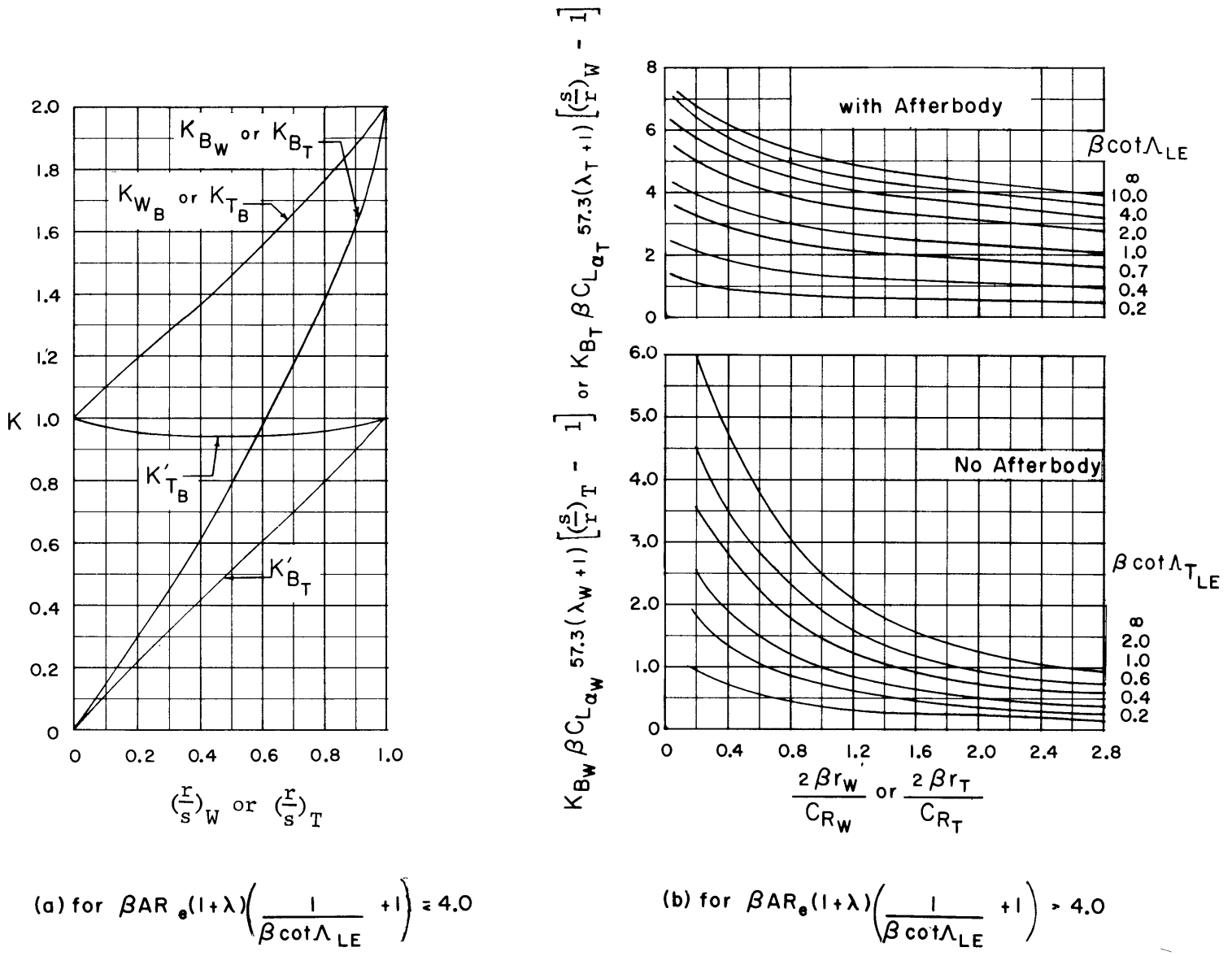

Figure 6 - Wing-Body and Tail-Body Lift Carryover Constants

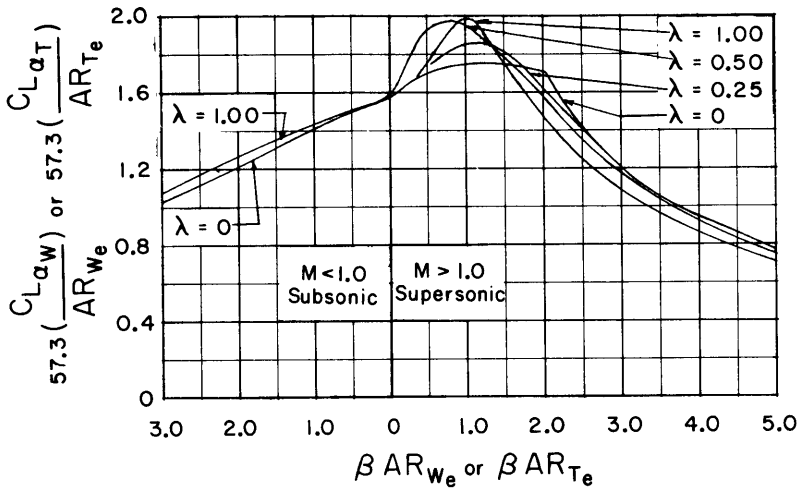

(a) Lifting Surfaces with Unswept Mid-Chords

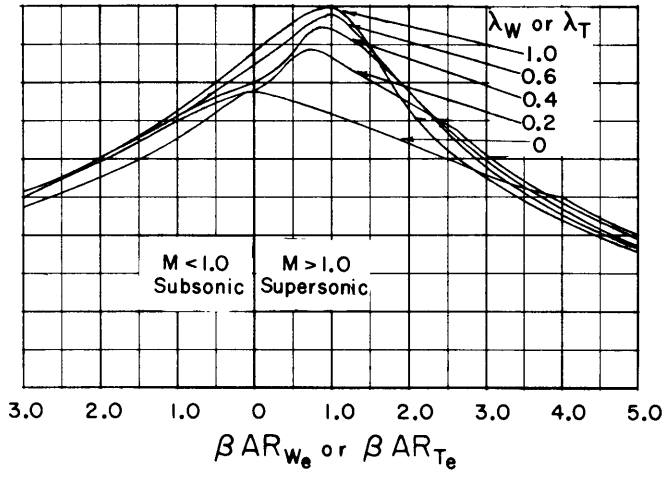

(b) Lifting Surface with Unswept Trailing Edges

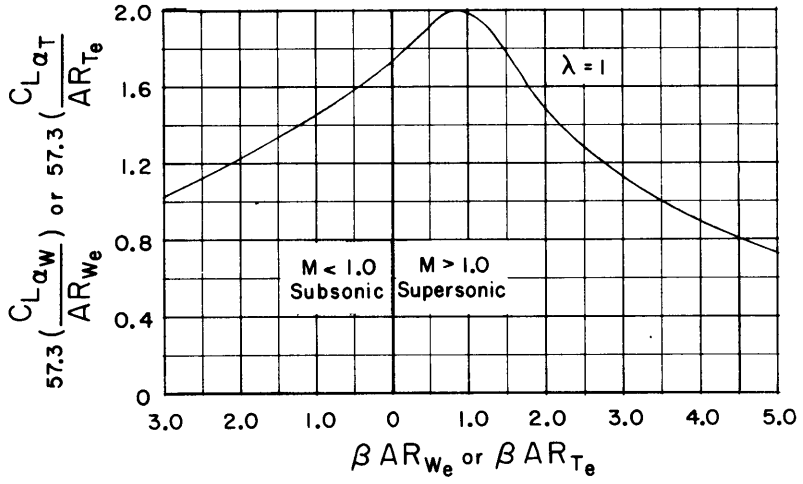

(c) Lifting Surfaces with Unswept Leading Edges

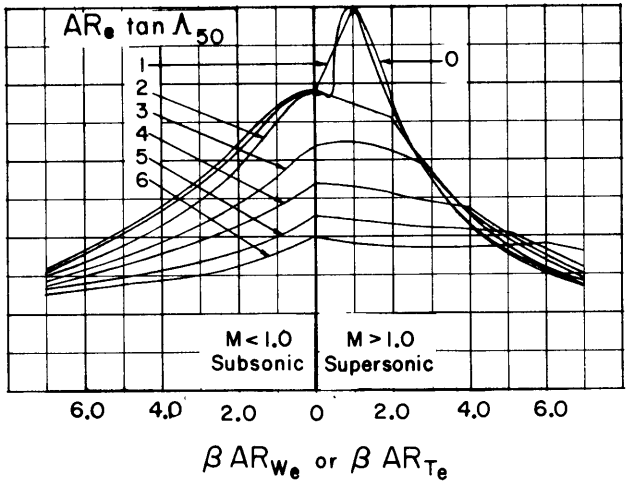

(d) Lifting Surfaces with Swept Leading and Trailing Edges

Figure 7 - Lift Curve Slopes of Low Aspect Ratio Wings or Tails

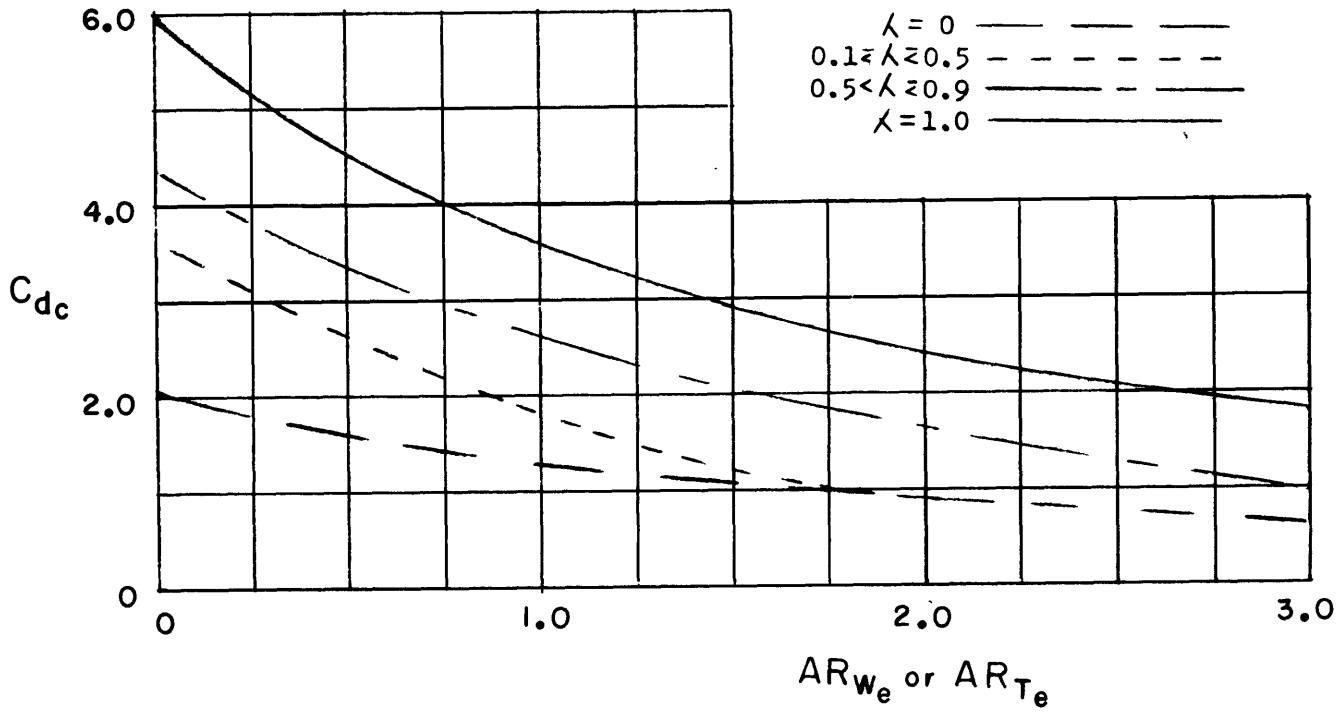

Figure 8 - Cross-Flow Constant for Nonlinear Lift on Wings and Tails

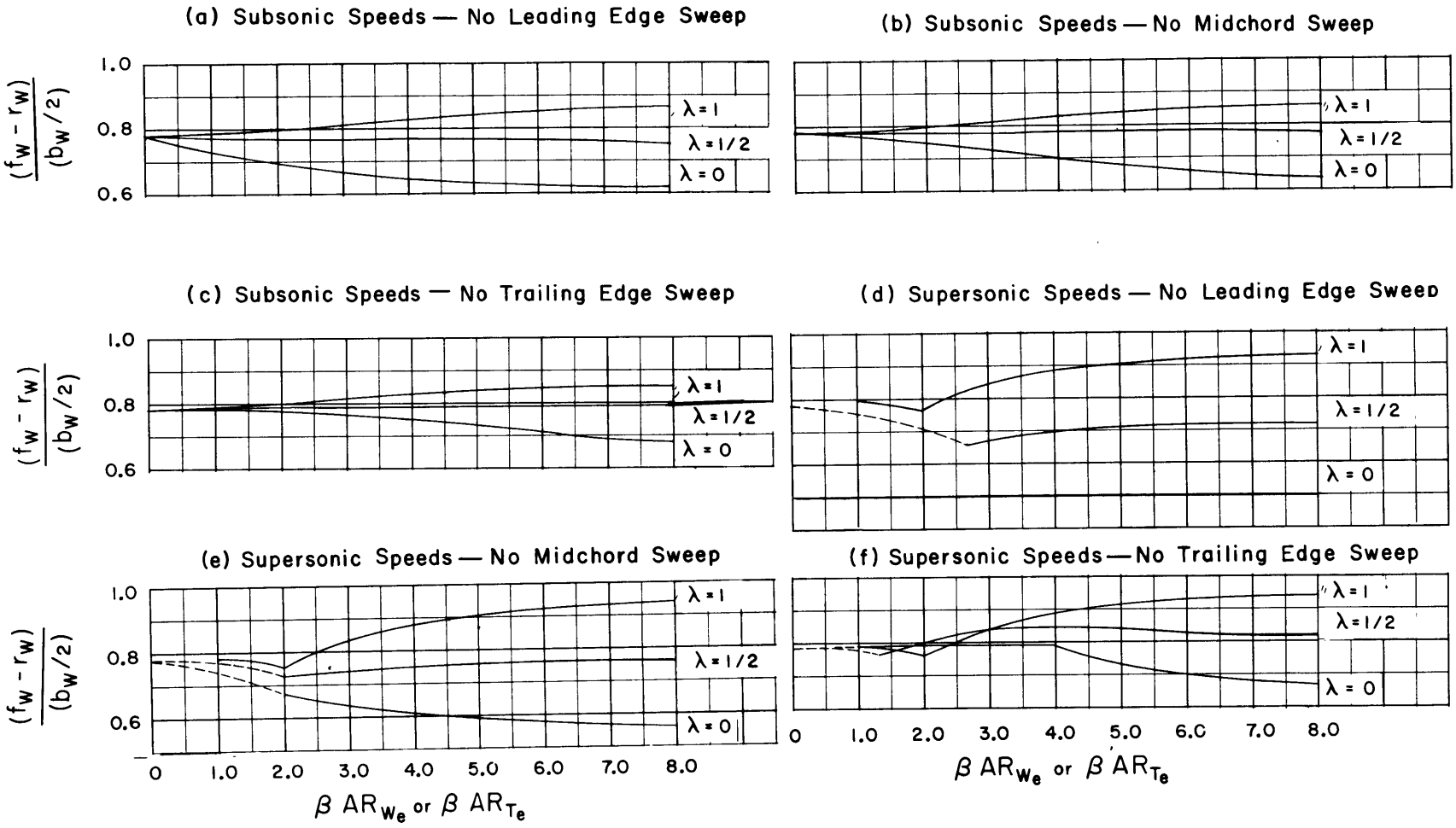

Figure 9 - Lateral Location of the Wing Vortex

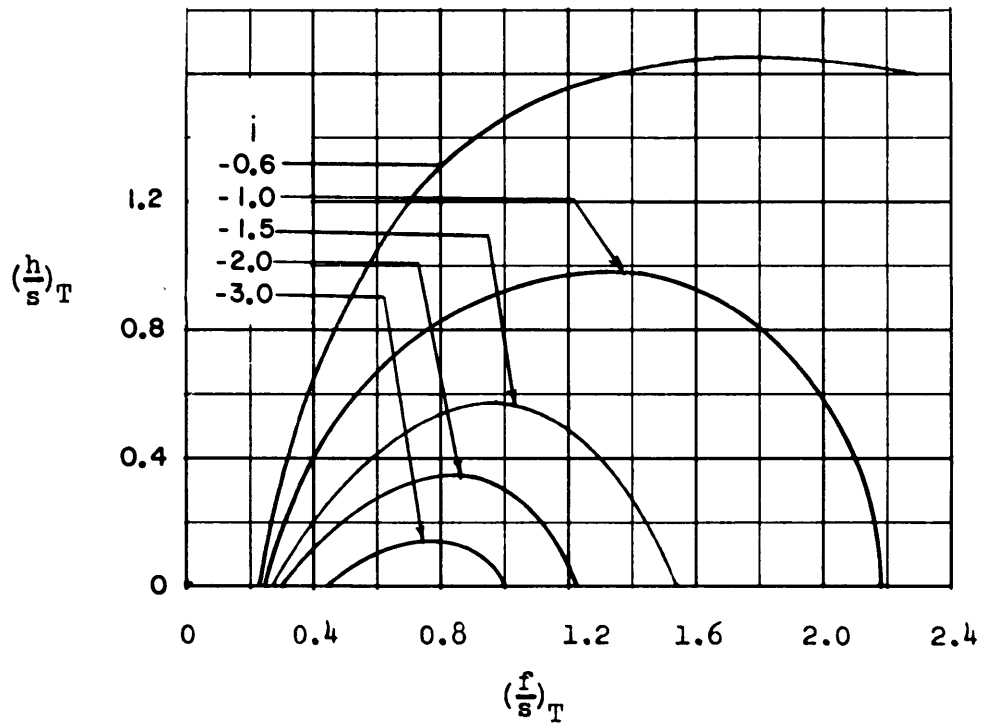

a) Λ_T=0 ; $(\frac{r}{s})_T$= 0 to 0.3

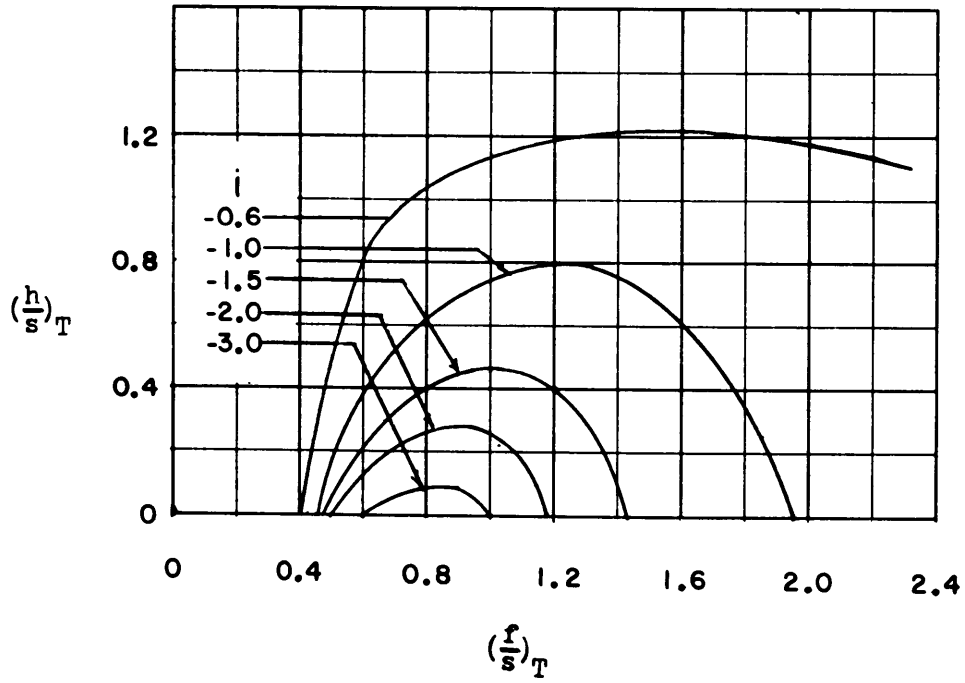

b) Λ_T=0 ; $(\frac{r}{s})_T$ = 0.3 to 0.5

Figure 10 - Charts for Determining the Wing-Tail Interference Constant (i)

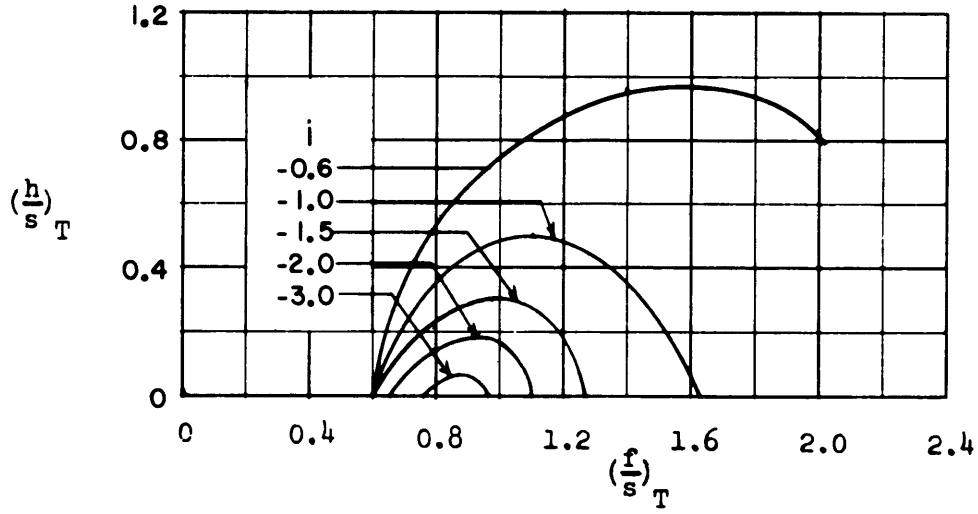

c) $\lambda_T = 0$; $(\frac{r}{s})_T$ = 0.5 to 1.0

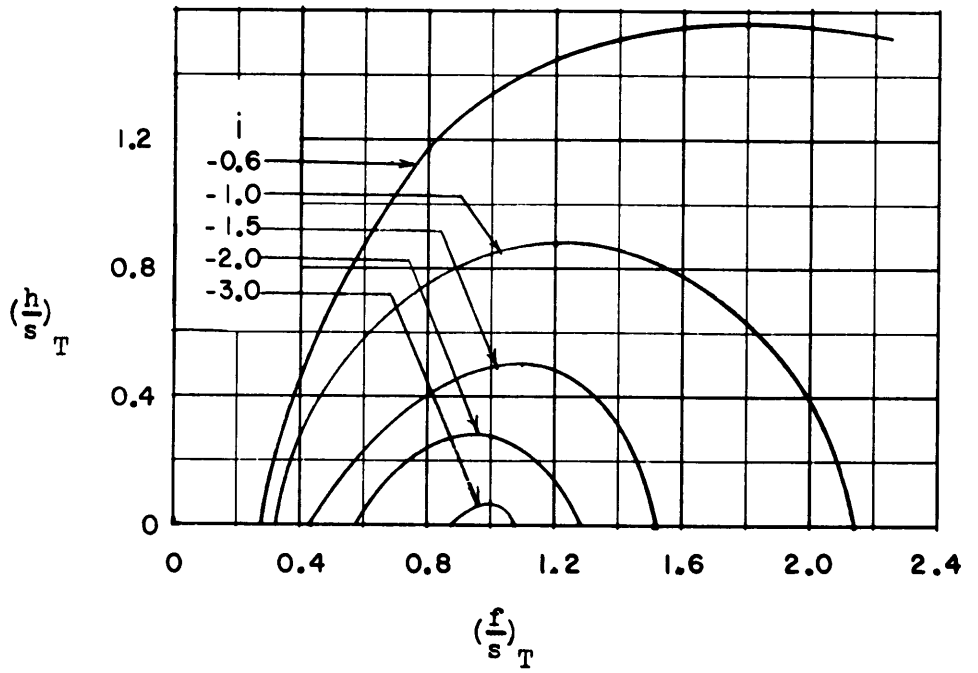

d) $\lambda_T = 0.5$; $(\frac{r}{s})_T$ = 0 to 0.3

Figure 10 (Continued)

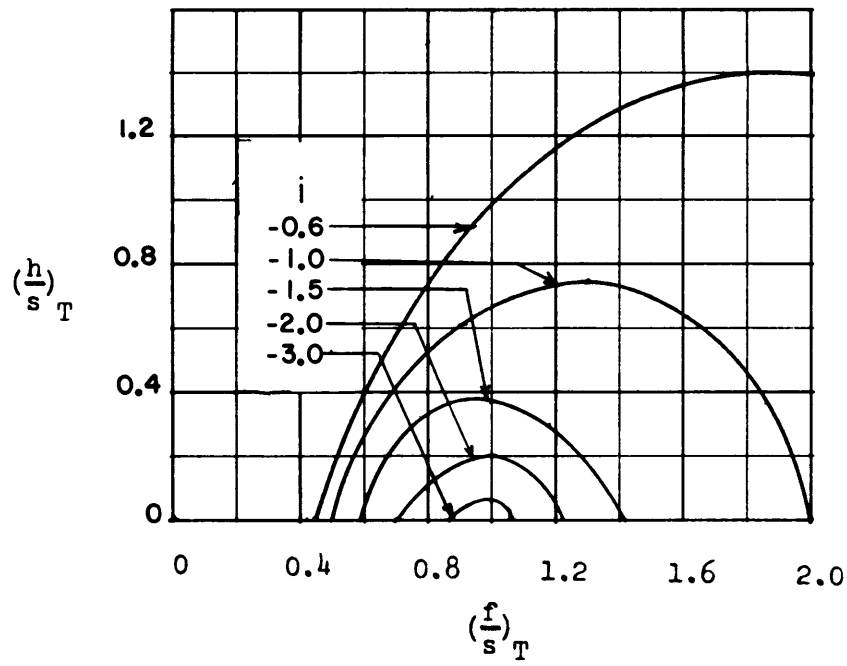

e) λ_T=0.5 ; $(\frac{r}{s})_T$ = 0.3 0.5

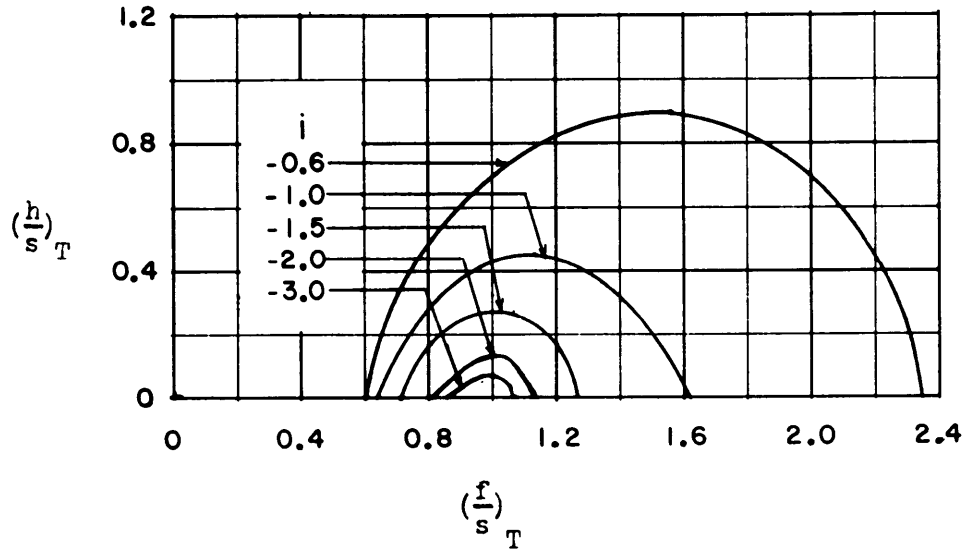

f) λ_T=0.5 ; $(\frac{r}{s})_T$ = 0.5 to 1.0

Figure 10 (Continued)

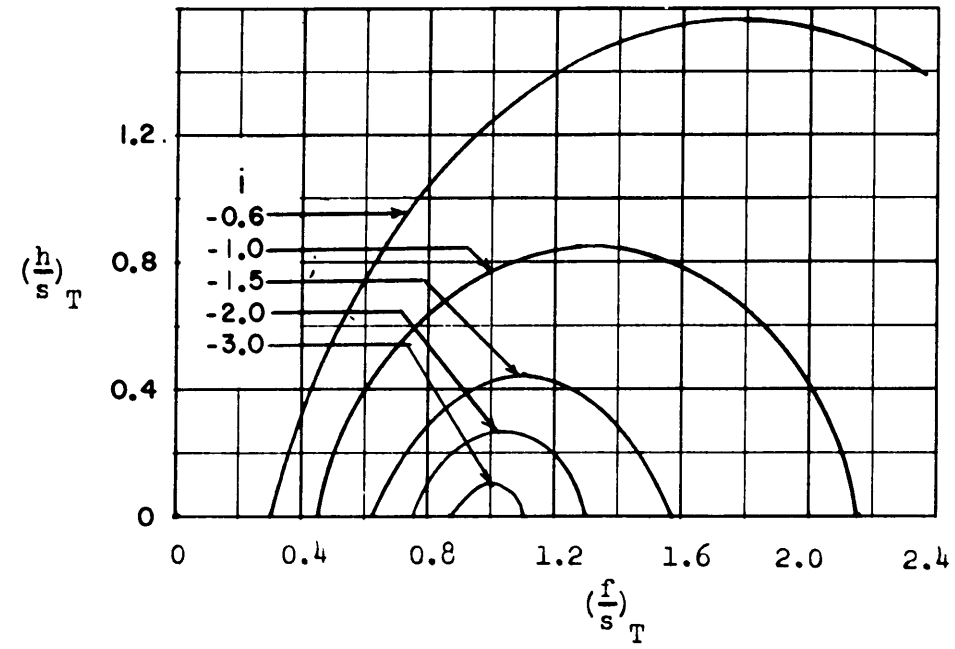

g) λ_T= 1.0 ; $(\frac{r}{s})_T$=0 to 0.1

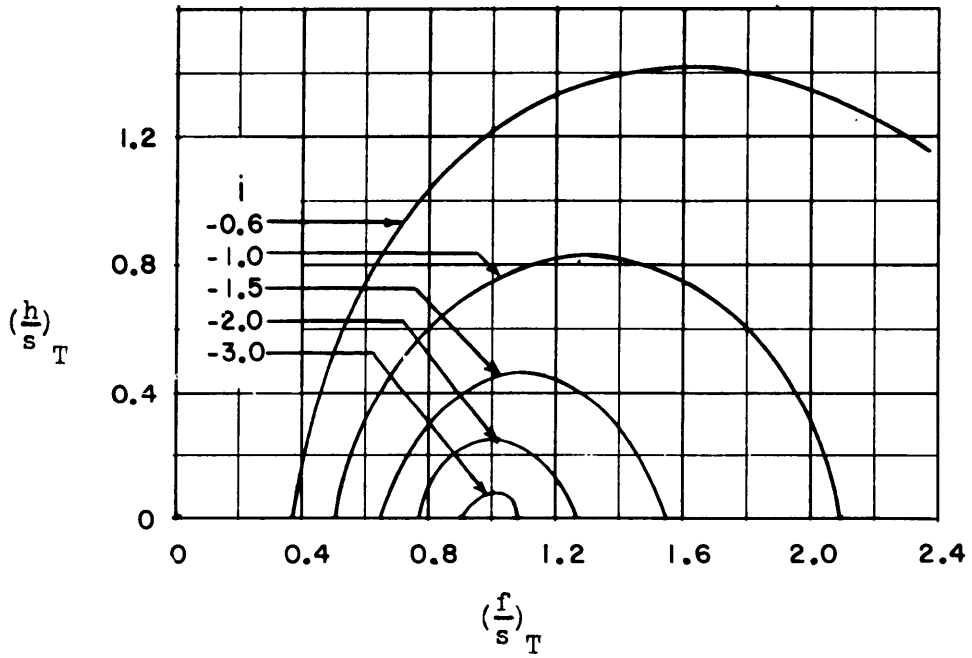

h) λ_T = 1.0 ; $(\frac{r}{s})_T$= 0.1 to 0.3

Figure 10 (Continued)

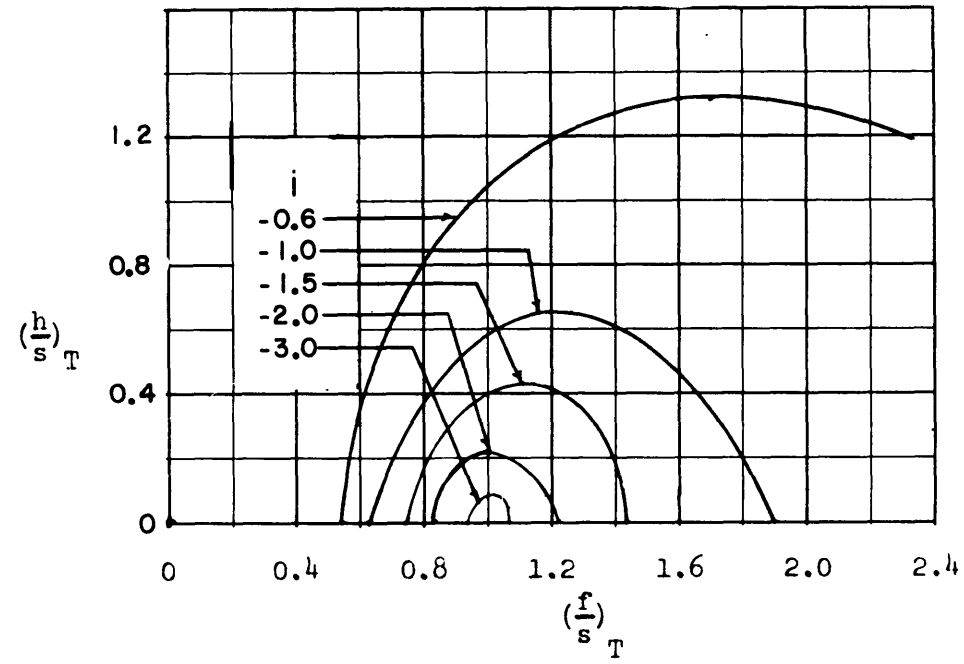

i) $\lambda_T = 1.0$; $(\frac{r}{s})_T = 0.3$ to 0.5

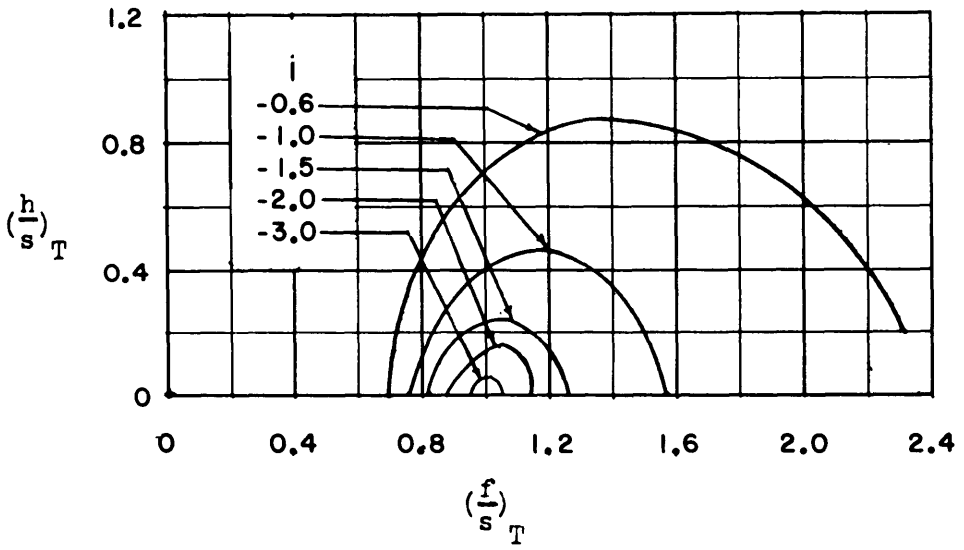

j) $\lambda_T = 1.0$; $(\frac{r}{s})_T = 0.5$ to 1.0

Figure 10 (Concluded)

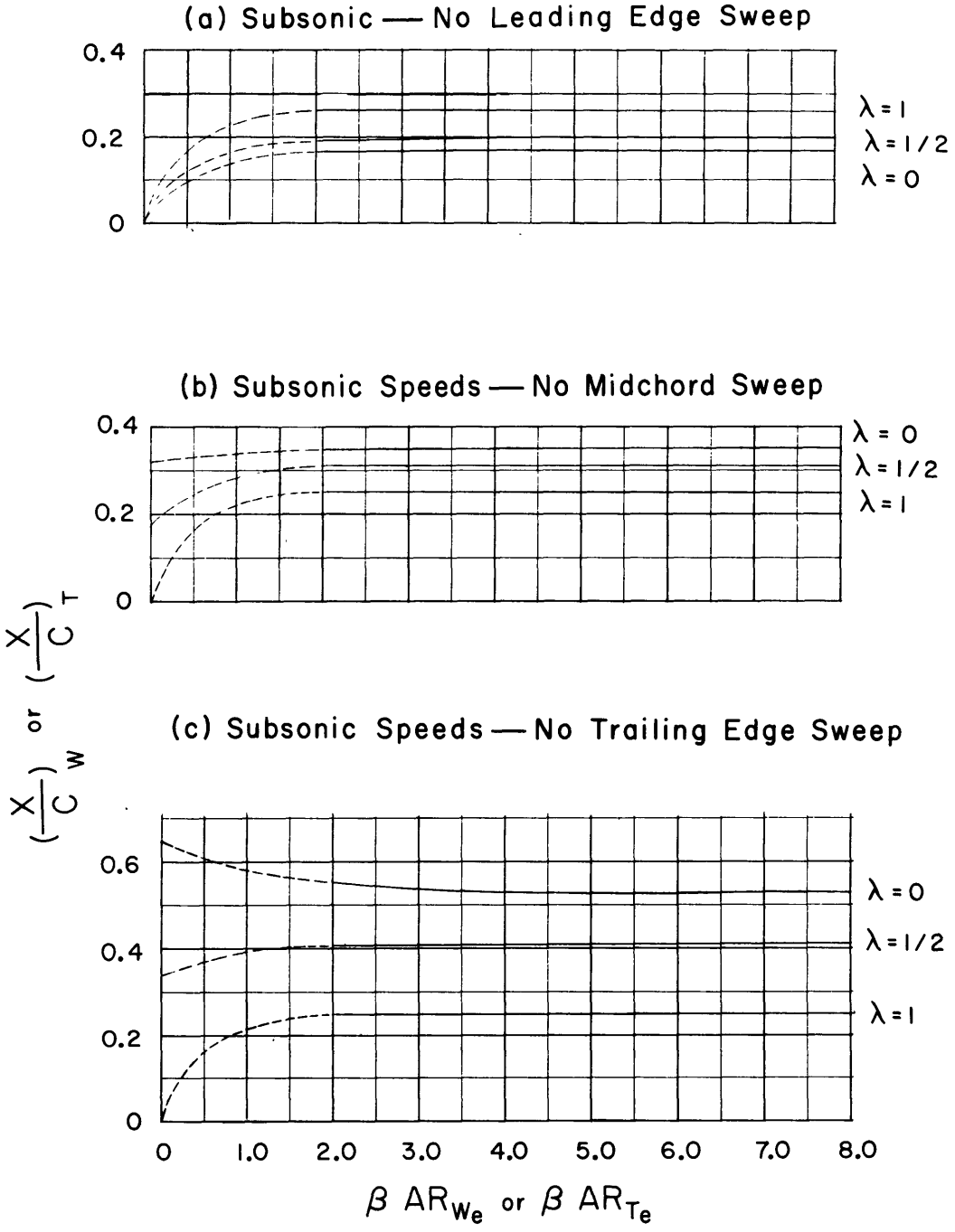

Figure 11 - Wing or Tail Center-of-Pressure Location as a Fraction of Exposed Root Chord

(d) Supersonic Speeds — No Leading Edge Sweep

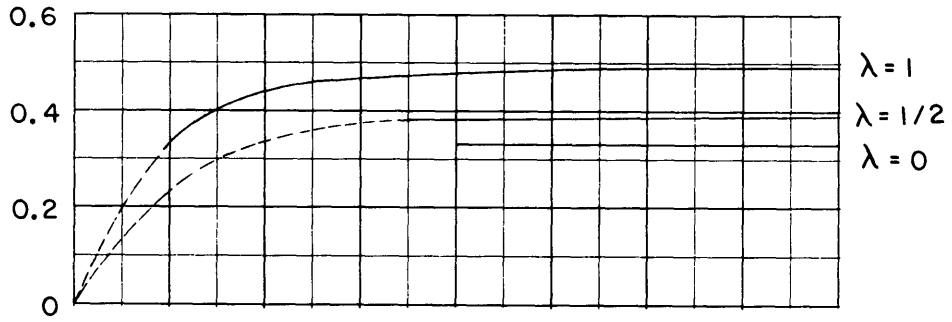

(e) Supersonic Speeds — No Midchord Sweep

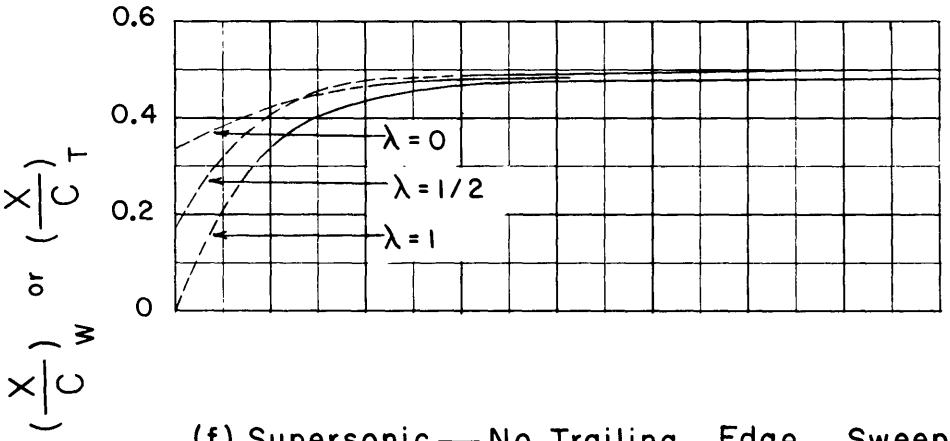

(f) Supersonic — No Trailing Edge Sweep

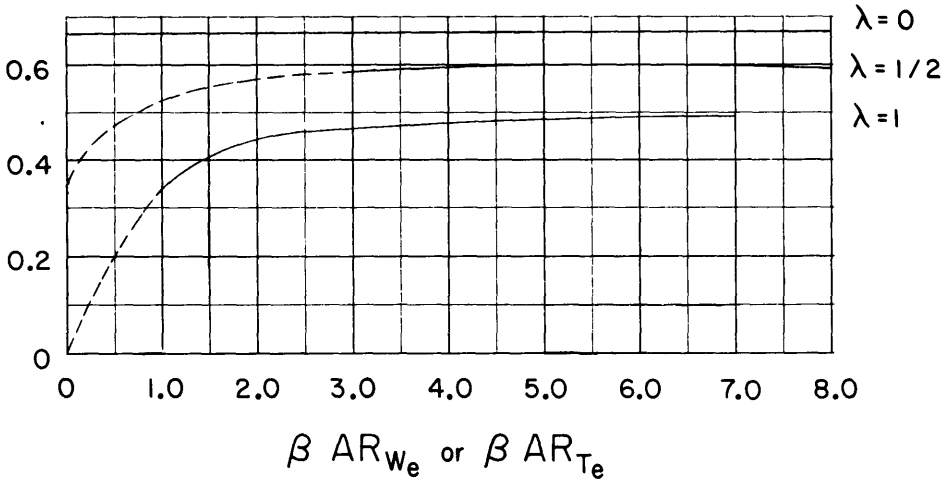

Figure 11 (Concluded)

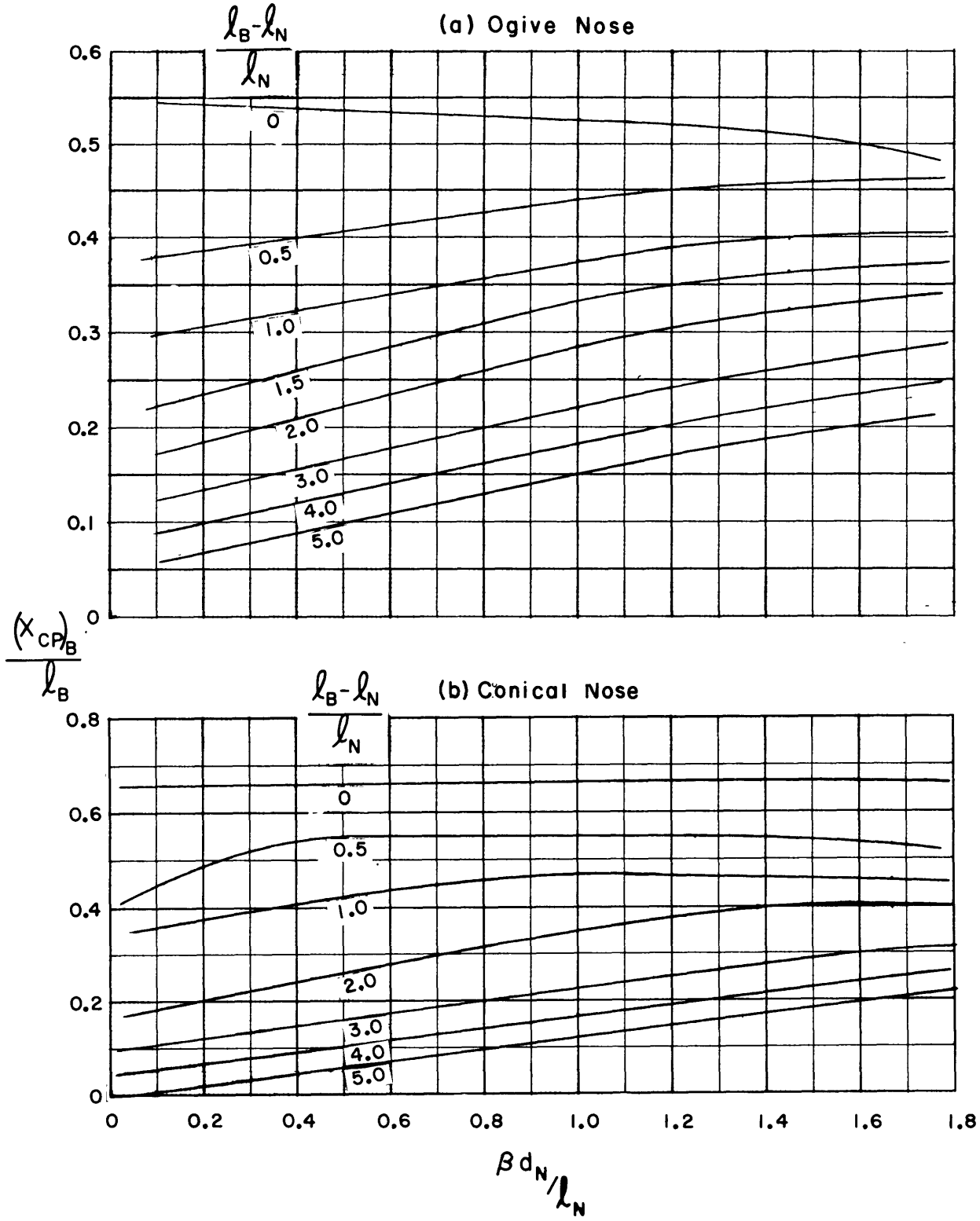

Figure 12 - Location of Center of Pressure of Linear Body Lift at Supersonic Speeds

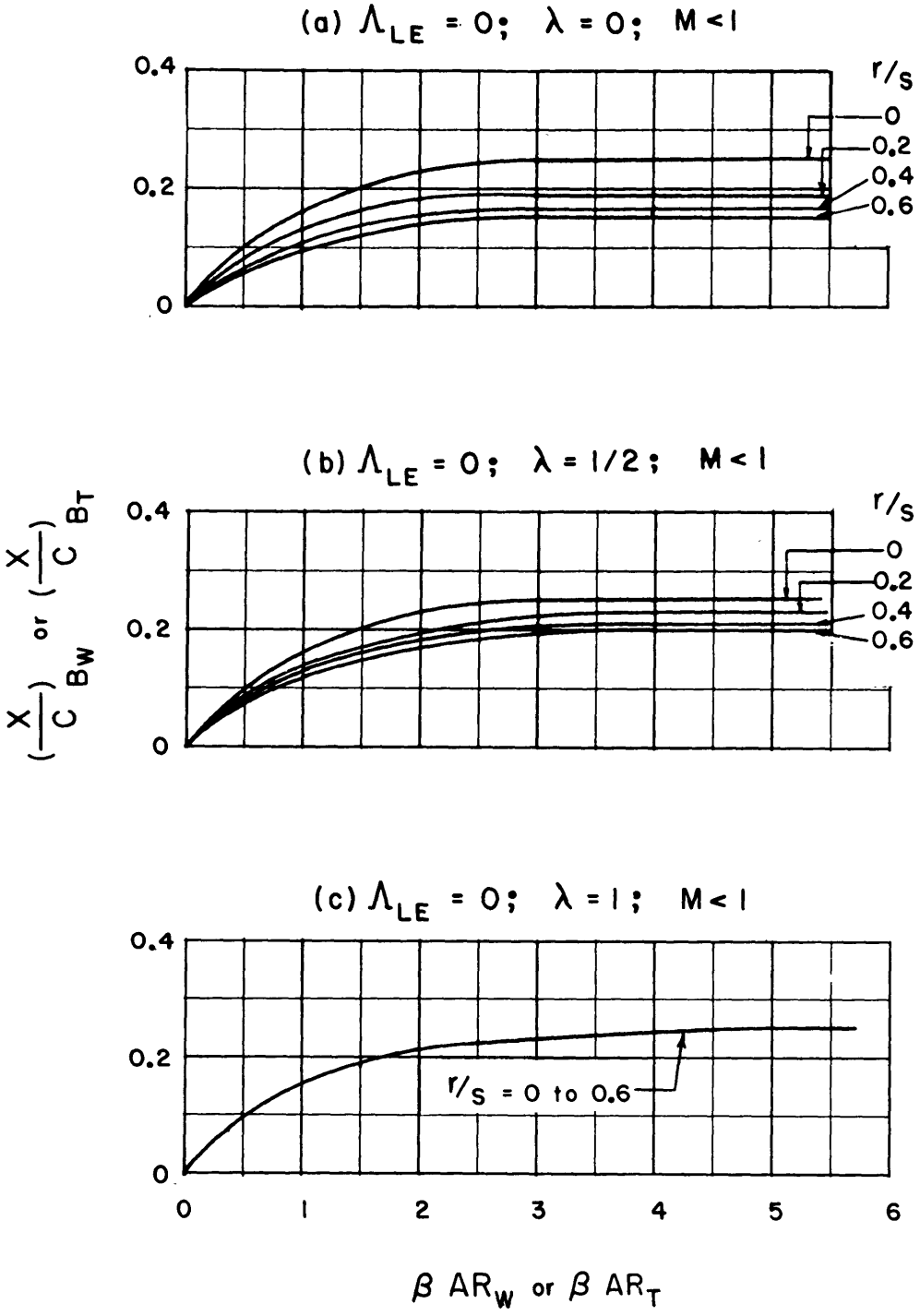

Figure 13 - Location Center of Pressure of Linear Lift on the Body in the Presence of the Wings or Tails

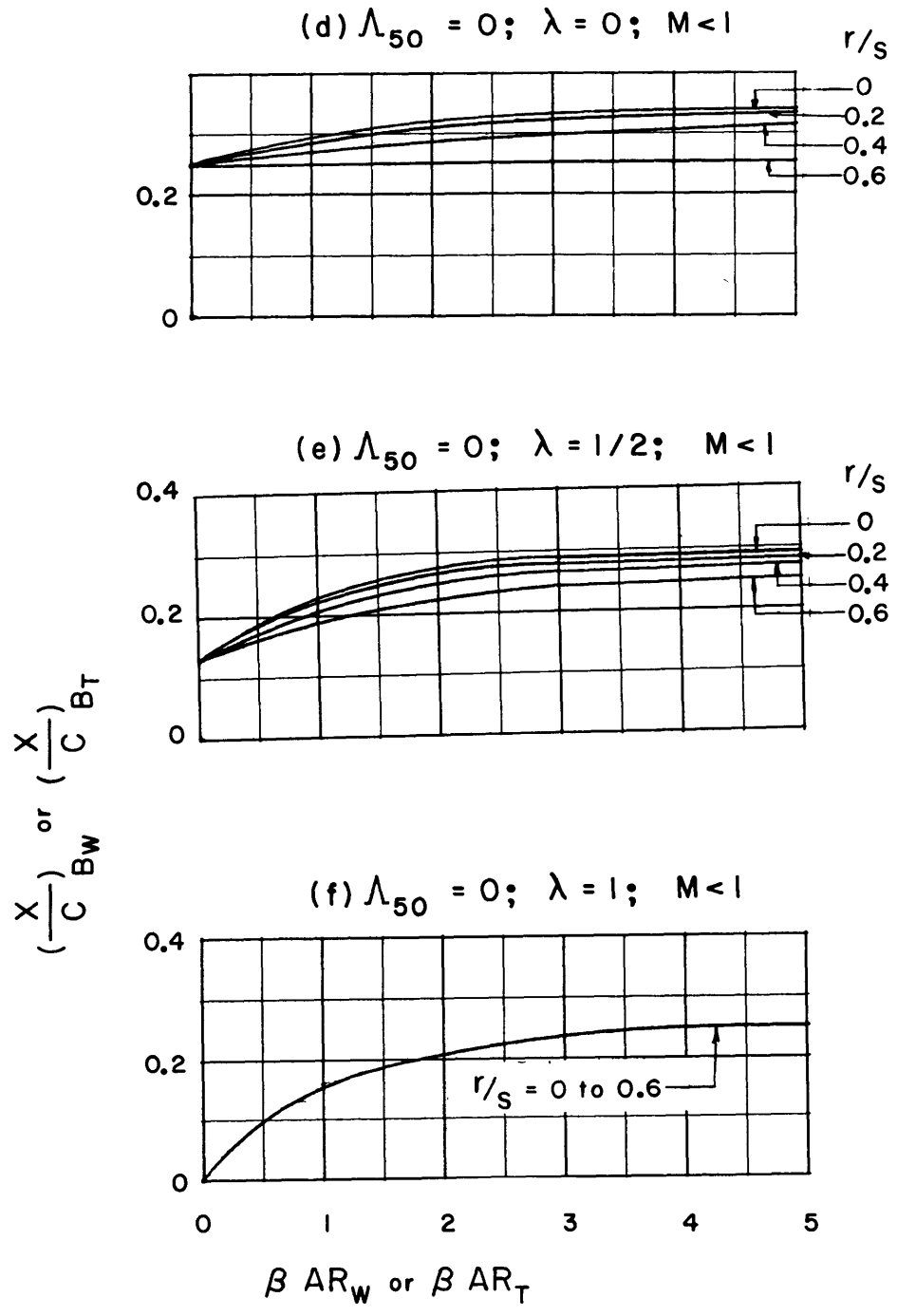

Figure 13 (Continued)

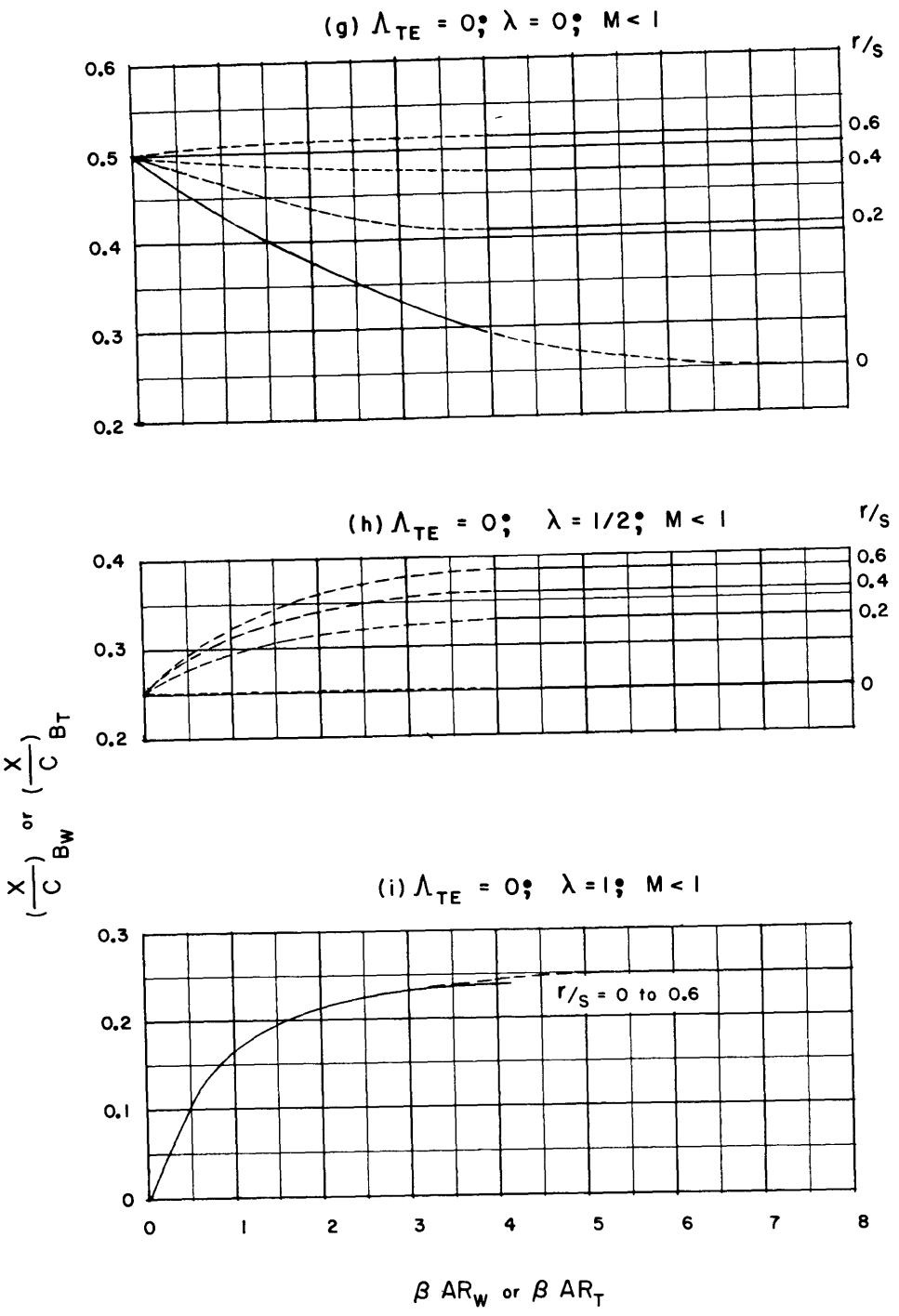

Figure 13 (Continued)

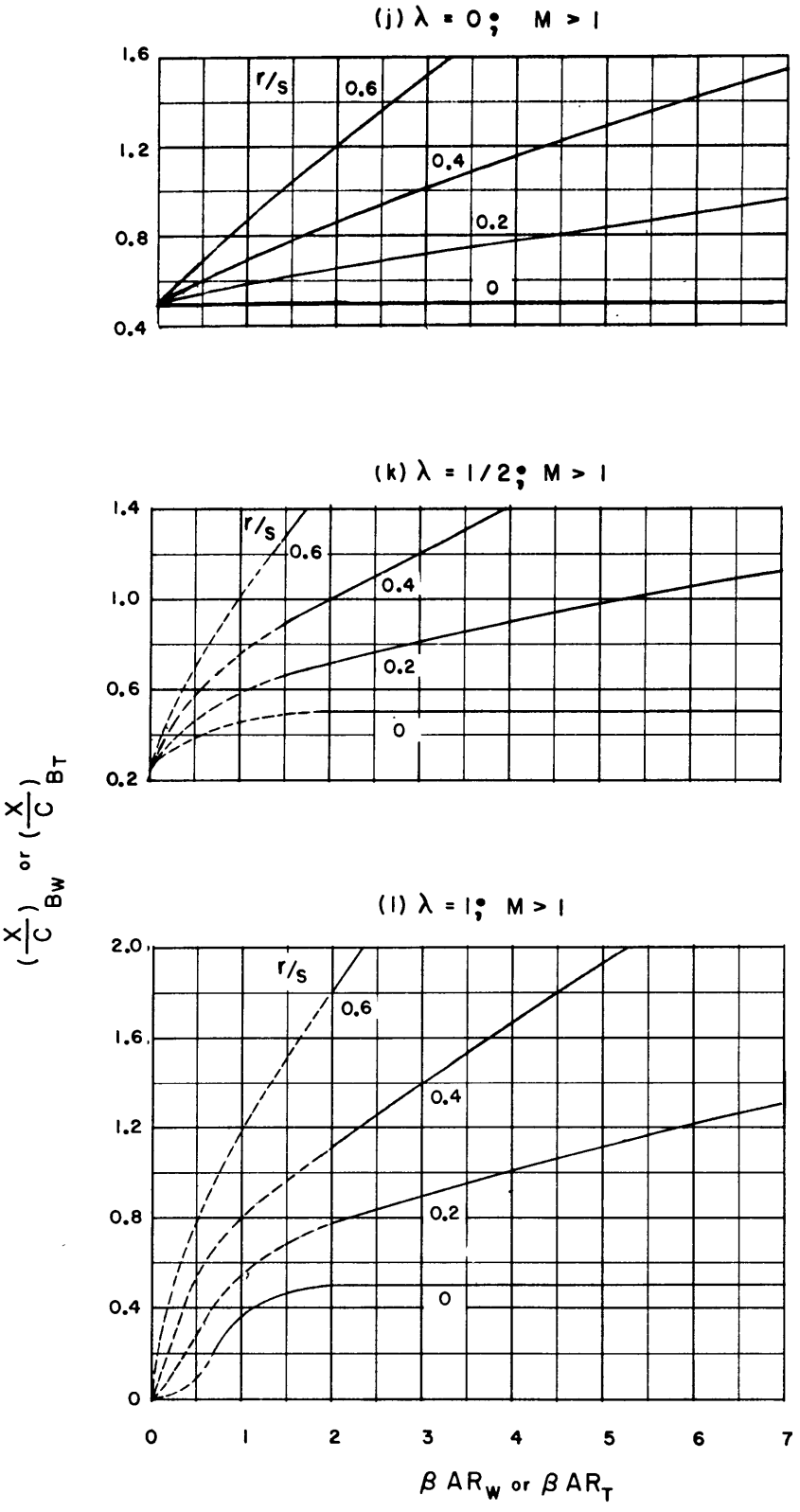

Figure 13 (Concluded)

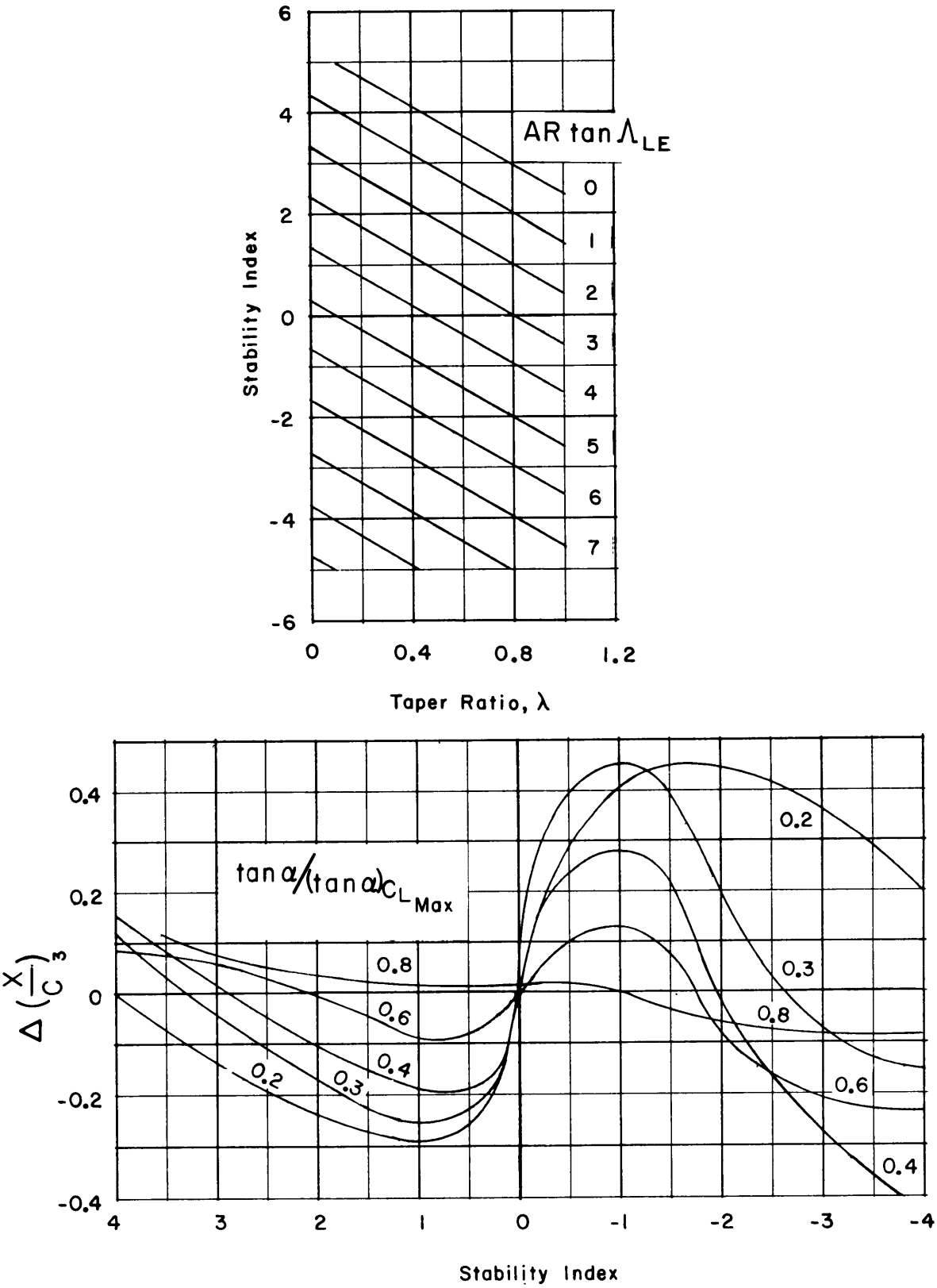

Figure 14 - Wing or Tail Center of Pressure Location Increment

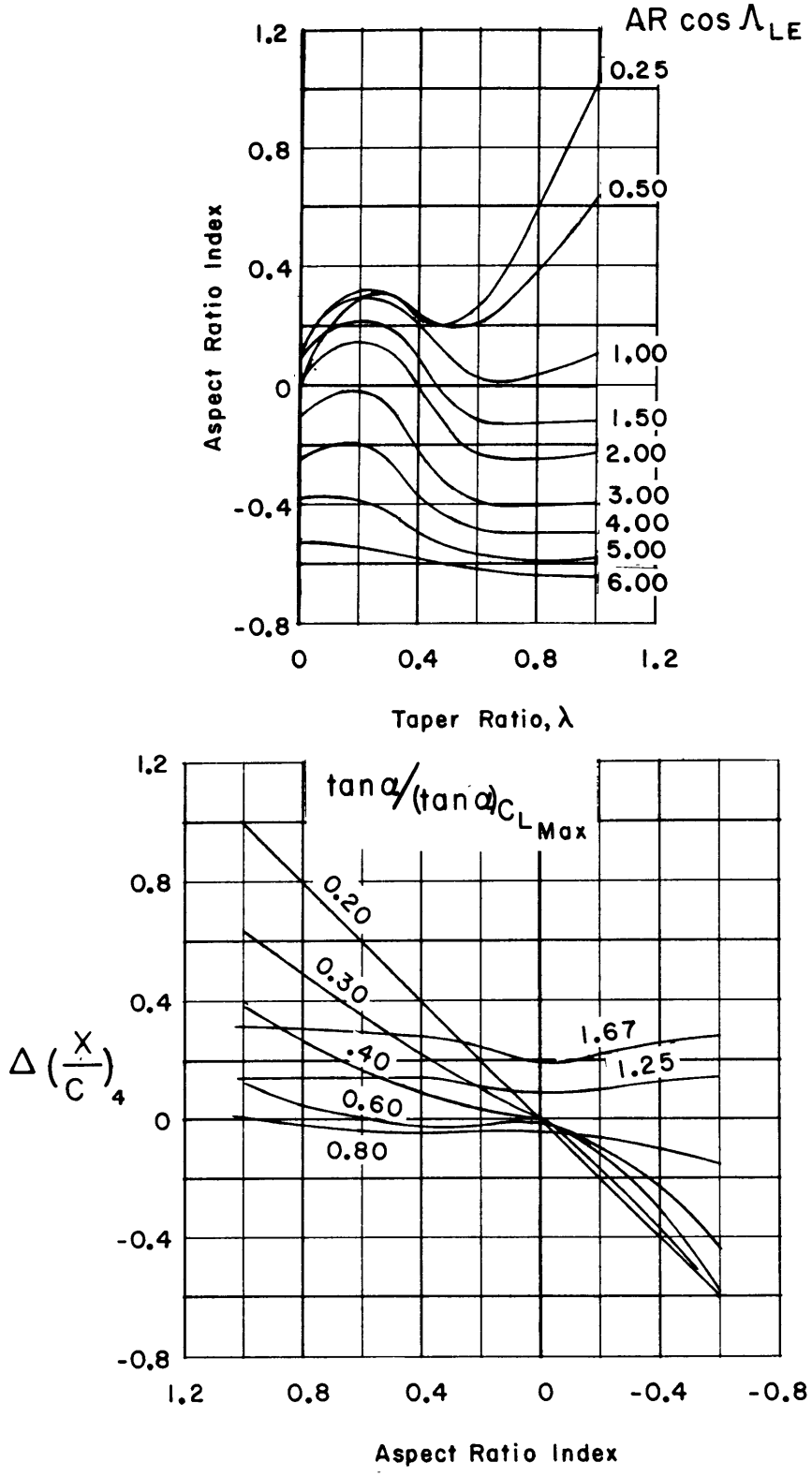

Figure 15 - Wing or Tail Center of Pressure Location Increment

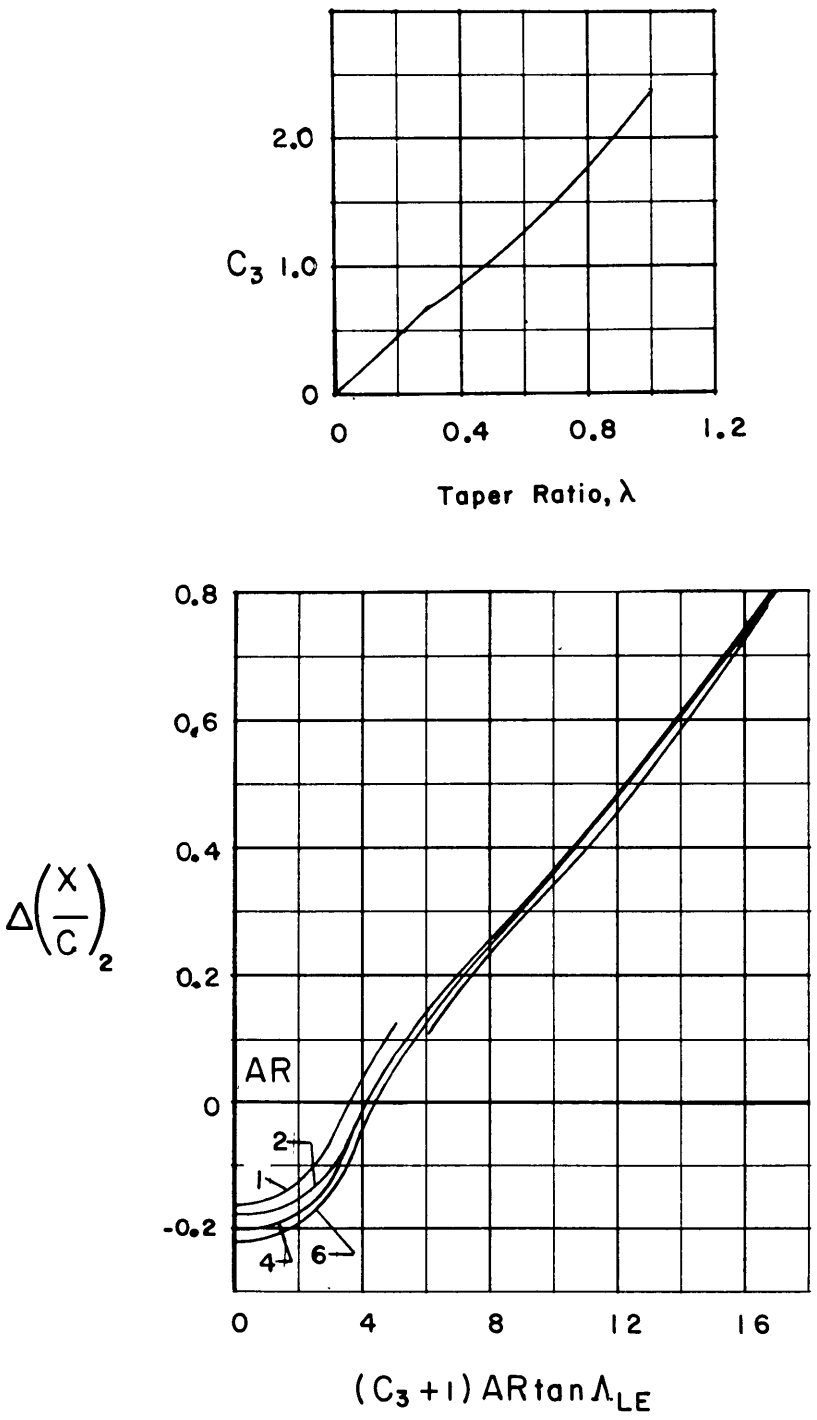

Figure 16 - Wing or Tail Center of Pressure Location Increment

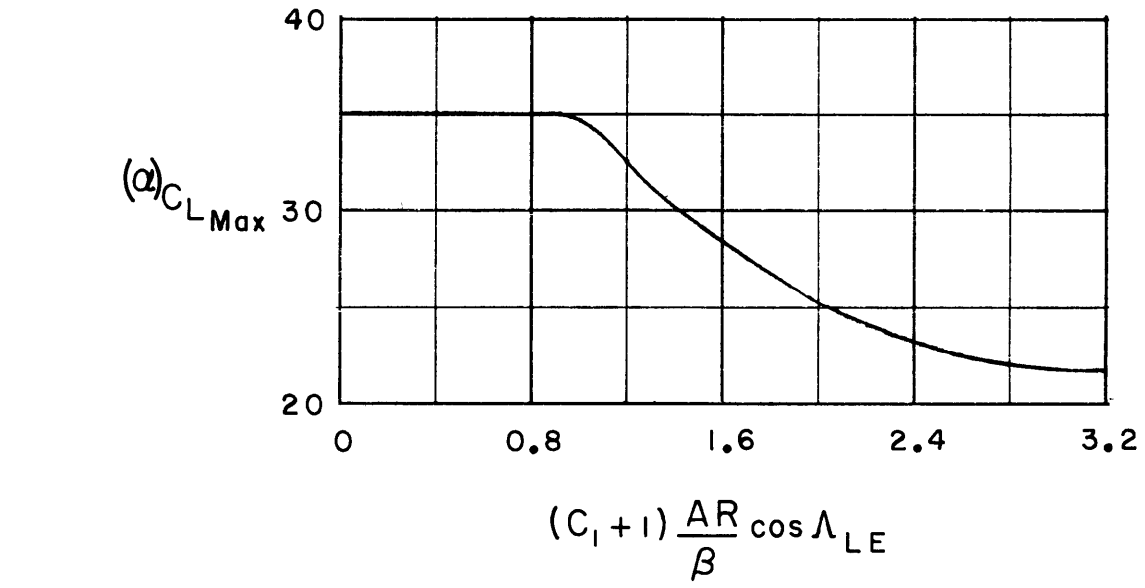

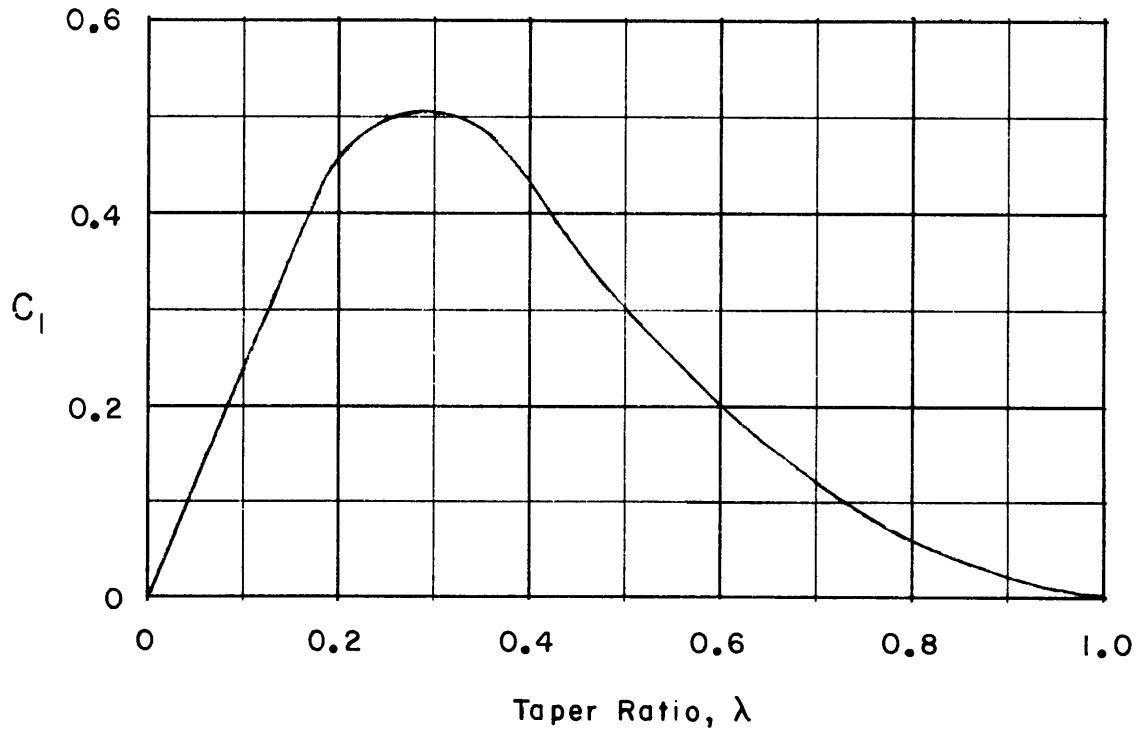

Figure 17 - Factors for Determining Angle of Attack for Maximum Lift

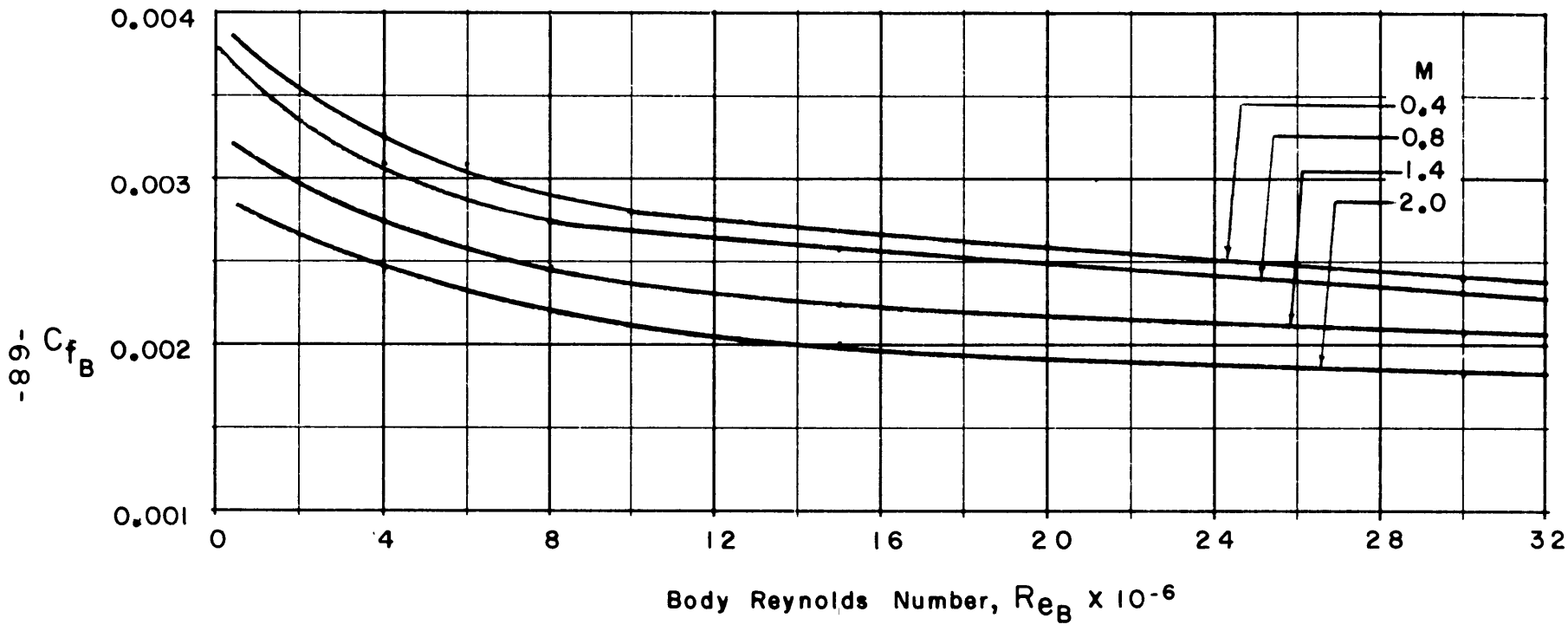

Figure 18 - Variation of Body Friction Coefficient with Mach Number and Reynolds Number

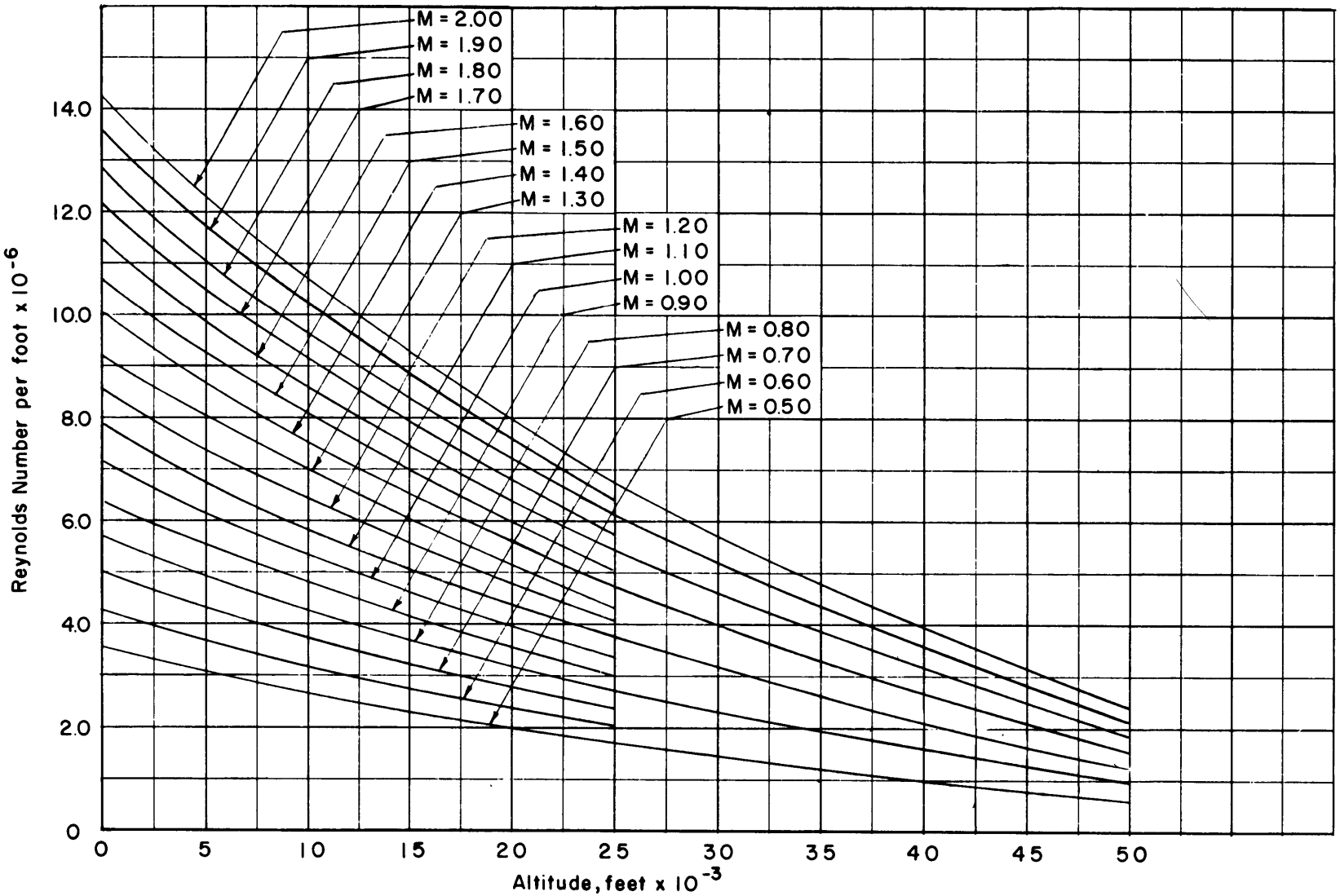

Figure 19 - Reynolds Number versus Altitude for Different Mach Numbers

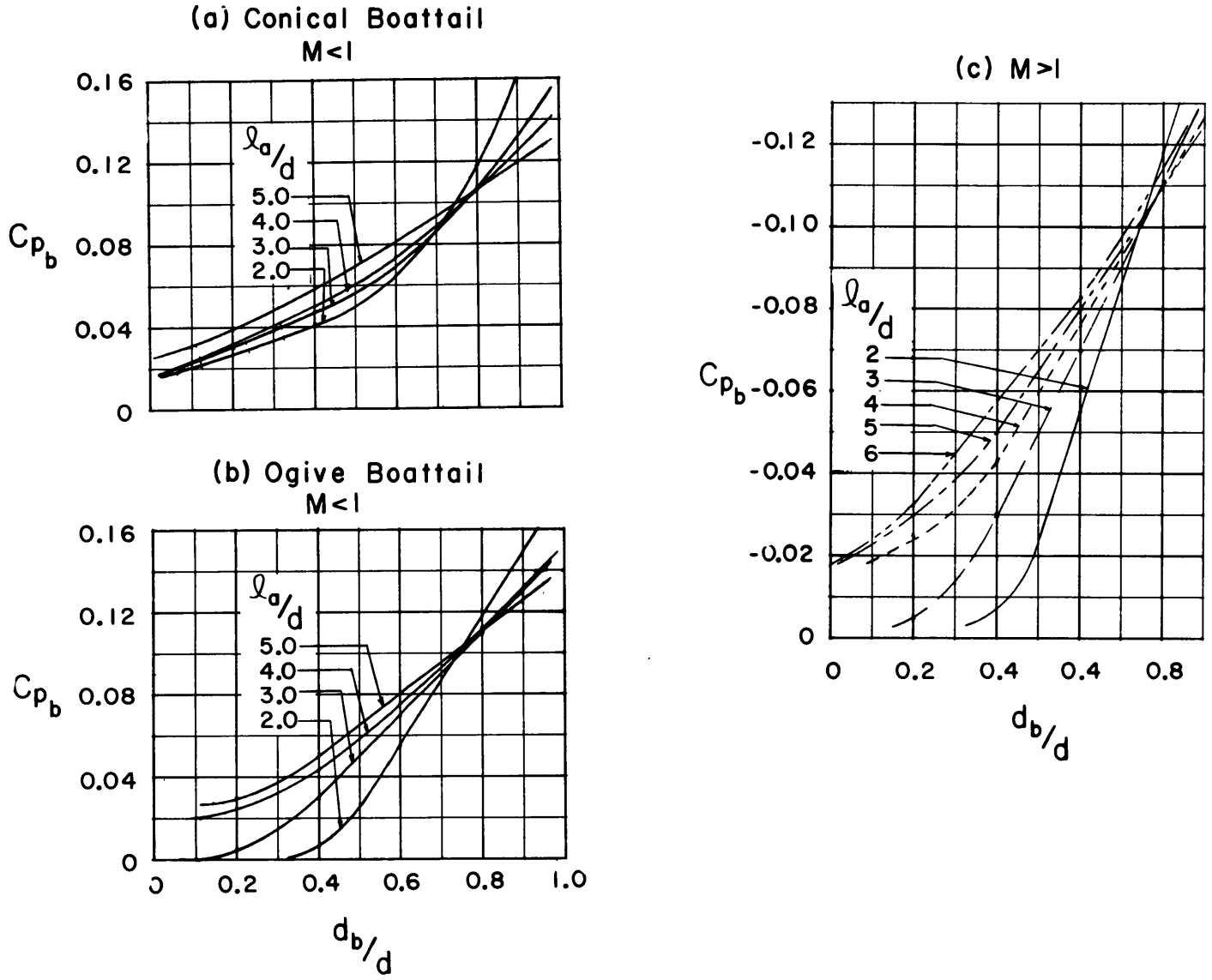

Figure 20 - Base Pressure Coefficient for Boattailed Bodies

(a) Conical Noses

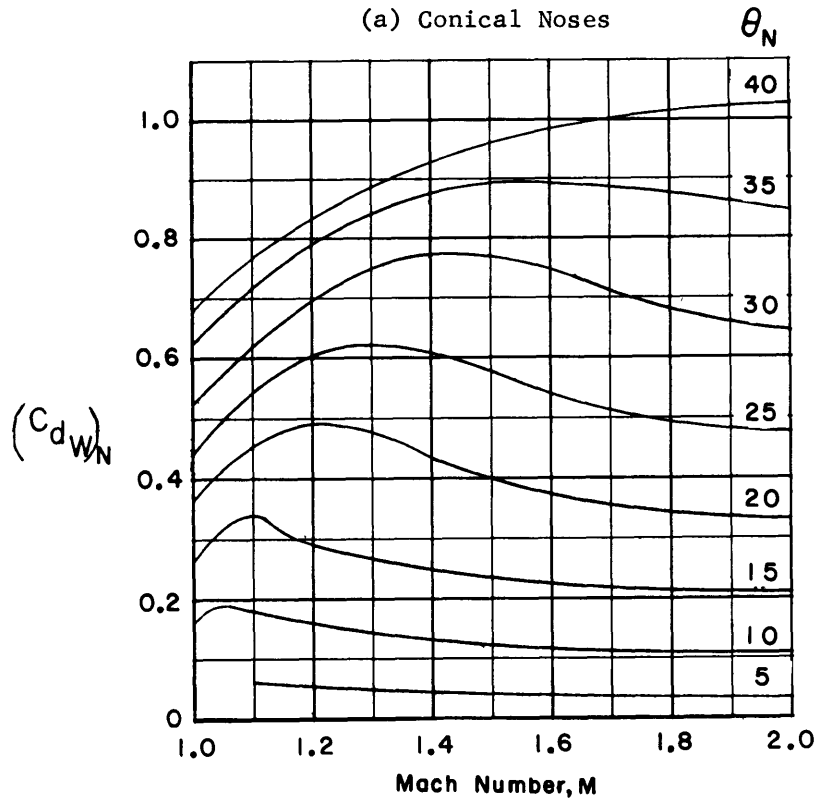

(b) Ogive Noses

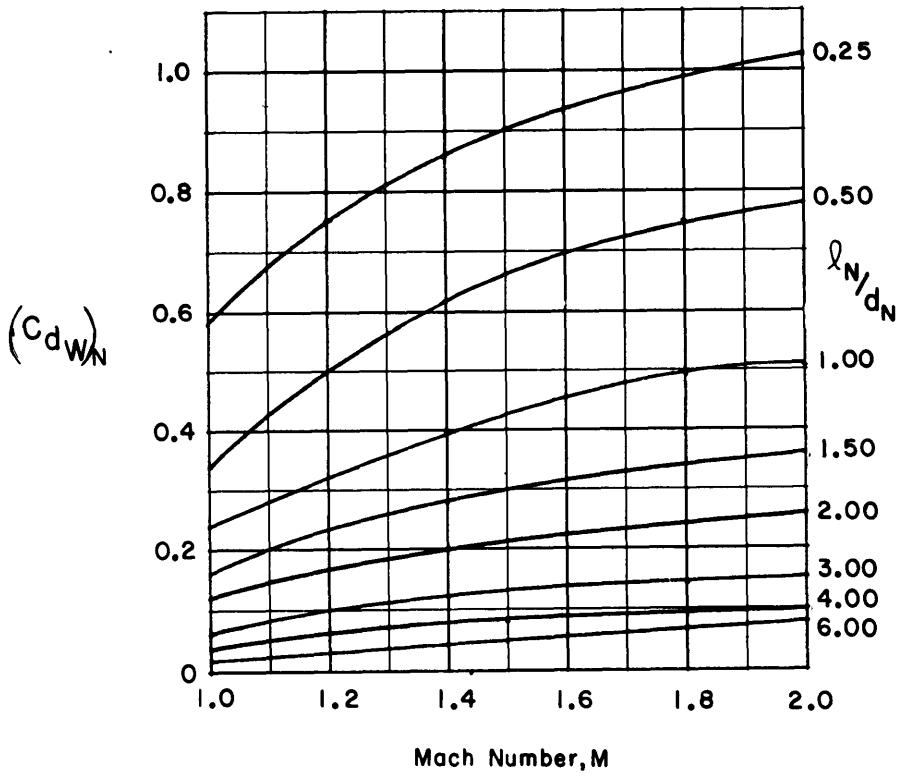

Figure 21 - Wave Drag of Nose-Cylinder Type Bodies

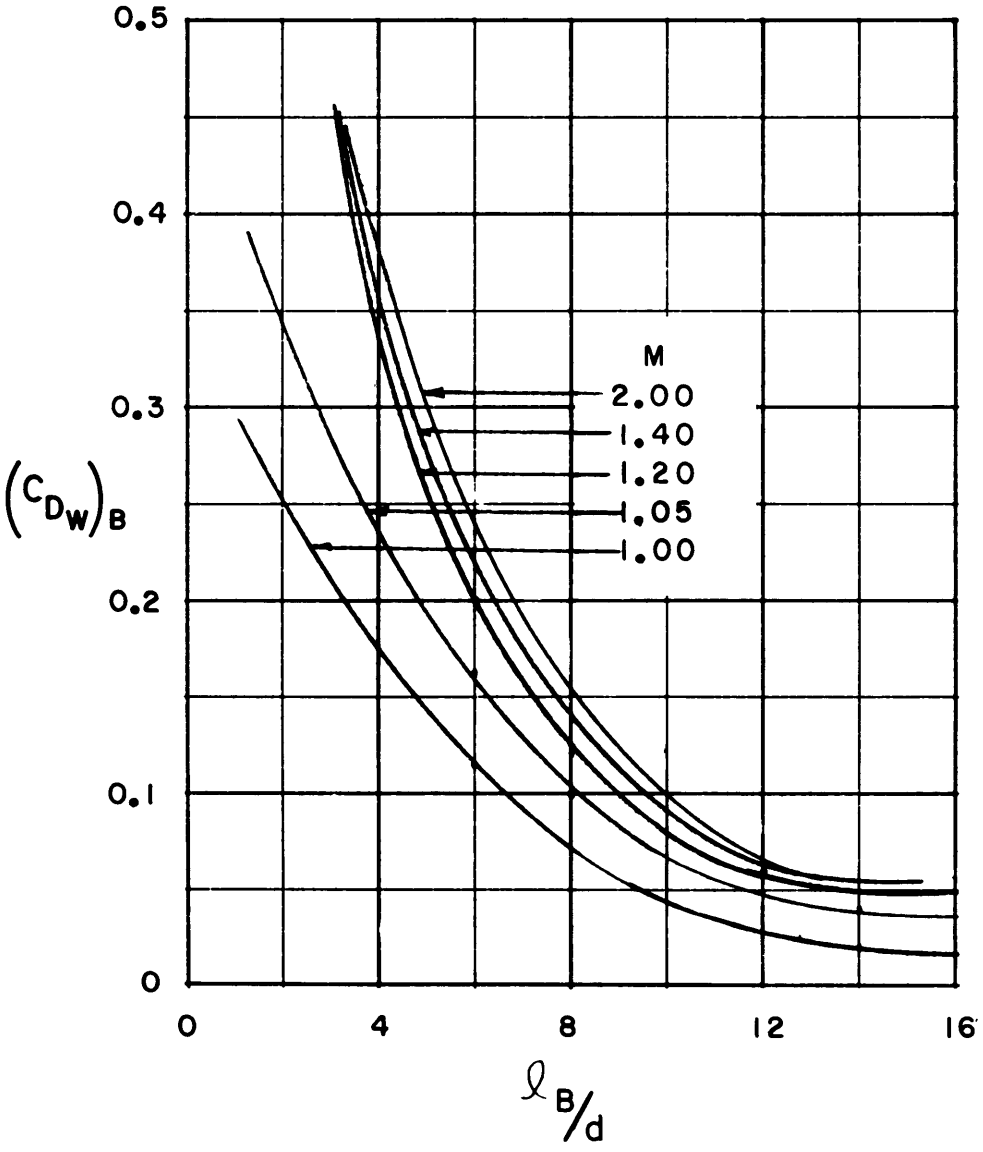

Figure 22 - Wave Drag of Parabolic Bodies of Revolution

(a) Conical Boattails

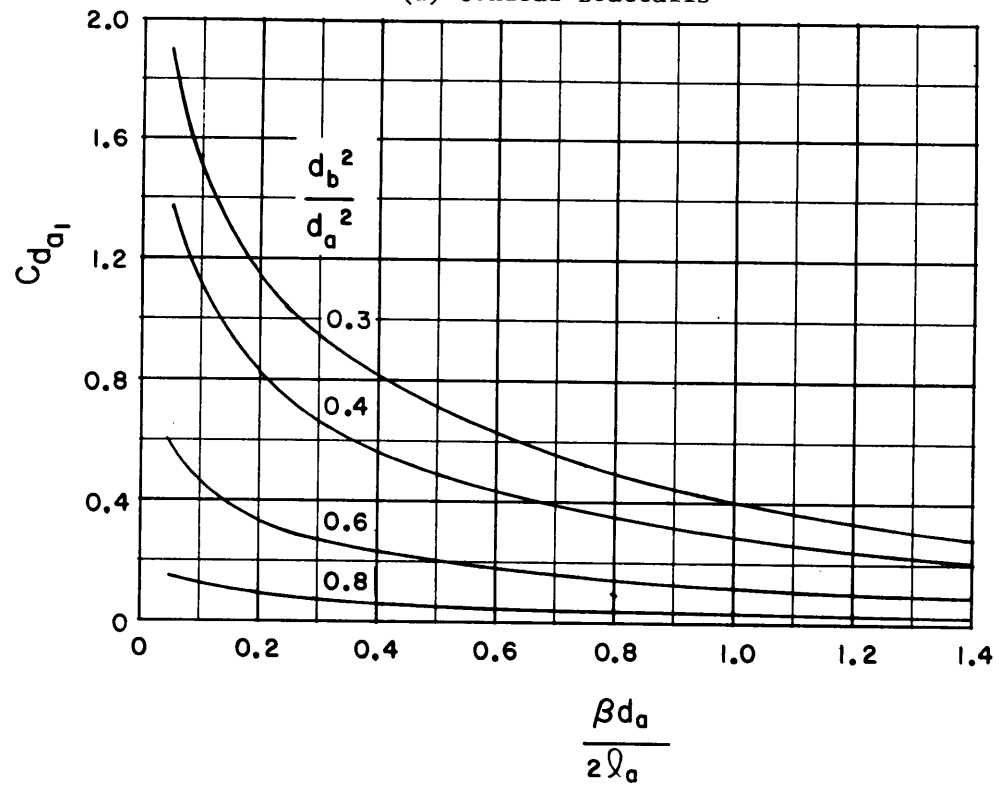

(b) Ogive Boattails

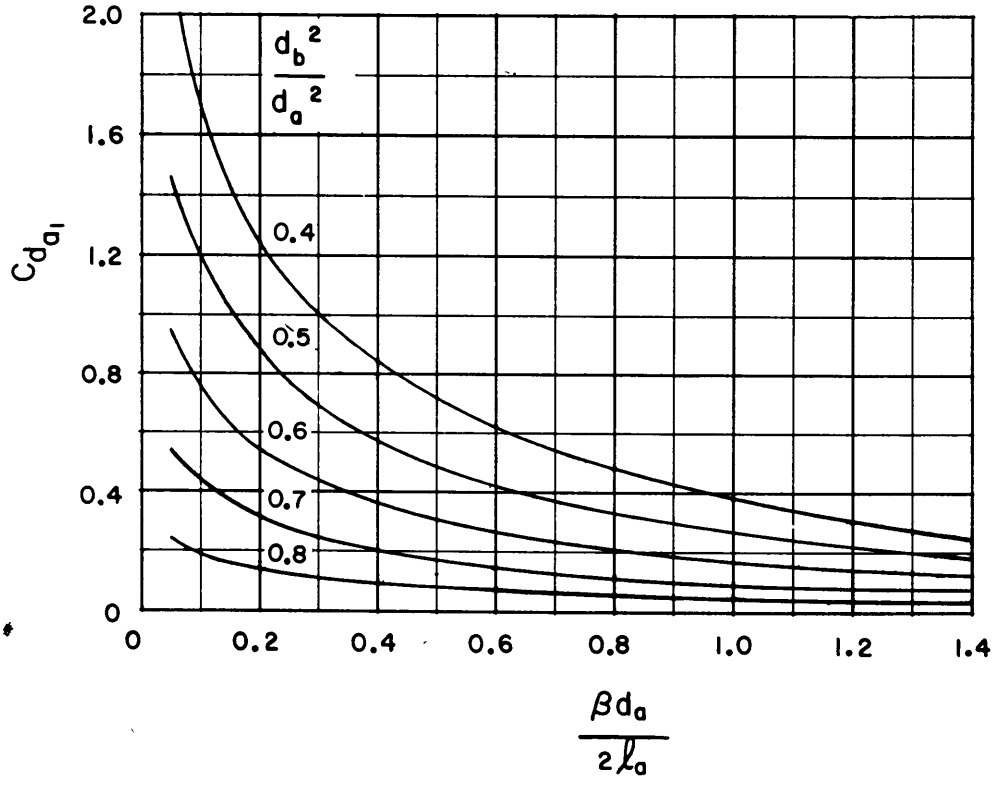

Figure 23 - Wave Drag of Boattails on Cylindrical-Type Bodies

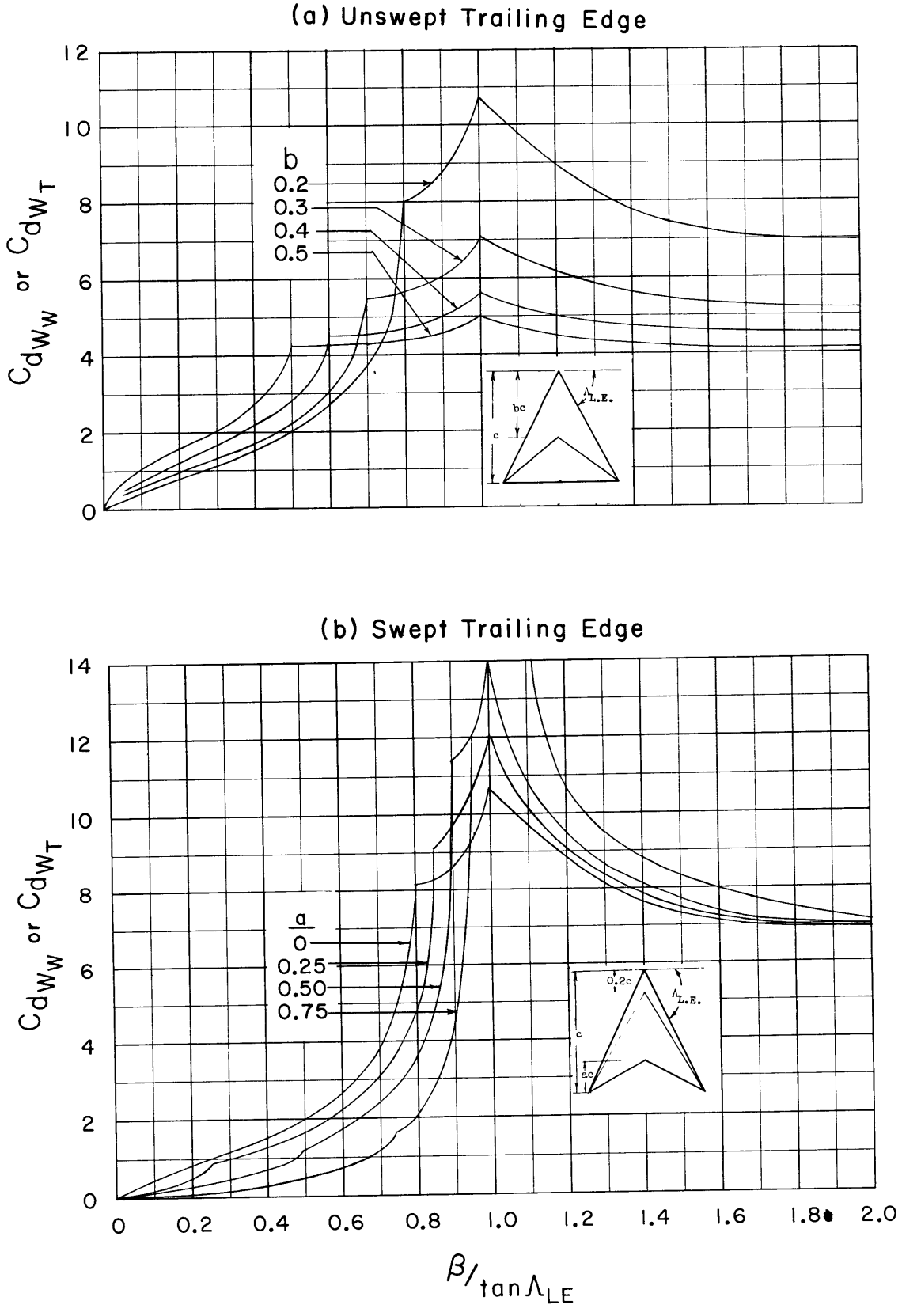

Figure 24 - Wave Drag of Zero Taper Ratio Lifting Surfaces (Wings or Tails) ($\lambda_W \leq 0.15$)

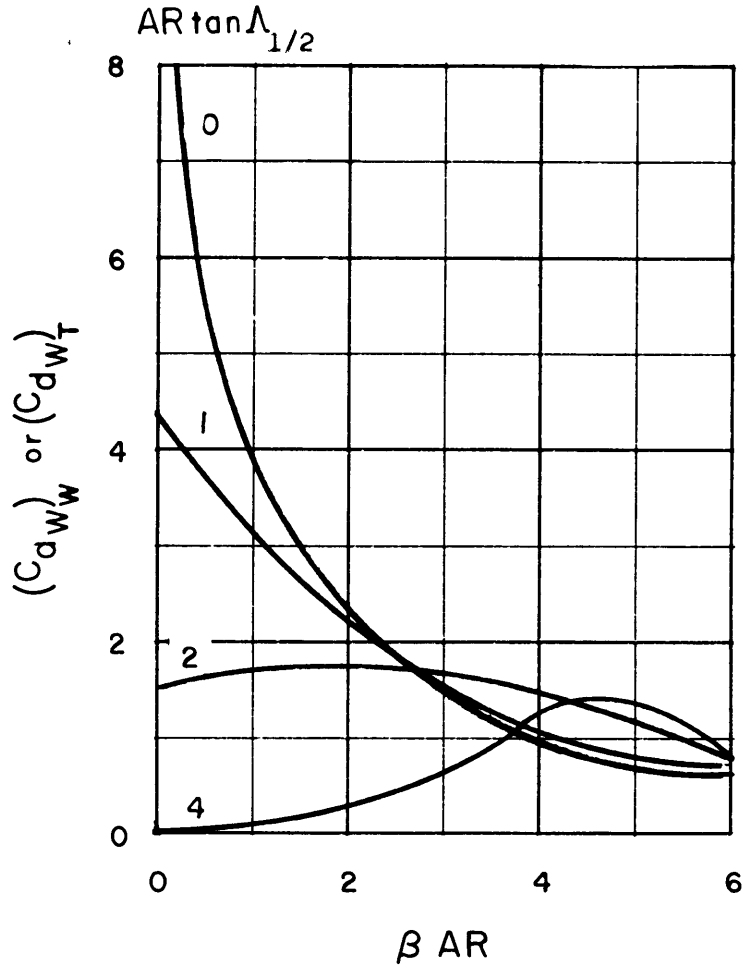

Figure 25 - Wave Drag of Lifting Surfaces (Wings or Tails) Whose Taper Ratio is Greater Than 0.15

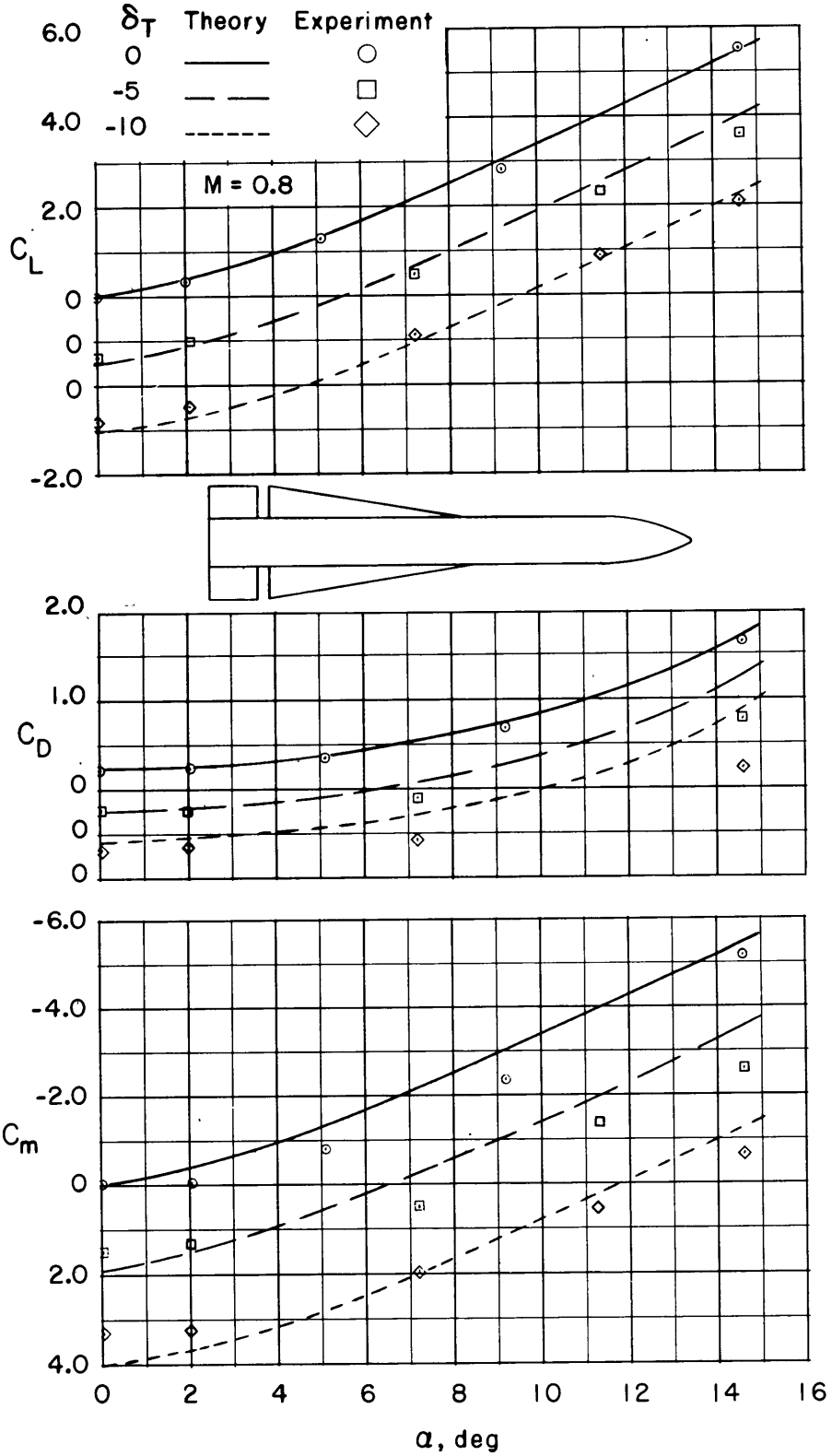

Figure 26 - Comparison of Theoretical Characteristics Obtained by the Method Herein with Experimental DTMB Unpublished Data

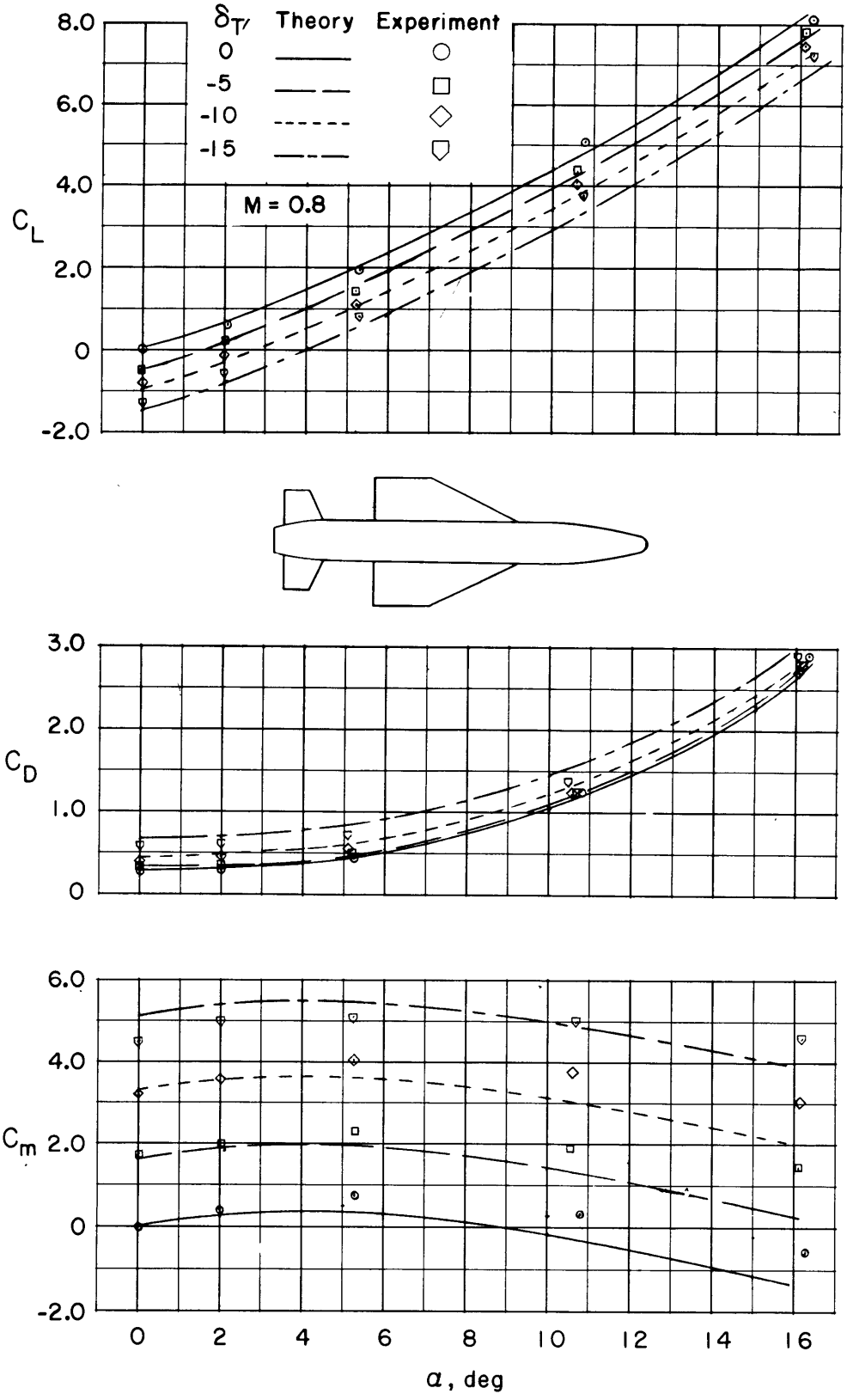

Figure 26 (Continued)

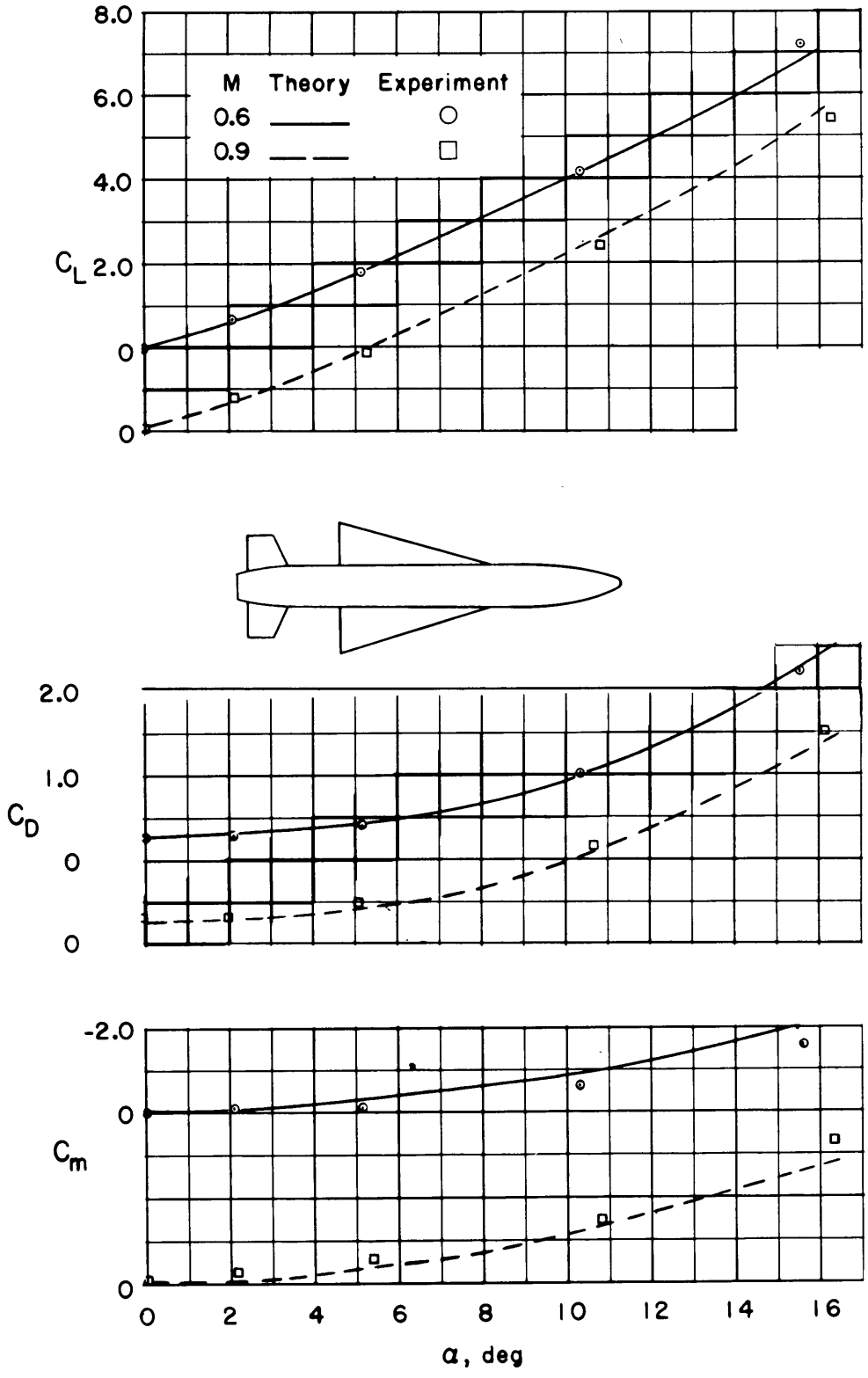

Figure 26 (Continued)

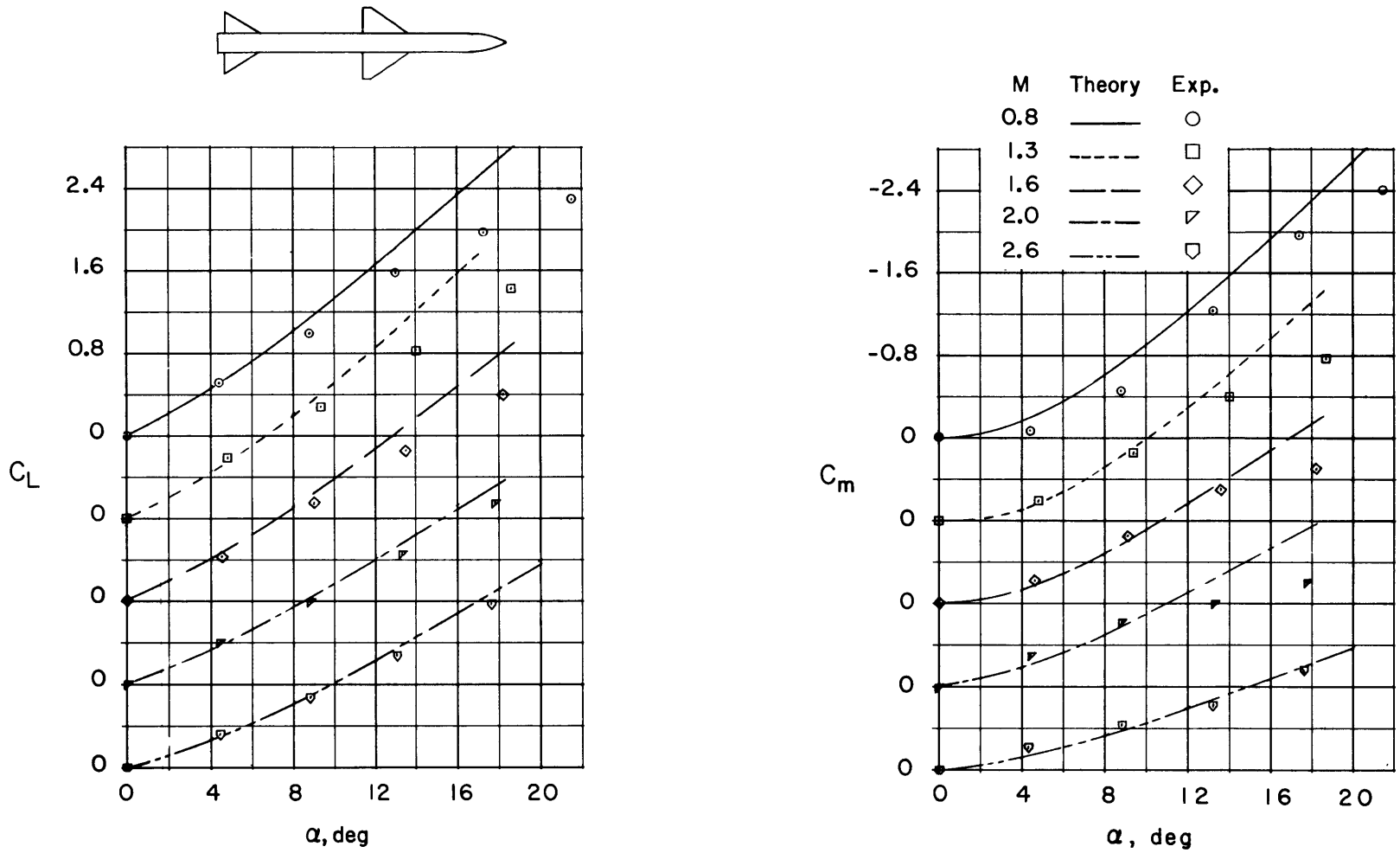

Figure 26 (Continued)

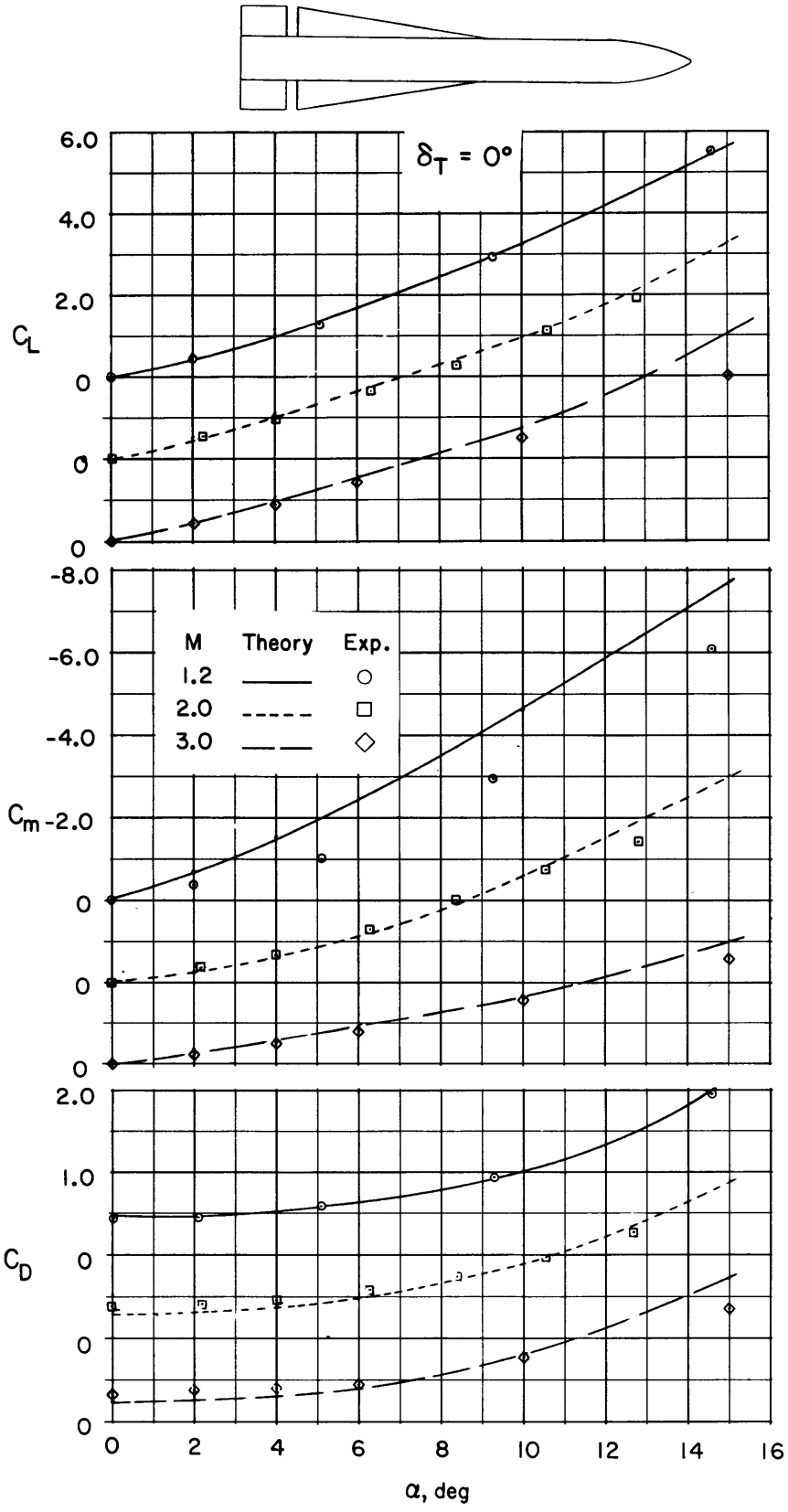

Figure 26 (Continued)

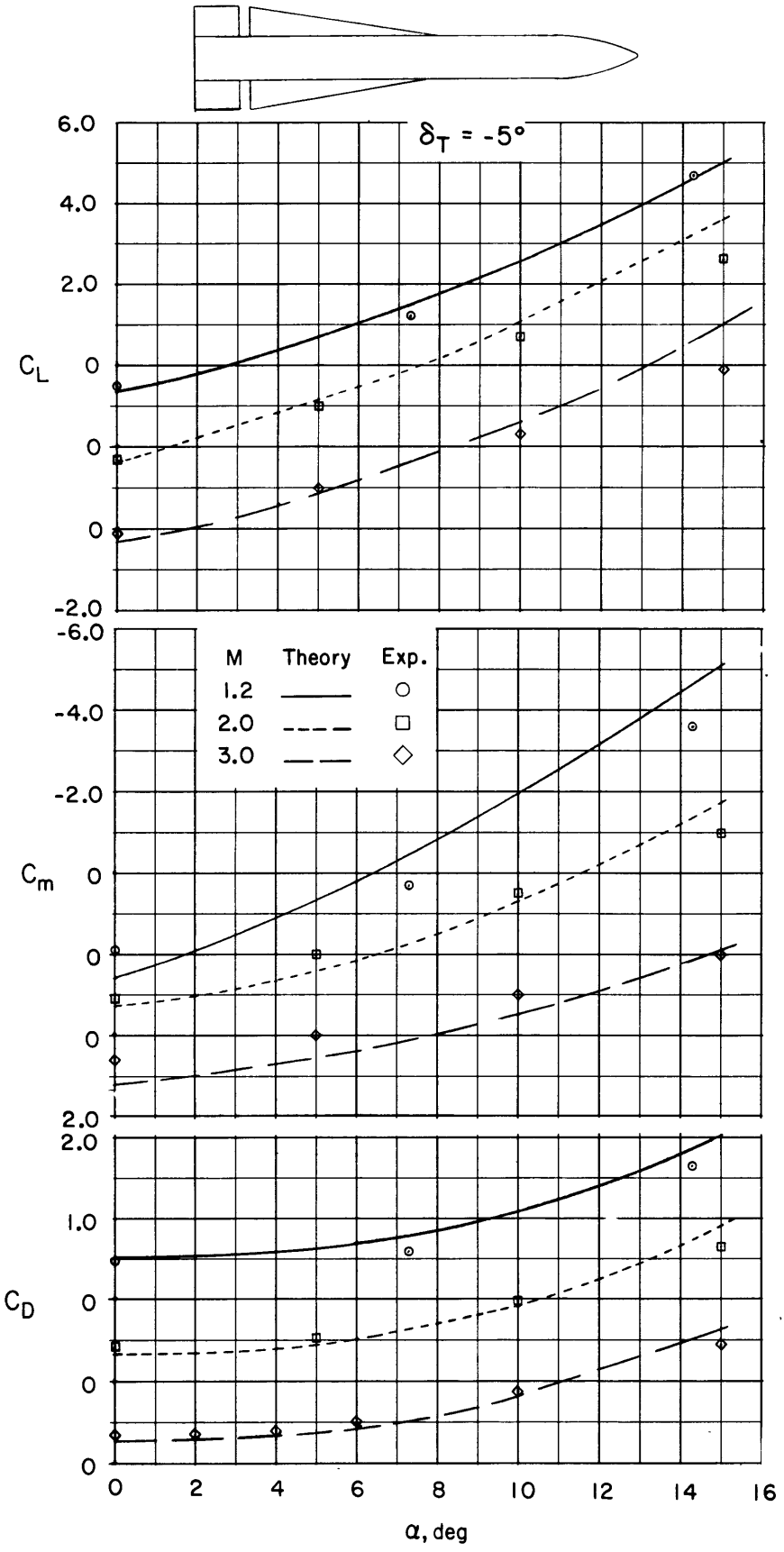

Figure 26 (Continued)

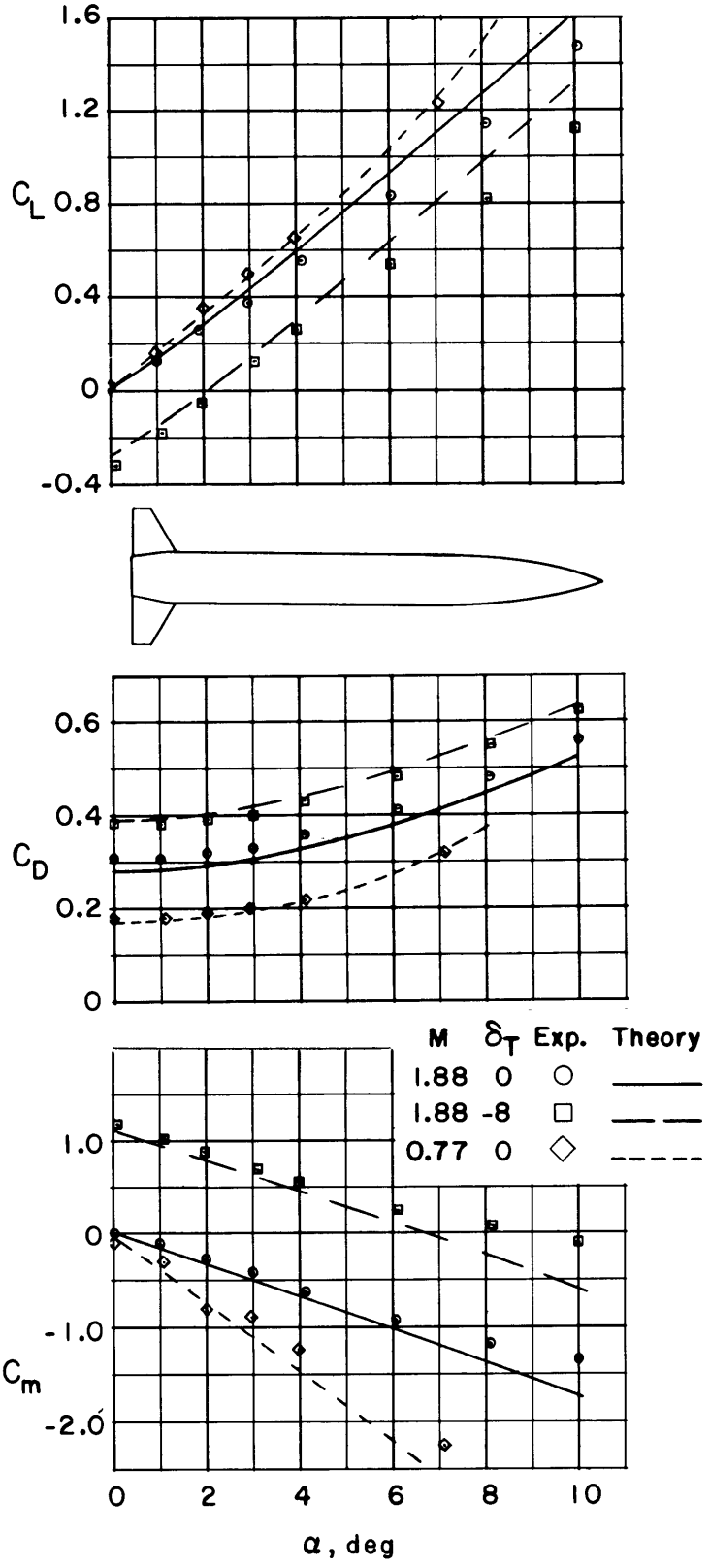

Figure 26 (Continued)

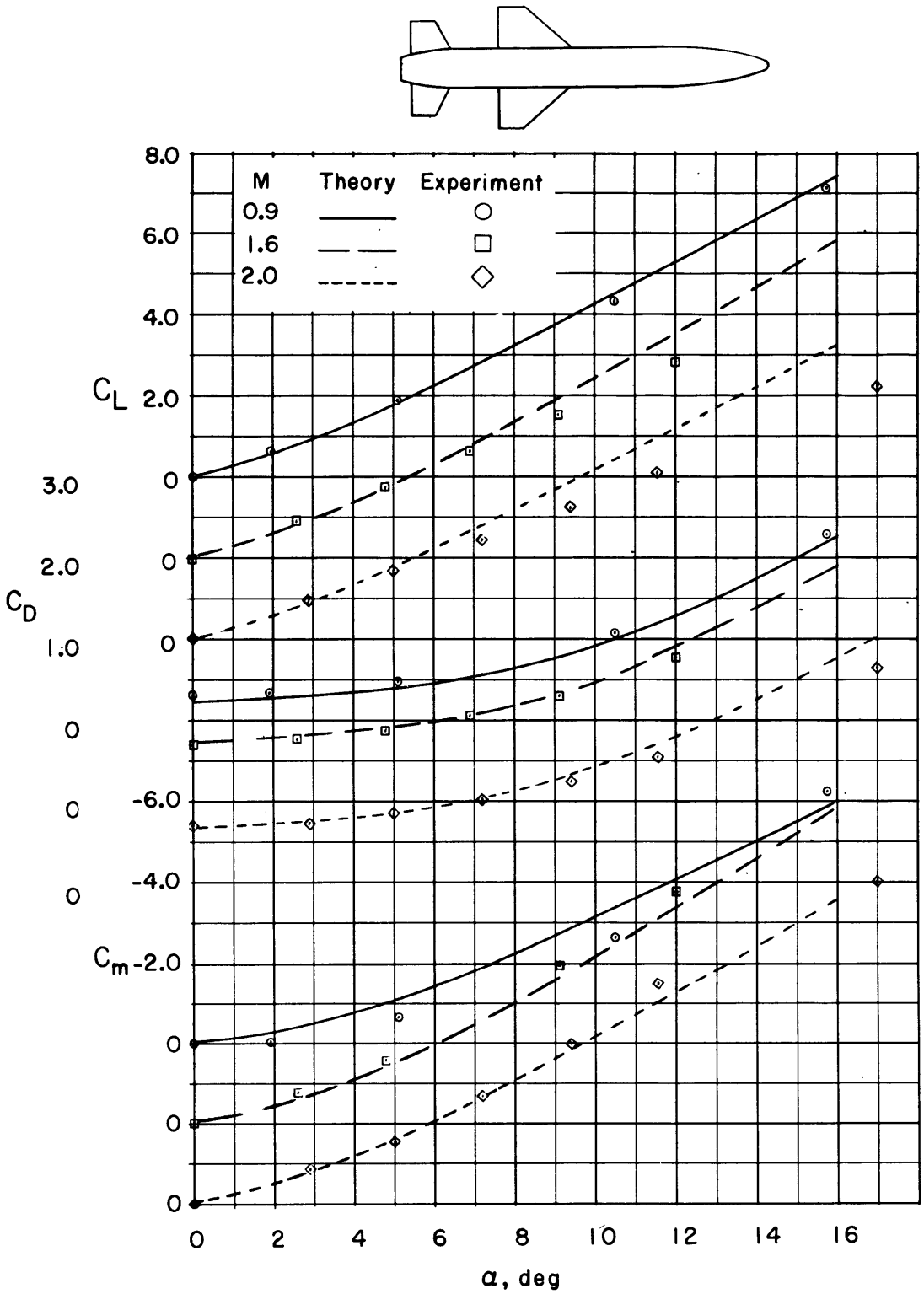

Figure 26 (Continued)

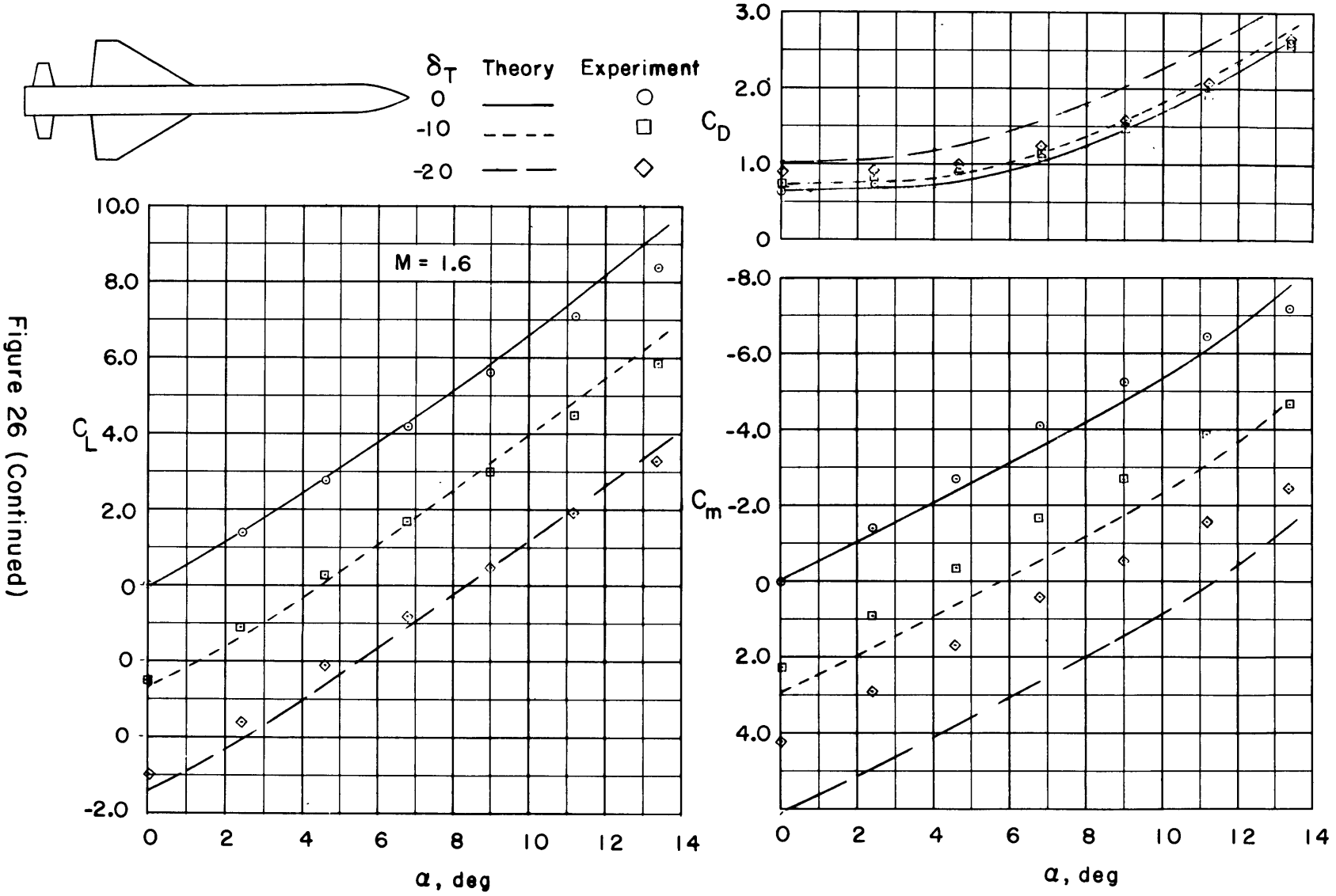

Figure 26 (Continued)

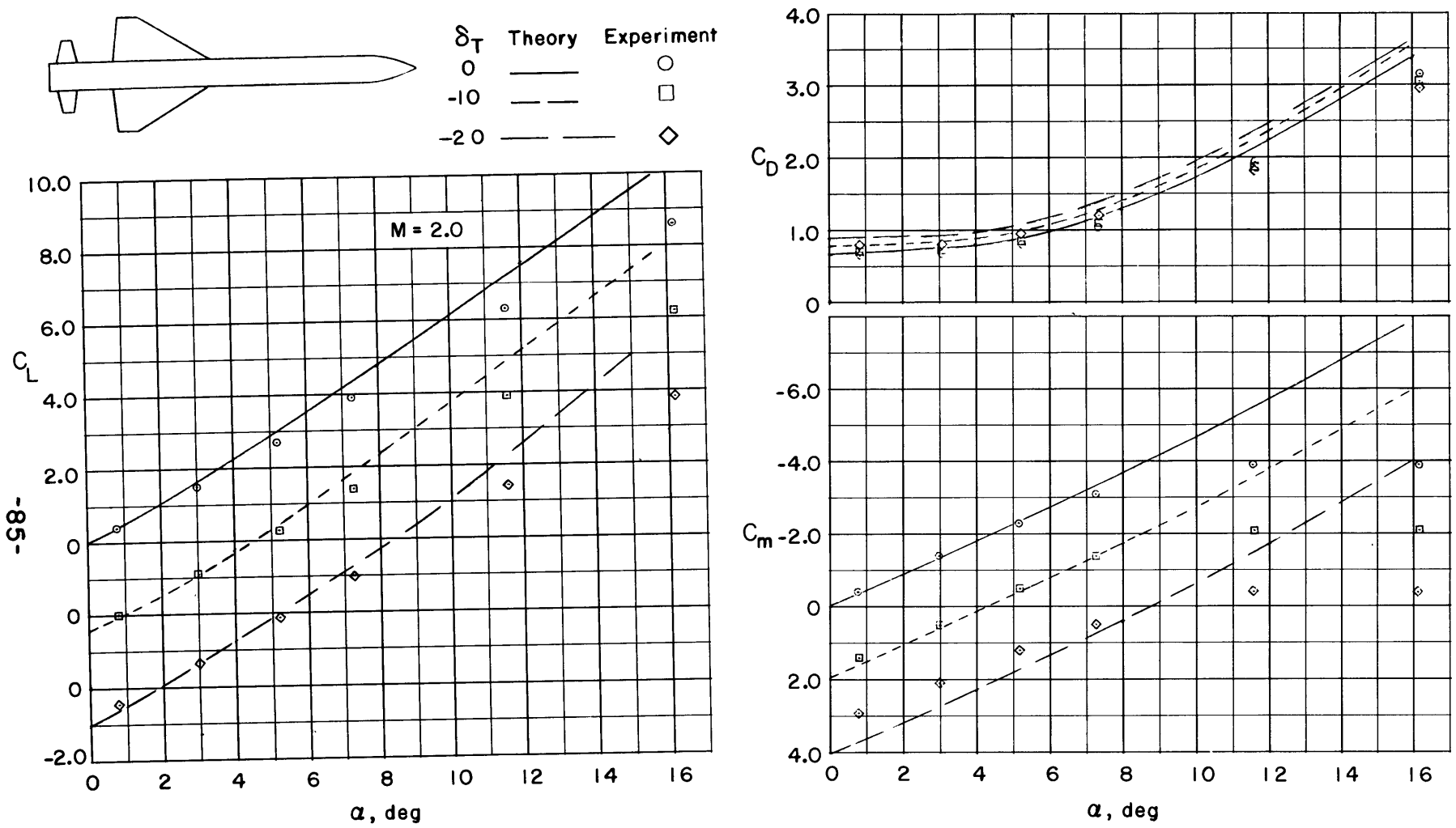

Figure 26 (Concluded)

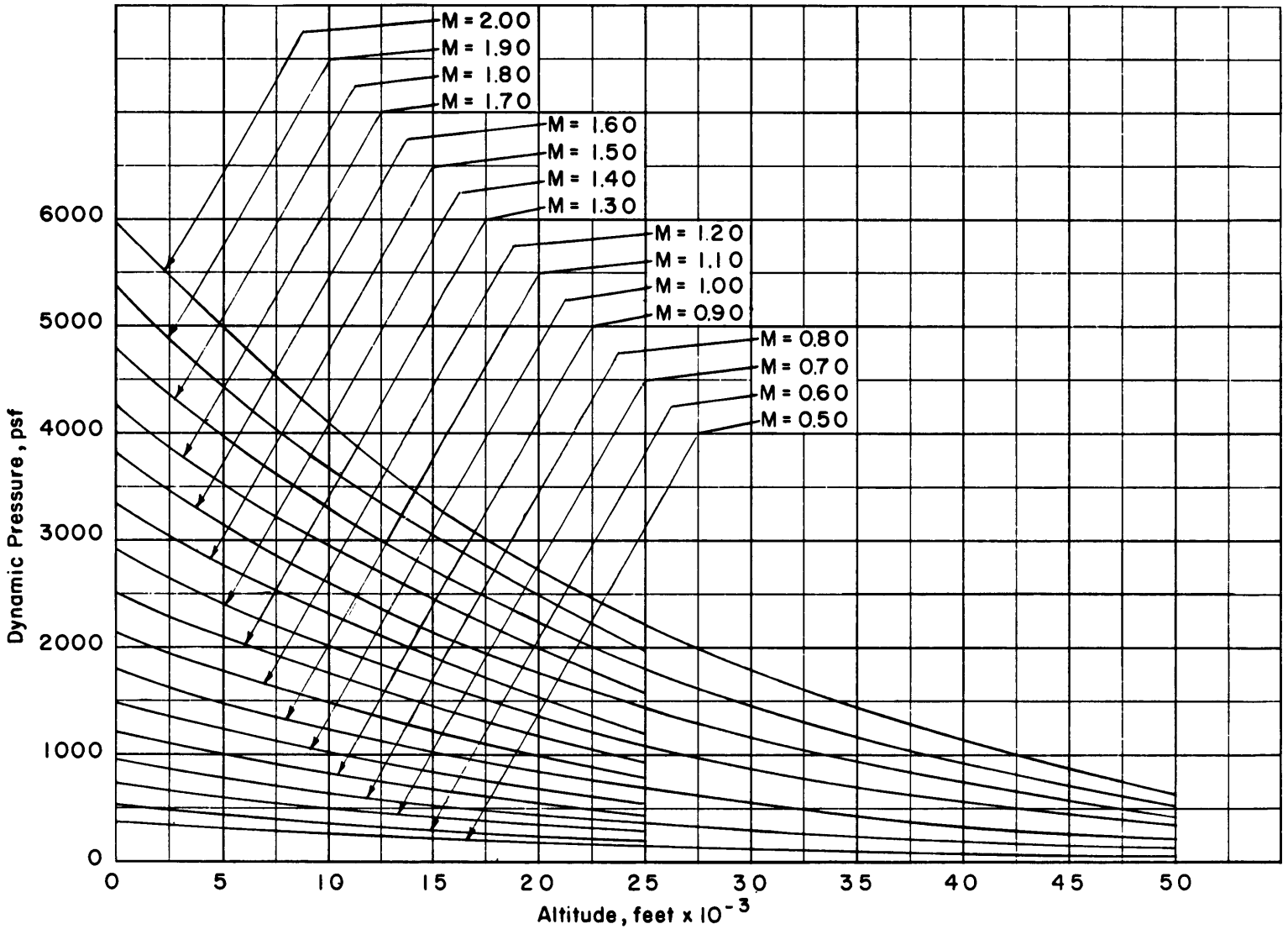

Figure 27 - Dynamic Pressure versus Altitude for Different Mach Numbers

DISTRIBUTION LIST

Copies	
1	NASC(530C)
4	NASC(604)
20	DDC
1	CDR,NATC(Dir., TPS)
1	CO, NADC
5	Scientific & Tech. Info. Facility Bethesda, Md. Attn: NASA Rep. (S-AK/DL)
2	ONR(461)
1	DIR, NRL(2027)
1	Supt. Naval Post-graduate Sch. Monterey, Calif.
3	NSSC(335)
1	NSSC(421)
1	Commandant, U.S. Marine Corps(A04E) GS-4 Div.
1	CNO(Op 07T6)
1	CNO(Op 0725)
1	DIR, Langley Res. Center Attn: Tech. Lib.
1	Chief of Transportation (TCDRD), Army
1	Chief of Transportation (TCDTE), Army

Copies	
1	CO, U.S. Army Transportation Research Command Fort Eustis, Virginia
1	Chief of Research and Development Department of the Army Attn: Res. Support Div.
1	Aerophysics Co.
1	Aerospace Corp. Los Angeles, Calif. Attn: Lib. Tech. Doc. Grp.
1	Air Vehicle Corp. San Diego, Calif.
1	Allis-Chalmers Mfg. Co. Milwaukee, Wisc.
1	American Mach. & Foundry Co. Mechanics Research Div. Niles, Illinois
1	Avco Corp. New York, N.Y.
1	Beech Aircraft Corp. Wichita, Kansas
1	Bell Aerosystems Co. Buffalo, N.Y. Attn: Chief Lib.
1	Chief of Transportation (TCAFO-C)
1	Bell Helicopter Co. Fort Worth, Texas
1	Bertelsen Mfg. Co. Neponset, Ill.

DISTRIBUTION LIST

1 Boeing Company
Wichita, Kansas
Attn: Chief Engr.

1 Boeing Company
Transport Div.
Seattle, Wash.
Attn: Libr.

1 Boeing Company
Vertol Div.
Morton, Pa.

1 Booz-Allen Applied Res. Inc.
Bethesda, Md.

1 Borg-Warner Corp.
Ingersoll Kalamazoo Div.
Kalamazoo, Mich.

1 Cessna Aircraft Co.
Research Dept.
Wichita, Kansas

1 Chrysler Corp.
Defense Operations Div.
Detroit, Mich.
Attn: Libr.

1 Collins Construction Co.
Port Lavaca, Texas

1 Cornell Aeronautical Lab., Inc.
Buffalo, New York

1 Cornell-Guggenheim
Avia. Safety Center
New York, N.Y.

1 Curtiss-Wright Corp.
Wash., D.C.

1 Curtiss-Wright Corp.
Wright Aeronautical Div.
Wood-Ridge, N.J.
Attn: Tech. Lib.

1 Fairchild Stratos Corp.
Hagerstown, Md.

1 Food Machinery & Chem. Corp.
San Jose, Calif.

1 The Ford Motor Co.
Aeronutronic Div.
Newport Beach, Calif.

1 Engineering Development Corp.
Englewood, Colo.

1 The Garrett Corp.
Airesearch Mfg. Co.
Phoenix, Arizona
Attn: Libr.

1 General Electric Co.
FPD Tech. Info. Center
Cincinnati, Ohio

1 General Electric Co.
Small Acft. Engine Dept.
West Lynn, Mass.

1 General Dynamics Corp.
Convair Fort Worth Oper. Div.
Fort Worth, Texas
Attn: Lib.

1 General Dynamics Corp.
Convair Div.
Dept. of Aero. Engrg.
San Diego, Calif.

1 Goodyear Aircraft Corp.
Akron, Ohio

1 Grumman Aircraft Engr. Corp.
Bethpage, L.I., N.Y.

1 Gyrodyne Co. of America, Inc.
Dept. of Aero. Engineering
St. James, L.I., N.Y.

DISTRIBUTION LIST

1 Hiller Aircraft Corp.
Advanced Res. Dept.
Palo Alto, Calif.

1 Hughes Tool Co.
Air-Craft Div.
Culver City, Calif.
Attn: Chief, Tech. Engr.

1 Jered Industries, Inc.
Hazel Park, Mich.

1 Kaiser Industries Corp.
Wash. D.C.

1 Kaman Aircraft Corp.
Bloomfield, Conn.

1 Kellett Acft. Corp.
Willow Grove, Pa.

1 Kettenberg Boats, Inc.
San Diego, Calif.

1 Ling-Temco Vought, Inc.
Dallas, Texas

1 Lockheed Aircraft Corp.
Burbank, Calif.

1 Martin-Marietta Corp.
Baltimore, Md.
Attn: Lib. & Doc Sec.

1 McDonnell Aircraft Corp.
St. Louis, Missouri

1 National Res. Associates, Inc.
Laurel, Md.

1 North American Aviation, Inc.
Autonetics Div.
Downey, Calif.

1 North American Avia. Inc.
Columbus, Ohio

1 Northrop Corp.
Hawthorne, Calif.

1 Piasecki Aircraft Corp.
Phila, Pa.

1 Radio Corp. of America
Missile Electronics & Controls
Burlington, Mass.
Attn: Lib.

1 Republic Avia. Corp.
Farmingdale, L.I., N.Y.
Attn: Mil. Contr. Dept.

1 Ryan Aeronautical Co.
San Diego, Calif.
Attn: Chief Engr.

1 Solar Aircraft Co.
San Diego, Calif.

1 Tacoma Boat Bldg. Co., Inc.
Tacoma, Wash.

1 H.M. Tiedemann & Co., Inc.
New York, N.Y.

1 United Aircraft Corp.
Sikorsky Aircraft Div.
Stratford, Conn.

1 United Aircraft Corp.
Research Dept.
East Hartford, Conn.

1 Vehicle Research Corp.
Pasadena, Calif.

1 Martin-Marietta Corp.
Orlando Div.
Orlando, Fla.

1 Univ. of Calif.
Berkeley, Calif.

1 Univ. of Calif.
Dept. of Engr.
Los Angeles, Calif.

1 Catholic Univ.
Dept. of Mech. and Aero. Engr.
Washington, D.C.

DISTRIBUTION LIST

1 Johns Hopkins Univ.
Dept. of Aeronautics
Baltimore, Md.

1 Univ. of Louisville
Speed Scientific Sch. Lib.
Louisville, Ky.

1 MIT, Hayden Lib.
Ser. & Documents Div.
Cambridge, Mass.

1 Iowa State Univ.
Iowa Inst. for Hydraulic Res.
Iowa City, I.

1 Univ. of Minn.
Rosemount Aeronautical Labs.
Dept. of Engrg.
Minneapolis, Minn.

1 Miss. State College
Aerophysics Dept.
State College, Miss.

1 Princeton Univ.
Forrestal Res. Center
Princeton, N.J.
Attn: Libr.

1 Rensselaer Polytechnic Inst.
Dept. of Aero. Engrg.
Troy, New York

1 Univ. of Southern Calif.
Engr. Center
Los Angeles, Calif.

1 Stevens Institute of Tech.
Hobeken, N.J.

1 Virginia Poly. Inst.
Carol M. Newman Library
Blacksburg, Va.

1 Univ. of Wichita
Dept. of Engrg.
Wichita, Kansas

1 Air War College, Air Univ.
Maxwell AFB, Alabama
Attn: Eval. Staff

1 Hdqs, U.S. Air Force (AFRDT-EX)
Deputy Chief of Staff
Research & Technology
Wash., D.C.

1 Executive Director
Air Force Office of
Scientific Research(SRIL)
Dept of the Air Force
Wash., D.C.

1 Chief, Office of
Research and Development
Maritime Adm.
Wash., D.C.

Unclassified
Security Classification

DOCUMENT CONTROL DATA - R&D

(Security classification of title, body of abstract and indexing annotation must be entered when the overall report is classified)

1 ORIGINATING ACTIVITY *(Corporate author)* Aerodynamics Laboratory David Taylor Model Basin Washington, D. C. 20007	2a REPORT SECURITY CLASSIFICATION Unclassified 2b GROUP

3 REPORT TITLE

A METHOD FOR PREDICTING THE STATIC AERODYNAMIC CHARACTERISTICS OF LOW-ASPECT-Ratio Configurations

4. DESCRIPTIVE NOTES *(Type of report and inclusive dates)*

5. AUTHOR(S) *(Last name, first name, initial)*

Eaton, Peter T.

6. REPORT DATE	7a. TOTAL NO OF PAGES	7b. NO. OF REFS
June 1966	102	21

8a. CONTRACT OR GRANT NO. b. PROJECT NO. WR 011-0101 c. DTMB 640-155 d.	9a. ORIGINATOR'S REPORT NUMBER(S) Report 2216 9b. OTHER REPORT NO(S) *(Any other numbers that may be assigned this report)* Aero Report 1112

10 AVAILABILITY/LIMITATION NOTICES

The distribution of this document is unlimited.

11. SUPPLEMENTARY NOTES	12. SPONSORING MILITARY ACTIVITY
	Naval Air Systems Command Department of the Navy Washington, D. C. 20360

13. ABSTRACT

A procedure has been derived for theoretically predicting the static aerodynamic characteristics (except rolling moment) of low-aspect-ratio configurations. This procedure is based on existing linear and nonlinear theories with some empirical modifications and has been programmed for the IBM 7090 computer so that the geometric characteristics of the configuration are the only required inputs. Correlation of theoretical and experimental results indicates that the procedure is applicable at Mach numbers up to 3.0, angle of attack up to 20° and tail deflection angles up to 10°.

DD FORM 1 JAN 64 1473

Unclassified
Security Classification

14 KEY WORDS	LINK A		LINK B		LINK C	
	ROLE	WT	ROLE	WT	ROLE	WT
Missiles Theory Performance Lift Stability Drag Angle of Attack Tail Deflection Angle Subsonic, Transonic, Supersonic Body Shape Lifting Surface Planform Low-Aspect-Ratio Automated Procedures						

INSTRUCTIONS

1. ORIGINATING ACTIVITY: Enter the name and address of the contractor, subcontractor, grantee, Department of Defense activity or other organization *(corporate author)* issuing the report.

2a. REPORT SECURITY CLASSIFICATION: Enter the overall security classification of the report. Indicate whether "Restricted Data" is included. Marking is to be in accordance with appropriate security regulations.

2b. GROUP: Automatic downgrading is specified in DoD Directive 5200.10 and Armed Forces Industrial Manual. Enter the group number. Also, when applicable, show that optional markings have been used for Group 3 and Group 4 as authorized.

3. REPORT TITLE: Enter the complete report title in all capital letters. Titles in all cases should be unclassified. If a meaningful title cannot be selected without classification, show title classification in all capitals in parenthesis immediately following the title.

4. DESCRIPTIVE NOTES: If appropriate, enter the type of report, e.g., interim, progress, summary, annual, or final. Give the inclusive dates when a specific reporting period is covered.

5. AUTHOR(S): Enter the name(s) of author(s) as shown on or in the report. Enter last name, first name, middle initial. If military, show rank and branch of service. The name of the principal author is an absolute minimum requirement.

6. REPORT DATE: Enter the date of the report as day, month, year; or month, year. If more than one date appears on the report, use date of publication.

7a. TOTAL NUMBER OF PAGES: The total page count should follow normal pagination procedures, i.e., enter the number of pages containing information.

7b. NUMBER OF REFERENCES: Enter the total number of references cited in the report.

8a. CONTRACT OR GRANT NUMBER: If appropriate, enter the applicable number of the contract or grant under which the report was written.

8b, 8c, & 8d. PROJECT NUMBER: Enter the appropriate military department identification, such as project number, subproject number, system numbers, task number, etc.

9a. ORIGINATOR'S REPORT NUMBER(S): Enter the official report number by which the document will be identified and controlled by the originating activity. This number must be unique to this report.

9b. OTHER REPORT NUMBER(S): If the report has been assigned any other report numbers *(either by the originator or by the sponsor)*, also enter this number(s).

10. AVAILABILITY/LIMITATION NOTICES: Enter any limitations on further dissemination of the report, other than those imposed by security classification, using standard statements such as:

(1) "Qualified requesters may obtain copies of this report from DDC."

(2) "Foreign announcement and dissemination of this report by DDC is not authorized."

(3) "U. S. Government agencies may obtain copies of this report directly from DDC. Other qualified DDC users shall request through _____."

(4) "U. S. military agencies may obtain copies of this report directly from DDC. Other qualified users shall request through _____."

(5) "All distribution of this report is controlled. Qualified DDC users shall request through _____."

If the report has been furnished to the Office of Technical Services, Department of Commerce, for sale to the public, indicate this fact and enter the price, if known.

11. SUPPLEMENTARY NOTES: Use for additional explanatory notes.

12. SPONSORING MILITARY ACTIVITY: Enter the name of the departmental project office or laboratory sponsoring *(paying for)* the research and development. Include address.

13. ABSTRACT: Enter an abstract giving a brief and factual summary of the document indicative of the report, even though it may also appear elsewhere in the body of the technical report. If additional space is required, a continuation sheet shall be attached.

It is highly desirable that the abstract of classified reports be unclassified. Each paragraph of the abstract shall end with an indication of the military security classification of the information in the paragraph, represented as *(TS), (S), (C), or (U)*

There is no limitation on the length of the abstract. However, the suggested length is from 150 to 225 words.

14. KEY WORDS: Key words are technically meaningful terms or short phrases that characterize a report and may be used as index entries for cataloging the report. Key words must be selected so that no security classification is required. Identifiers, such as equipment model designation, trade name, military project code name, geographic location, may be used as key words but will be followed by an indication of technical context. The assignment of links, roles, and weights is optional.